

UNIVERSITY OF PADOVA

DOCTORATE SCHOOL: INFORMATION ENGINEERING

INFORMATION SCIENCE AND TECHNOLOGY

XXVI CICLO

---

---

# Movement-Related Desynchronization in EEG-based Brain-Computer Interface applications for stroke motor rehabilitation

---

---

*Supervisor:*

Ch.mo Prof. Silvano PUPOLIN

*Ph.D. Candidate:*

Giulia CISOTTO

*School Director:*

Ch.mo Prof. Matteo BERTOCCO

Academic Year 2013-2014

# Contents

<b>Abstract</b>	<b>3</b>
<b>List of Acronyms</b>	<b>4</b>
<b>Introduction</b>	<b>7</b>
<b>1 Sensorimotor System and Stroke</b>	<b>9</b>
1.1 Sensorimotor System . . . . .	9
1.2 Stroke . . . . .	15
<b>2 Electroencephalography based Brain Computer Interface</b>	<b>19</b>
2.1 Electroencephalography (EEG) . . . . .	19
2.1.1 Basic Principles . . . . .	20
2.1.2 Rhythms . . . . .	23
2.2 Brain Computer Interface (BCI) . . . . .	25
2.2.1 Background and Applications . . . . .	25
2.2.2 Principles and Setups . . . . .	27
<b>3 An Example of EEG based BCI Platform for Stroke Motor Recovery</b>	<b>33</b>
3.1 Study Protocol and Participants . . . . .	33
3.2 System Description . . . . .	37
3.3 Performance Evaluation . . . . .	41
3.4 Strong Points and Further Improvements . . . . .	43
<b>4 EEG Signal Processing for BCI based Motor Rehabilitation</b>	<b>49</b>
4.1 Electrode Pop Artefacts . . . . .	49
4.1.1 Description . . . . .	49
4.1.2 Literature Solutions . . . . .	50
4.1.3 Proposal for a Rejection Algorithm . . . . .	51
4.2 Energy Analysis . . . . .	60
4.2.1 Preliminary Steps . . . . .	60
4.2.2 Energy Computation . . . . .	63
4.3 Movement Related Desynchronization (MRD) Quantification . . . . .	64
4.3.1 MRD Definition . . . . .	64
4.3.2 BCI2000 Software . . . . .	68
4.3.3 Proposal for an MRD Quantification Algorithm . . . . .	70

<b>5 Results and Discussion</b>	<b>73</b>
5.1 Results from the Signal Processing . . . . .	73
5.2 Discussion . . . . .	76
5.3 Future Perspectives . . . . .	78
<b>Conclusion</b>	<b>87</b>
<b>References</b>	<b>89</b>
<b>List of Figures</b>	<b>96</b>

# Abstract

Neurological degenerative diseases like stroke, Alzheimer, Amyotrophic Lateral Sclerosis (ALS), Parkinson and many others are constantly increasing their incidence in the world health statistics as far as the mean age of the global population is getting higher and higher.

This leads to a general need for effective, at-home and low-cost rehabilitative and health-daily-care tools. The latter should consist either of technological devices implemented for operating in a remote way, i.e. tele-medicine is quickly spreading around the world, or very-advanced computer-based and robotic systems to realize intense and repetitive trainings. This is the challenge in which Information and Communications Technology (ICT) is asked to play a major role in order to bring medicine to reach further advancements.

Indeed, no way to cope with these issues is possible outside a strong and vivid cooperation among multi-disciplinary teams of clinicians, physicians, biologists, neuropsychologists and engineers and without a resolute pushing towards a widespread interoperability between Institutes, Hospitals and Universities all over the world, as recently highlighted during the main International conferences on ICT in healthcare. The establishment of well-defined standards for gathering and sharing data will then represent a key element to enhance the efficacy of the aforementioned collaborations.

Among the others, stroke is one of the most common neurological pathologies being the second or third cause of mortality in the world; moreover, it causes more than sixty percent survivors remain with severe cognitive and motor impairments that impede them in living normal lives and require a twenty-four-hours daily care. As a consequent, on one side stroke survivors experience a frustrating condition of being completely dependent on other people even to perform simple daily actions like reach and grasp an object, hold a glass of water to drink it and so on. States, by their side, have to take into account additional costs to provide stroke patients and their families with appropriate cares and supports to cope with their needs. For this reason, more and more fundings are recently made available by means of grants, European and International projects, programs to exchange different expertise among various countries with the aim to study how to accelerate and make more effective the recovery process of chronic stroke patients.

The global research about this topic is conducted on several parallel aspects: as regard as the basic knowledge of brain processes, neurophysiologists, biologists and engineers are particularly interested in an in-depth understanding of the so-called neuroplastic changes that brain daily operates in order to adapt individuals to life changes, experiences and to realize more extensively their own potentialities.

Neuroplasticity is indeed the corner stone for most of the trainings nowadays adopted by the standard as well as the more innovative methods in the rehabilitative programs

for post-stroke recovery. Specifically speaking, motor rehabilitation usually includes long-term, repetitive and intense goal-directed exercises that promote neuroplastic mechanisms such as neural sprouting, synapto-genesis and dendritic branching. These processes are strictly related with motor improvements and their study could - one day - serve as prognostic measures of the recovery.

Another aspect of this field of neuroscience research is the number of applications that it makes feasible. One of the most exciting is to connect an injured brain to a computer or a robotic device in a Brain-Computer or Brain-Machine Interface (BCI or BMI) scheme aiming at bypassing the impairments of the patient and make him/her autonomously move again or train his/her motor abilities in a more effective way. This kind of research can already count an amount of literature that provides several proofs of concept that these heterogeneous systems constituted by humans and robots can work at the purpose.

A particular application of BCI for restoring or enhancing, at least, the reaching abilities of chronic stroke survivors was implemented and is still currently being improved at I.R.C.C.S. San Camillo Hospital Foundation, an Institute for the rehabilitation from neurological diseases located in Lido of Venice and partially technically supported by the Department of Information Engineering of Padua in range of an agreement signed in 2009. This specific BCI platform allows patients to train and improve their reaching movements by means of a robotic arm that provides a force that helps patients in completing the training exercise, i.e. to hit a predetermined target. This force feedback is however subject to a strict condition: during the movement, the person has to produce the expected pattern of cerebral activity. Whenever this is accomplished, a force is delivered proportionally to the entity of the latter activity, otherwise the patient is obliged to operate without any help. In this way, this platform implements the so-called operant-learning, that is one of the most effective conditioning techniques to make a subject learn or re-learn a task. If, on one hand, the primary and explicit task is to improve a movement, on the other side the secondary but most important task is to deploy the perilesional part of the brain - still healthy - in becoming responsible for the control of the movement. It is a popular and widely-accepted opinion within the neuroscience community, indeed, that a healthy region of the sensorimotor area nearby the damaged one - which was previously in charge of performing the (reaching) movement - can optimally accomplish the impaired motor function substituting the original control area.

Technically speaking, the main crucial feature that can ensure the effectiveness of the whole system is the precise and in real-time identification and quantification of the cerebral pattern associated with the movement, the worldwide named movement-related desynchronization (MRD). Starting from its original definition, passing through the most used techniques for its recognition, the thesis work presents a series of criticisms of the current signal processing method to detect the MRD and a complete analysis of the possible features that can better represent the movement condition and that can be more easily extracted during the on-line operations.

Brain - it is well-known - learns by trials and errors and it needs a slightly-delayed (in the range of fraction of seconds) feedback of its performance to learn a task in the best way. This BCI application was born with the purpose to provide the above-mentioned feedback: however, this is only feasible if a computationally easy and contingent signal processing technique is available. This thesis work would like to cope with the lack of a well-planned real-time signal analysis in the current experimental protocol.

## **Acronyms**

<b>ADC</b>	Analog-to-Digital Converter
<b>ADL</b>	Activities of Daily Life
<b>ALS</b>	Amyotrophic Lateral Sclerosis
<b>AVM</b>	Arterio-Vascular Malformation
<b>BBT</b>	Box and Blocks Test
<b>BCI</b>	Brain Computer Interface
<b>BMI</b>	Brain Machine Interface
<b>CAR</b>	Common Average Reference
<b>CNS</b>	Central Nervous System
<b>CSP</b>	Common Spatial Pattern
<b>DSP</b>	Digital Signal Processor
<b>ECoG</b>	Electrocorticogram
<b>EEG</b>	Electroencephalography
<b>EMG</b>	Electromyogram
<b>ERD</b>	Event-Related Desynchronization
<b>ERPs</b>	Evoked-Related Potentials
<b>ERS</b>	Event-Related Synchronization
<b>FES</b>	Functional Electrical Stimulation
<b>FFT</b>	Fast Fourier Transform
<b>FIR</b>	Finite Impulse Response
<b>FIM</b>	Functional Independence Measure
<b>FMA-UE</b>	Fugl-Meyer Assessment for the Upper Extremity
<b>fMRI</b>	Functional Magnetic Resonance Imaging
<b>fNIRS</b>	Functional Near Infrared Spectroscopy
<b>HMI</b>	Human Machine Interface
<b>ICA</b>	Independent Component Analysis
<b>ICT</b>	Information and Communication Technology

**IFSECN** International Federation of Societies for Electroencephalography and Clinical Neurophysiology

**IRCCS** Istituto di Ricovero e Cura a Carattere Scientifico (Scientific Institute for Research, Hospitalisation and Health Care)

**LFPs** Local Field Potentials

**LORETA** Low Resolution Brain Electromagnetic Tomography

**MAS** Modified Ashworth Scale

**MEG** Magnetic Encephalography

**MEM** Maximum Entropy Method

**MI** Motor Imagery

**MRD** Movement-Related Desynchronization

**MRS** Movement-Related Synchronization

**MUSIC** Multiple Signal Classification

**NFB** Neurofeedback

**NHPT** Nine Hole Peg Test

**NS** Nervous System

**PNS** Peripheral Nervous System

**RS** Reaching Score

**SCI** Spinal Cord Injury

**SCPs** Slow Cortical Potentials

**SIR** Signal-to-Interference Ratio

**SMR** Sensorimotor Rhythms

**SNR** Signal-to-Noise Ratio

**TDCS** Transcranial Direct Current Stimulation

**TMS** Transcranial Magnetic Stimulation

**VEPs** Visual Evoked Potentials

**VR** Virtual Reality

# Introduction

Detection and quantification of the cerebral activity patterns related to the movement is one of the most crucial aspects to be addressed in the context of Brain Computer Interface (BCI) [1] applications of rehabilitative medicine in favour of chronic stroke patients.

Recovery from stroke and particularly rehabilitation of impaired motor functions [2], basically aims at restoring the so-called *sensorimotor system* [3], that complex of cortical areas and sub-cortical structures that allow an individual to receive somatosensory feedback from the external environment and react by means of a suitable motor behaviour accomplished through the final actuators of the movement, the muscles.

In pursuit of this goal, the most rehabilitative techniques and BCI as well put a great effort in exploiting and promoting the spontaneous processes brain constantly performs to improve its functionalities, adapt to new environmental conditions and even try to recover impaired capabilities after an injury. These phenomena are generally referred as *neuroplasticity* [4] and they have been extensively exploited for years in the clinical practise, but only recently studied from a more rigorous and scientific point of view by the contributions of many neuroscientists with different backgrounds, i.e. neurophysiology, biology, physical therapy, engineering and so on.

In the particular context of the rehabilitation of motor functions [5] [6] that basically points at restarting learning mechanisms of motor behaviours in the brain of a stroke survivor, recent literature about neuroplasticity highlighted the significant effectiveness of the so-called *operant-conditioning* [7].

Through a repetitive reinforcement by means of specific kinds of *rewards* of the contingency between a *correct* cerebral pattern and a *good* motor output, brain is conditioned to exploit the redundant cerebral pathways from the Central Nervous System (CNS) to the muscles still healthy after the traumatic injury, leading to a generally observed functional motor improvement.

This specifically means that with a suitable operant-conditioning paradigm, one can voluntarily - although almost unconsciously - modify or *modulate* the amplitude and the frequency of his/her cerebral activity.

As a consequence then, the Information and Communication Technology (ICT) and the signal processing community strongly have a part in the completion of this kind of rehabilitative strategy: accurate and customized algorithms and software implementations are needed to detect and quantify in real-time the aforementioned correct cerebral patterns, indeed, along with the whole technical expertise about kinematics and control theory for human motor output evaluations and robot-aided rehabilitative technologies.

In this Ph.D. thesis work, after the introductory Chapter 1 about the neurophysiological basis of the sensorimotor system and the essential background on stroke disease,

the following Chapter 2 will include a description of the fundamentals of the Electroencephalography (EEG) and a brief overview about the BCIs.

Then, a specific EEG-based BCI system for the recovery of the reaching function of mildly impaired stroke patients implemented at Istituto di Ricovero e Cura a Carattere Scientifico (Scientific Institute for Research, Hospitalisation and Health Care) (IRCCS) San Camillo Hospital Foundation at Lido of Venice, Italy, will be presented in Chapter 3. In that Chapter the typical BCI structure made by the basic units for acquiring and processing the EEG signals, extracting its most relevant features and transforming them into commands for a robotic output will be explained by means of the specific platform implemented at the clinical Institute. In particular, the output is represented by an haptic device that helps subjects in completing a movement of reaching on a plane. Its operation is controlled by the cerebral activity of the subject performing the reaching task closing, in this way, the loop between the human brain and the machine.

To establish this mutual dependence in which the machine is driven by the voluntarily modulation of the cerebral pattern accomplished by the subject and the human has to learn how to control in a self-paced mode the machine in order to receive the help, an underlying robust and *user-friendly* signal processing module has to capture the relevant EEG features related to the intention to move, including a certain level of adaptation that could take into account the physiological variations of the cerebral activity, and finally continuously control the machine's response to the human behaviour.

One of the most crucial issues to cope with towards such a successful identification mentioned so far is to detect and remove, in real-time as well, both the non-physiological and the non task-related components of the signals acquired by the EEG. For this reason, part of the Ph.D. work was dedicated to such a study and the initial section of Chapter 4 will deal with this topic.

In the rest of that Chapter a comprehensive analysis of the energy of the EEG signals in every different phase of the experiment, e.g. rest, planning of the movement and actual task performance, will provide a detailed description of the cerebral changes at the scalp level during the experiment. Afterwards, a new quantitative method for the computation of the cerebral pattern associated with the reaching movement and its timing along all the trials of the experiment could be defined.

Chapter 5 will finally provide the promising results of the previously presented new algorithm of movement-related cerebral pattern computation. In particular, it will be highlighted how its capacity to early identify such patterns leads to save longer time for operating further signal processing to transform the cerebral activity in an optimal output command for the robotic actuator before the beginning of the actual movement performed by the subject. In the same Chapter further considerations around this new algorithm will be presented in the discussion section.

As already mentioned, it has to be strongly pointed out that providing in real-time the optimal feedback to the subject perfectly matches the neurophysiological requirements to achieve an effective operant-learning mechanism of conditioning and, as a consequence, a larger, faster and longer lasting functional recovery.

Thesis will conclude sketching open issues still remained to be addressed and future perspective that are most likely going to be reached in a near future.

# Chapter 1

## Sensorimotor System and Stroke

As mentioned in the introduction, this Chapter is devoted to the description of the sensorimotor system starting from the general notions about the Nervous System (NS), its components and functionalities with a final insight on the elementary module of the NS, the neuron.

In the second section of the Chapter, then, a brief overview about the stroke pathology, its aetiology and the most common rehabilitative approaches is provided.

### 1.1 Sensorimotor System

In order to discuss about the central topic of this thesis work, some concepts regarding the neuroanatomy and the neurophysiology of the human body and some basic principles of motor control have to be outlined.

NS is in charge of all the sensory information gathering, thoughts formation, and processing and control of the functions of the whole body [8]. Specifically, it accomplishes to three main functions:

- the sensory one;
- the integration one (including memory and thoughts);
- and the motor one.

To implement them the two main subsystems of the NS, the CNS and the Peripheral Nervous System (PNS) have to cooperate, as sketched in Fig.1.1.

Specifically, the CNS is made by the brain and the spinal cord. While the brain is the main area in charge of the integration activity of the NS including emotion, thoughts and control of organs, the spinal cord acts as a transmission line for signals from and towards brain and participates to the control of coordination.

On the other side, the PNS is constituted by a nerves network where *afferent fibers* and *efferent* ones can be distinguished. Precisely speaking, afferent fibres conduct sensorial information from the peripheral areas to the spinal cord and the brain; efferent fibres, instead, represent the vias to send motor commands from the CNS to the distant areas of the body, e.g. the muscular-skeletal apparatus. For the sake of completeness, cranial nerves - nervous fibres that origin from the brain - and spinal nerves - arising from the spinal cord - belong to the PNS.

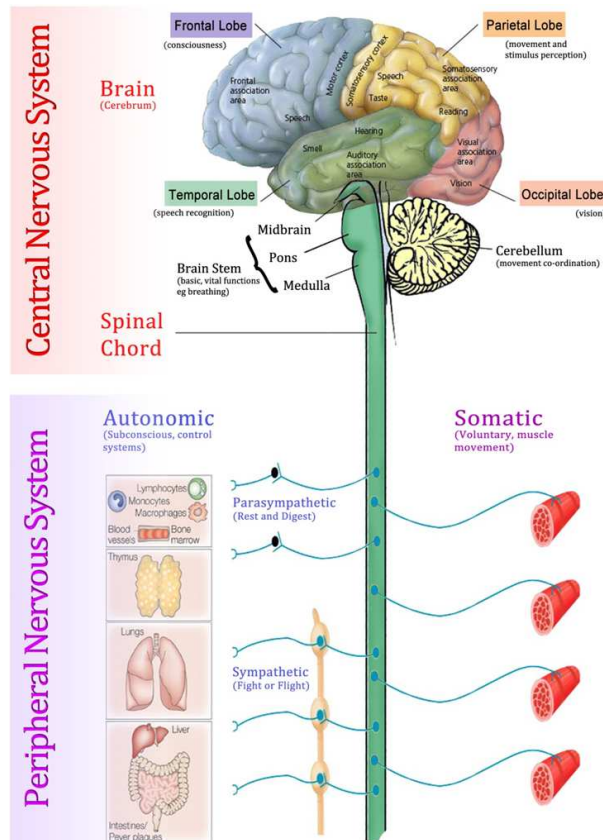


Figure 1.1: The nervous system.

Within the NS, brain performs a major role as control centre for the most functionalities that allow the individual to perform all the activities of his/her life as well as the body to survive thanks to all the feeding mechanisms the brain also coordinates. As captured by Fig.1.2, two main *hemispheres* can be distinguished in the brain; they are separated by the *central sulcus* but they can communicate each others by the *corpus callosum* and the *anterior commissure*, two sets of nervous fibres connecting the two hemispheres.

Then, going further into details, four *lobes* can be recognized in both the hemispheres: the *frontal*, the *parietal*, the *temporal* and the *occipital* one.

During the first World War, many persons were injured by several kinds of brain damages and, contextually, a series of systematic studies were carried on by many neurologists and neurosurgeons on the modifications due to the lesions in different parts of the brain. From this extensive analysis the functional mapping of the cerebral cortex could be suggested. Those studies brought a further contribution and confirmation to what Korbinian Brodmann published in 1909 ([9],[10]) and was known as the 52 Brodmann's areas distinguishing the different brain areas by their functions [11]. The result of all these works is shown in Fig.1.3.

However, the most significant areas from a motor rehabilitation point of view are illustrated by Fig.1.4 [8].

Indeed, the principal areas involved in the auditory, visual and somatosensory stimuli acquisition and integration are highlighted. In particular, it can be noted:

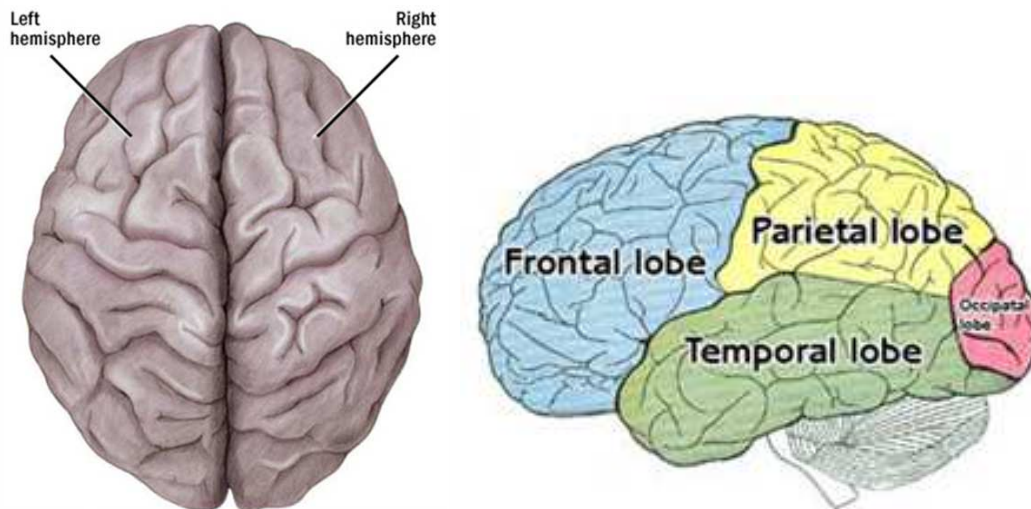


Figure 1.2: Brain hemispheres and lobes.

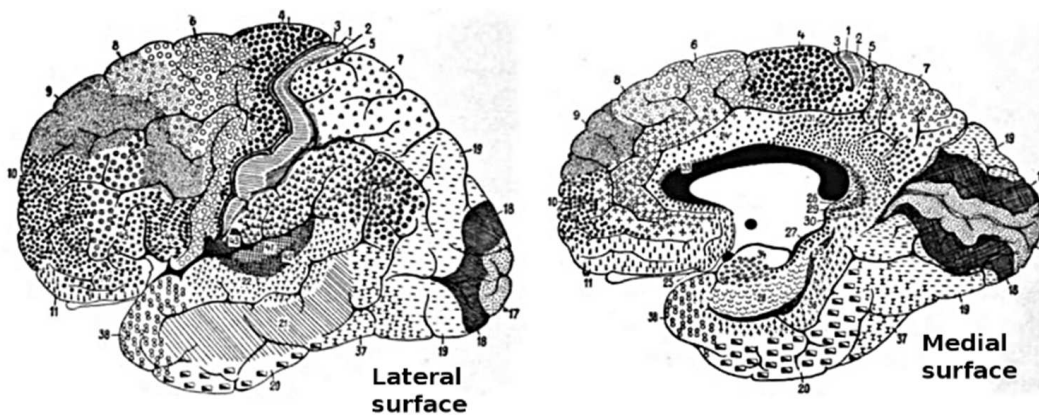


Figure 1.3: The Brodmann areas.

- the *motor area* further subdivided in:
  - the primary motor cortex which receives external stimuli through the peripheral afferent vias and is responsible for giving commands for muscles activation via the efferent pathways;
  - the premotor area that also receives sensory input but it is mainly in charge of the planning of the motor commands;
  - the supplemental area that is significantly involved in the coordination of different groups of muscles for programming complex sequences of movement.
- the *somatosensory cortex* that accounts for tactile sensations, pain and temperature stimuli. This area, located in the parietal lobe, could be also subdivided in a primary and in a secondary area. While the first one receives signals directly from the mechanoreceptors and sensory receptors placed all over the body, the second one is given by pre-processed signals coming from the primary area and it further

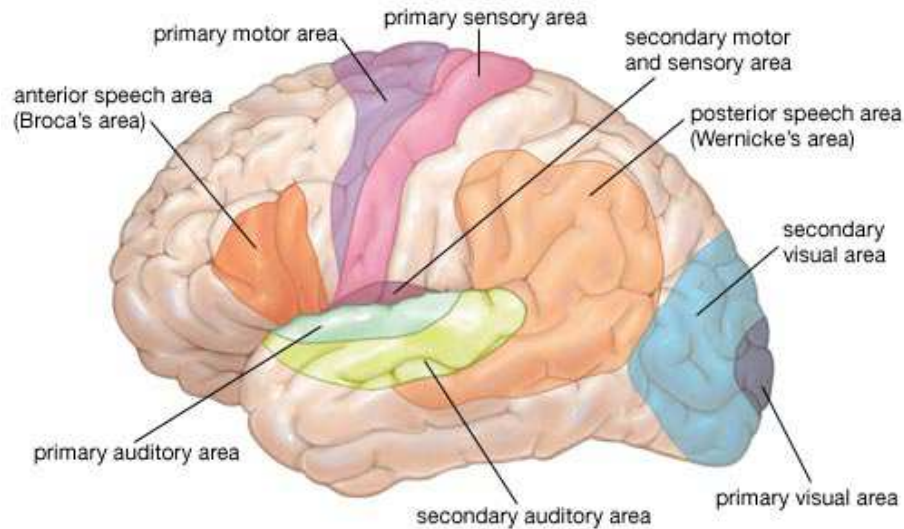


Figure 1.4: The main functional areas.

transforms these inputs into convenient outputs mainly sent to the motor areas to integrate somatosensory information to accomplish motor functions.

- the *visual cortex*. Mainly occupying the occipital lobe, it performs basic image processing like the distinction of bright and dark points or the definition of image boundaries (primary visual cortex) as well as more sophisticated image processing that allows to recognize objects and faces, for example (secondary visual cortex).
- the *auditory area* located in the temporal lobes accomplishes to sound, speech and music processing by means of a double layers structure made by a primary and a secondary auditory area.
- the *Wernicke's area* that is involved in the somatosensory integration thanks to convergence of projection from the parietal, the occipital and the temporal lobes.
- the *short-term memory area* that was mapped in the lower part of the temporal lobe and is involved in the storing of information from few minutes up to few weeks.
- the *prefrontal area* which seems to be correlated with the highest faculty of the brain, as the thought processing and the concentration ability.

Functional areas aforementioned are only the cortical representations of complex *circuits* or *systems* involving several areas of the whole NS. Among others i.e. the dorso-lateral-prefrontal and the visual circuit for example, the most important system for the scopes of this thesis work is the sensorimotor circuit [3], illustrated by Fig.1.5.

As already hint at in the introduction, the sensorimotor system accomplishes to the generally referred as motor control. This includes the integration of somatosensory, visual and vestibular inputs for performing two kinds of motor activities: the *feedback control* and the *feedforward control* [12]. If, on one hand, the stimulation of corrective responses after a sensory detection is defined as feedback control, on the other hand feedforward

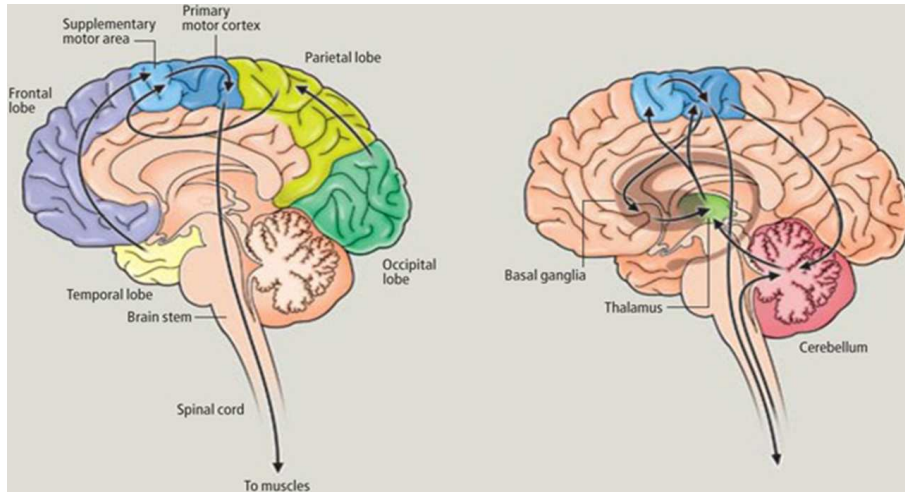


Figure 1.5: The sensorimotor system.

control describes actions occurring upon the identification of their beginning, in an anticipatory way. Sometimes the combination of these two types of control is needed, as in the maintenance of the postural control.

It has also to be observed that the sensorimotor system is hierarchical organized: a *central axis* constituted by three levels that are the spinal cord, the brain stem and the cortex reaches the motor control with a *functional segregation* scheme, where at each hierarchical level different units simultaneously perform a variety of functions. Furthermore, two associate areas, cerebellum and basal ganglia, are responsible for modulating and regulating the motor commands.

Spinal cord gives rise to direct responses to peripheral sensory information and to elementary patterns of motor coordination.

Brain stem represents, instead, the main storage element for automatic and stereotyped movements. Moreover, at this level the integration of sensory information from vestibular, visual and somatosensory sources is performed.

The third and last level is the cerebral cortex that is responsible for initiating and controlling more complex and discrete voluntary movements. Three main areas, already described before, act a major role in this hierarchical control of movement: the primary motor cortex, the secondary one and the supplemental motor area.

Moreover, the *corticospinal tract* i.e. the tract of the NS that conducts impulses from the brain to the spinal cord, contains the most important descending (i.e. efferent) direct pathways from the motor cortex to the motor neurons, the elementary units of the neural motor system.

Along with the three main levels, cerebellum and basal ganglia play a fundamental role in the motor control, especially for the execution of coordinated movements. Cerebellum, specifically, is responsible for the continuous comparison of the intended movement with the outcome one. Furthermore, it is also implicated in the motor learning. On their side, basal ganglia consist of five subcortical nuclei (groups of cells) that include the *caudate nucleus*, the *putamen*, the *globus pallidus*, the *claustrum* and the *amygdala*, and they are directly connected only with the cerebral cortex at the higher level of the hierarchical

organization. Particularly, input and output connections passing through the *thalamus*. As regards as basal ganglia implication in motor control, they are believed to be involved in cognitive aspects of motor control.

In the final part of this section, it has to be described the primary component of the whole NS: the nervous tissue [8] which is, in turn, constituted by neurons and glia cells. The latter are the elementary units of the NS and they act as control center for every kind of activity performed by the individual, from cognitive to motor ones.

Specifically, neurons conduct signals from nervous sources to the various parts of the body.

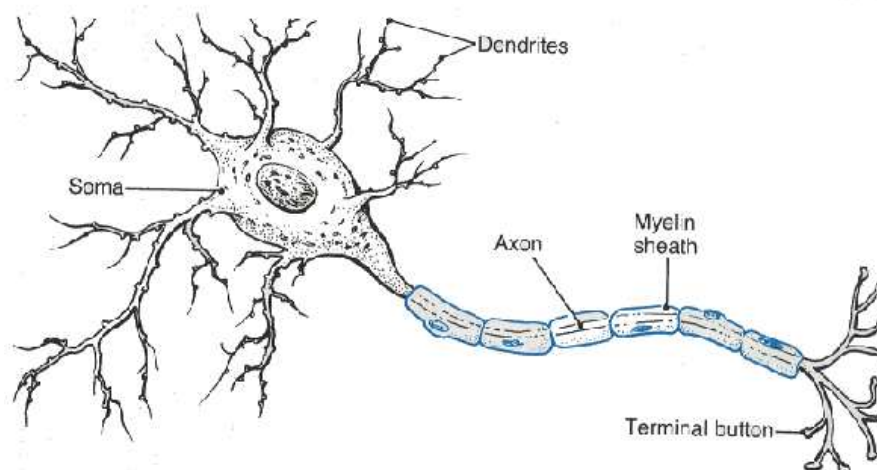


Figure 1.6: The neuron.

As provided by Fig.1.6, the main components of a neuron are:

- the *cellular body* where functions for ensuring the cellular life are accomplished;
- the *dendrites*, projections of the cellular body to other neurons for communications purposes;
- the *axon* or *nervous fibre*. It can be few millimetres up to 1 metre long. Axons transport the nervous signals to the next neuron of the CNS or the PNS.
- the *synaptic terminals* that are represented by the final parts of an axon and are used by the neuron to establish a communication with other nervous cells. Indeed, when two neurons are in contact with each others - forming a *synapse*- the presynaptic neuron releases into the synaptic space between its termination and either the dendrite or the cellular body of another neuron a *neurotransmitter*, a protein that has special properties and it is able to activate, i.e. transmit the electrical information in form of chemical signal, (to) the post-synaptic neuron.

If, on one side, neurons represent the elementary and fundamental units for the neuro-transmission of information, glia cells play the major and complementary role to maintain the nervous system compact.

By now, the complete description of the sensorimotor system can be recalled in further detail. As shown in Fig.1.7, the whole motor pathway from the central nervous system, i.e. the primary motor area, to the muscle through all the components of the of an efferent via of the NS is shown.

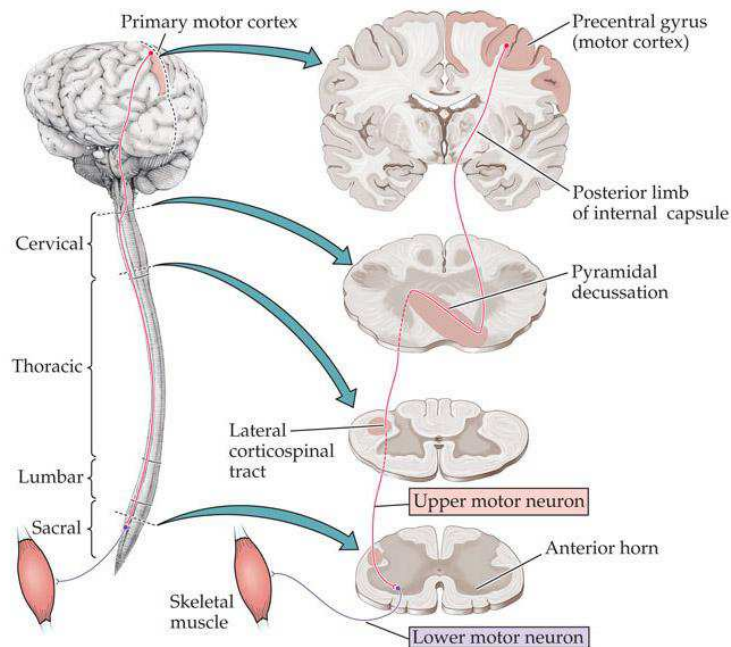


Figure 1.7: Pathway from the CNS to the muscles.

Concluding, it can be observed that in case of neuro-degenerative disorders (above all, the Amyotrophic Lateral Sclerosis (ALS)) neural loss or dysfunction occur in the sensorimotor system in a long time even before the clinical diagnosis. On the opposite, an abrupt loss of the neural functions could be caused by severe traumatic or cerebrovascular disease, stroke among others. In both cases, neurons death causes severe impairments that in most cases could only partially be recovered.

As anticipated at the beginning of this Chapter, in the following an overview about stroke will be presented along with a brief excursus of the most common rehabilitative techniques to restore a particular class of functions, the motor ones.

## 1.2 Stroke

World health reports [13] usually show severe traumatic neural injuries, particularly stroke, as the second or third most common cause of mortality in the majority of the Countries of the world. This clue is constantly increasing with the ageing of the global population and with the worsening of food habits and environmental conditions of life.

By now the sixty percentage survivors remains with permanent disabilities that cause them long-term impairments and psychological consequences for themselves and also their families. Among others, motor functions of the extremities are the most commonly damaged ones and this kind of impairment represents an important element of disability:

patients with gait, reaching, grasping and holding difficulties are severely compromised in the Activities of Daily Life (ADL) and lose their independence needing a twenty-four-hours care assistance.

Clinically speaking, stroke can be caused by an ischemia or an hemorrhage. In the first case, the most common one with an occurrence of the 87%, an interruption of blood feeding to a part of the brain occurs, while in the hemorrhagic stroke a blood loss injures the surrounding cerebral tissues. As a result, in both cases, this cerebrovascular disease causes - if not death - mild to severe impairments affecting the functions normally performed by the damaged areas of the brain.

However, fortunately, it is well-known that after stroke spontaneous processes of recovery take place [14] [15] [16] [17]: synapto-genesis increase, dendritic branching along with neural sprouting have already been observed and are currently under deep investigation all over the world. These changes inside the brain are generally referred with the previous mentioned name of neuroplasticity [4] and, as already said in the introduction they can be addressed as promising prognostic clues of the best recovery towards health.

Despite this kind of phenomena and although notable advancements recently reached in the clinical management of stroke, a good practise of rehabilitation after the injury plays a crucial role in the recovery of a high quality of life.

To this purpose, literature [2] [18] highlights the effectiveness of high-intensity, repetitive and goal-directed training: the latter indeed have been correlated with advantageous changes in the neural architecture. Thus, these activities were found to be beneficial in promoting the above mentioned neuroplastic brain changes and, as a consequence, a more effective recovery.

In line with literature, international guidelines for a good rehabilitation practice [19] establish the importance of such task-specific and intense activities to promote neural plasticity and spontaneous recovery of lost functions. In this context, occupational therapy is highly recommended as an effective trade off between the pure physiotherapeutic exercise at the rehabilitation Institutes and the normal daily life which patients aim to return as soon as possible.

Moreover, manipulations by the physical therapists, pharmacological treatments and physical therapies with lasers or magnetic fields are also typically included in every rehabilitative programs for post-stroke patients [2] [18].

Besides this kind of standard therapies, many other alternative and more innovative methods have already been used and have shown their effectiveness in promoting beneficial anatomical and physiological changes in the brain [2] [18]. Among others, bilateral training was introduced to induce patients to regain lost functions of their affected limb taking advantage of the comparison with the healthy one. On the contrary, constraint-induced therapy forces patients to use the only affected limb, since the healthy one is immobilized.

Another major class of rehabilitative methods includes the use of some kind of feedback in the protocol: for instance, while a patient is performing an exercise of isotonic contraction of his/her hand, a feedback of his/her muscles activity is measured by an Electromyogram (EMG) and shown to the patient. On its turn, the latter has to adjust the effort of the contraction following the information provided by its own EMG along with some guidelines from the physical therapist that conducts the exercise. During Virtual Reality (VR) training, instead, correct motor behaviours are feedback by real-world

scenes in a virtual environment such as a kitchen, a bar or a supermarket. All these kinds of feedback-supported trainings have been shown to be effective to make patients improve their motor abilities and to cope with the annoying repetitiveness of the standard training exercises.

A final particular class of recovery strategies has to be mentioned: the Motor Imagery (MI) one [20]. During motor imagery tasks the patients have to imagine the movement of a limb or a hand, a foot or even the tongue. In some cases, his/her cerebral activity could be also acquired and used to provide him/her information about the quality of his/her performance or, as it happens in a BCI platform, this activity is used to control an external device.

BCIs are indeed the youngest motor rehabilitative methods but they have already shown their effectiveness and potentialities [1] [21].

Moreover, BCIs along with training environments enriched by VRs, biofeedbacks (like the EMG-feedback), Functional Electrical Stimulation (FES)-based feedbacks [22] and any kind of robotics [23] are in general almost-autonomously operating system that can provide that intense and repetitive training assistance that have already been proved to be highly beneficial to stroke survivors. Furthermore, technology can add quantification and a very detailed customization of the rehabilitation program based on the specific characteristics of each patient.

This makes health-care in neuroscience one of the most technology pervaded field of medicine nowadays.



# Chapter 2

## Electroencephalography based Brain Computer Interface

In this Chapter the particular class of BCI based on EEG is presented. Before that, an introductory section reports information about EEG, its original implementation, its operative acquisition and, more importantly, the physiological components that it can record.

### 2.1 Electroencephalography (EEG)

The EEG has a relatively old history and nowadays all Hospitals, clinical Institutes and even Universities have an EEG system to perform either daily clinical assessments of several kinds of patients or to study the cerebral activity of healthy and impaired people in a relaxation status and during any task execution.

Although its widespread availability, no gold standards for the analysis of the EEG traces are recognized all over the world. Instead most clinicians still analyse by-eye, only, the cerebral activity of their patients being satisfied to observe macroscopic phenomena like epileptic seizures or alternating phases of higher and lower levels of awareness represented by larger or smaller oscillations (*reactivity*) in the frequency band around 10 Hz, the so-called  $\alpha$  band [24].

However research has already shown, in many years of study, that an amount of information is hidden in that complex combination of waves that EEG is [25] [26]. Then several applications arose in many fields of neuroscience, e.g. cognitive assessments, evaluations of the effects of new kinds of brain stimulations such as Transcranial Direct Current Stimulation (TDCS) [27] [28] [29] or Transcranial Magnetic Stimulation (TMS) [27] [29] [30] and so on.

One of the most amazing field of the EEG employment is, without any doubt, the BCI where a subject can learn to operate a computer by the voluntary modulation of some of his/her EEG components to communicate in an alternative way with the external world or to move again by controlling a wheelchair or a robotic arm [1].



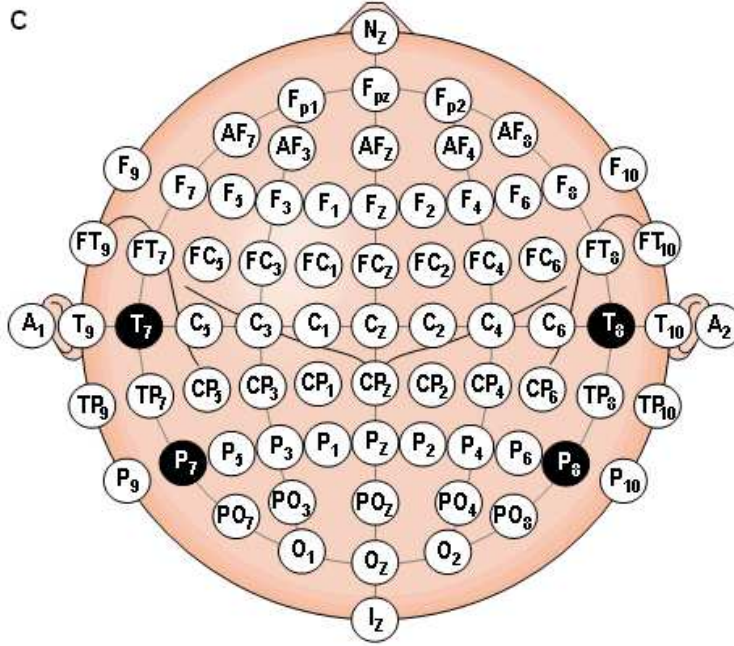


Figure 2.2: The 5-10 extended international EEG system.

2. an electrode should be placed at every 20% of this distance on the imaginary line that links the two reference points;
3. the analogous distance between the earlobes' centres ( $A_1$  being the standard name for the left one,  $A_2$  that of the opposite side) is measured;
4. as in 2. an electrode is located every 20% of the distance found in (3) on the line linking  $A_1$  and  $A_2$ ;
5. other sensors can fulfil the montage being added in the middle of every pair of already placed electrodes, that is the 10% of the reference distances;
6. further channels can be added outside the two perpendicular lines (crossing at the so-called *vertex*, indicated as  $C_z$ , of the scalp) following the 10%-20% rule similarly as what illustrated above.

Actually, nowadays all EEG producers have developed predefined EEG caps with places already allocated for electrodes.

Modified and world-wide accepted versions of this standard are further adopted in order to place a higher number of sensors on the scalp. For example, the 5%-10% system [34] (see Fig.2.2) allows clinicians and researchers to allocate up to 385 channels on the head of the subject, gathering much more information that can be then used for advanced applications.

Acquiring cerebral activity at the scalp requires, actually, to choose also a ground and a reference electrode. Usually, ground is placed on the EEG cap among the other electrodes, while the reference could be either located either on the scalp (as more usual

in clinics) or outside it. In research studies reference channel is usually located either on one earlobe or mastoid, or two references are selected and put on both the earlobes or the mastoids. Selecting an outside-scalp reference prevent experimenters to place it on particular areas of the brain in which special activity could be present (for example an epileptic focus). Moreover, all the scalp channels have to be monitored and can provide useful information while, if one of them (for example  $C_z$ ) was used as reference, its activity would be lost. Choosing both earlobes or mastoids would allow to record a more balanced activity: each scalp electrode would be indeed referred to the mean potential of the two references and distances from each sensor and one reference would be more comparable than in the asymmetrical situation of one reference only.

Indeed, operatively, recording the EEG of one single channel means to measure the voltage  $\Delta V_{e-ref}$  between each electrode and the reference as provided by the expression:

$$\Delta V_{e-ref} = (V_e - G) - (V_{ref} - G)$$

where  $V_e$  is the electrode potential,  $V_{ref}$  is the analogous quantity measured at the reference and  $G$  is the ground potential [25] [26].

Physiological range of voltages is limited to tens of  $\mu V$ , as already mentioned, while a broad frequency range from 0 Hz up to 100 Hz can be expected for such signals.

As outlined before, these kinds of signals are easily subjected to interferences and noises from outside as well as muscular activity. This leads EEG to be a very (and sometimes too much) sensitive device to record such a small cerebral activity. For the same reason, although an increasing number of electrodes could be placed on the most recent caps and pre-amplification stages were embedded in the most advanced *active* electrodes, EEG comes with a very low spatial resolution.

Indeed, multiple signal generators inside the brain have to be considered since several physiological sources can easily be simultaneously active. Then, each electrical signal originated from a different source propagates through several layers and tissues till the scalp surface where the EEG recording takes place. This cerebral environment leads the acquired signals suffer from reflections and diffractions phenomena. As a consequence, each original transmitted signal is received by many EEG electrodes with different amplitudes and delays, entailing that each EEG trace results from the combination of multiple transmitted signals transformed in amplitude (with a certain amount of attenuation) and time course (with some delay) during the pathway from the source to the scalp.

Moreover, voluntary as well as spontaneous muscular activity is also source of electrical signals which, propagating over the skin, reach the EEG recording electrode and contribute to the combined overall acquired signal. Nevertheless, this muscle activity is not of interest at all for the purposes of the BCI control and has to be rather excluded from the analysis because of its artefactual character.

In order to localise the physiological sources of the cerebral signals and their characteristics (amplitude and frequency distributions), sophisticated signal processing techniques are required and, specifically, the latter are asked to identify and remove muscular artefacts and, subsequently, spatially distinguish between the original transmitted signals. Literature offers several examples of such techniques, each of them with their own advantages as well as drawbacks. Among others, the most successful approach was described in [35] where Low Resolution Brain Electromagnetic Tomography (LORETA) algorithm was provided. Then, functional networks as in [36] with a *small world* logic are the trend of

the moment and they have already shown promising results in many fields of neuroscience (EEG as well as Functional Magnetic Resonance Imaging (fMRI)). Finally, other common approaches like Multiple Signal Classification (MUSIC), Bayesian or wavelets-based algorithms as in [37], [38], [39] and [40] can be also adopted.

Although clinicians (neurologists, neurophysiologists and technicians) can develop large expertise about the EEG traces evaluation, they can not in any way go further into EEG detailed characteristics by eye only. Then, engineers and physicians developed and implemented algorithms to accomplish to these more sophisticated functions making feasible many EEG-based advanced and automated applications.

Nevertheless, it has to be mentioned that EEG has also unique advantages in comparison with other possible brain recording techniques like fMRI, Magnetic Encephalography (MEG) or Electrocorticogram (ECoG): first of all, it is indeed a relatively cheap and portable device that every clinics owns and that could also be brought outside the hospital or the laboratory for continuing tests and experiments at patient's home with much longer monitoring time and/or training effects. Moreover, it is a completely non-invasive method that prevents people to be implanted with microelectrodes placed inside the scalp over the cerebral cortex (as in the ECoG case) to monitor specific neurophysiological activities. Finally, despite of its poor spatial resolution (fMRI and MEG overcomes it in this case), EEG can offer a very high temporal resolution on the order of milliseconds.

The previous mentioned advantages make this device probably the best candidate for real-time and portable health-care and rehabilitative applications in a near future.

## 2.1.2 Rhythms

EEG actually contained a lot of information regarding individual's health conditions, intentions, external and internal stimuli reactions, drowsiness, emotions and so on.

Mainly the most physiological information is carried by the so-called *rhythms*. EEG is indeed, as mentioned above, a combination of periodical signals originated from the synchronous behaviour of some neural mass [26] inside the brain and a large variety of signals coming from both inside and outside it, gathered by the EEG but not useful for the purposes of determine the physiological status of the subject. For this reason the latter are considered as disturbing phenomena and briefly labelled as *noise*.

Therefore rhythms is the term coined to indicate the oscillatory components belonging to a specific frequency band that is usually associated with the prevalence of a particular condition. Specifically, five standard most common rhythms were defined for clinical scopes and will be presented here:

- DELTA ( $\delta$ ) Ranging from 0.5 Hz to 3.5 Hz is the typical rhythm of the infants and which occur during deep sleep and in some organic brain disease (like persistent vegetative state) in a diffuse spatial distribution.
- THETA ( $\theta$ ) They are rhythms in the (4,7.5) Hz band associated with drowsiness and the earlier stages of life till the young adulthood. Waking normal adults show only small amount of this kind of rhythm, although theta were found to correlate with frustration and hedonic responses along with mental activity (mainly observed on the frontal mid-line).

- ALPHA ( $\alpha$ ) The International Federation of Societies for Electroencephalography and Clinical Neurophysiology (IFSECN) proposed in 1974 [41] the following definition of alpha rhythms:  
*Rhythm at 8-13 Hz occurring during wakefulness over the posterior regions of the head, generally higher voltage over the occipital areas. Amplitude is variable but is mostly below  $50\mu V$  in adults. Best seen with eyes closed and under conditions of physical relaxation and relative mental activity. Blocked or attenuated by attention, especially visual and mental effort. (IFSECN, 1974)*
- BETA ( $\beta$ ) Any rhythmical activity above 13 Hz and below 35 Hz may be regarded as beta activity. Usually non exceeding  $30\mu V$ , it can be found in almost every healthy adult over the frontal and central regions. It is of interest for the kind of application presented in the following that a central  $\beta$  activity is related to the movement and can be *blocked* by motor actions and tactile stimulation.
- GAMMA ( $\gamma$ ) Ranging between 35 Hz and 100 Hz,  $\gamma$  rhythms were found to be involved in higher mental activity including perception, problem solving, fear and consciousness.

Fig.2.3 shows an example of rhythms subdivision of a real EEG of a healthy adult.

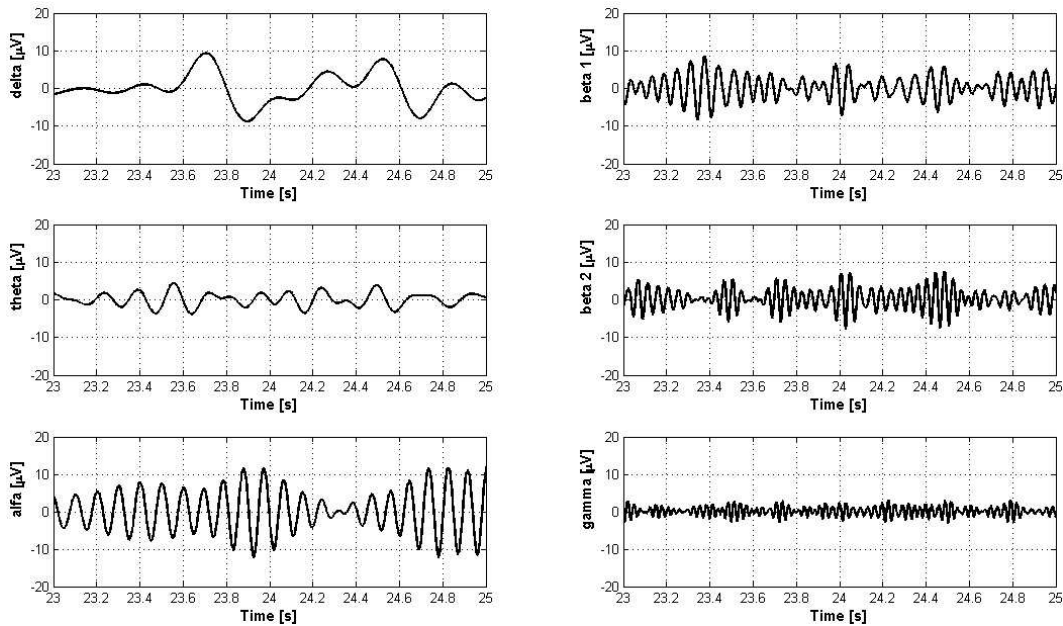


Figure 2.3: An example of cerebral rhythms.

A further class of oscillations has to be mentioned here: the Sensorimotor Rhythms (SMR) [42] [43] [44]. Two main components can be distinguished within this class, the MU ( $\mu$ ) rhythms and the lower  $\beta$  ones (as mentioned in the  $\beta$  rhythms definition). Although occurring in the same  $\alpha$  frequency band,  $\mu$  rhythms can be acquired over the sensorimotor area of the brain. Moreover, it is considered the sign of the movement

because its amplitude significantly decreases when a movement or even its imagination, observation or planning, is accomplished. This phenomenon is known as Movement-Related Desynchronization (MRD) and it will be further taken into consideration in the next Chapters.

This brings to highlight the important notion that a rhythm can not be completely defined by its frequency distribution and sometimes neither by the further spatial distribution over the scalp. The term rhythm, actually, means a more precise concept of electro-physiological phenomenon occurring in relation to a precise condition of the subject along with a specific frequency and spatial distribution.

Moreover, although international societies of EEG defined standard frequency ranges and occurrences to recognize the different rhythms, experience tells that no strict distinctions can be stated but subject-to subject studies have to be carried on. Indeed both inter-individuals and intra-individual differences were observed in literature. Among others, state of vigilance, age, gender, body temperature as well as different emotional states are common factors that can modify rhythms behaviour.

In this context, technology and signal processing techniques for cerebral activity identification and quantification have promised to bring electroencephalography much further the clinicians' experience based on by-eye expertise. Indeed, with an automatic recognition of individual frequency bands and their adaptation throughout every recording condition, diagnosis, prognosis and rehabilitation could be much more reliable and effective because individual-centred.

## 2.2 Brain Computer Interface (BCI)

### 2.2.1 Background and Applications

BCI or Human Machine Interface (HMI) systems were born at the end of the 70s to answer the increasing need for an advanced technology for the alternative communication of people who suffered from tetraplegia, Spinal Cord Injury (SCI), ALS or other traumatic cerebrovascular lesions that compromised their motor system forever. Such complete paralysed people, indeed, can not communicate with the external world through the standard physiological vias, anymore. In most cases, however, they remain with their cognitive functions completely intact.

If on one hand, this makes them experience the dramatic condition of being prisoner of their own body as Jean-Dominique Bauby wrote in his "*The diving-bell and the butterfly*", on the other side this could be also the key to help those kinds of patients in regaining a quasi-normal life thanks to technology.

Jacques Vidal, the BCI pioneer and its world-wide recognised father, in 1973 for the first time proved the feasibility to detect brain signals in real-time and use them to control the movement of a cursor on a computer screen [45]. Ten years later, in 1988, Farwell and Donchin implemented a P300 BCI system [46] that could be trained and used to write up to 2.3 characters per minute: that was the first example of the nowadays well-known as *P300 Speller* platform.

But the first claimed success in the BCI community was reached by Niels Birbaumer and his team in 1999 [47] [48] when in Tubingen they recruited for a BCI test two patients - called *Subject A* and *Subject B* suffered from a locked-in syndrome of an ALS disease.

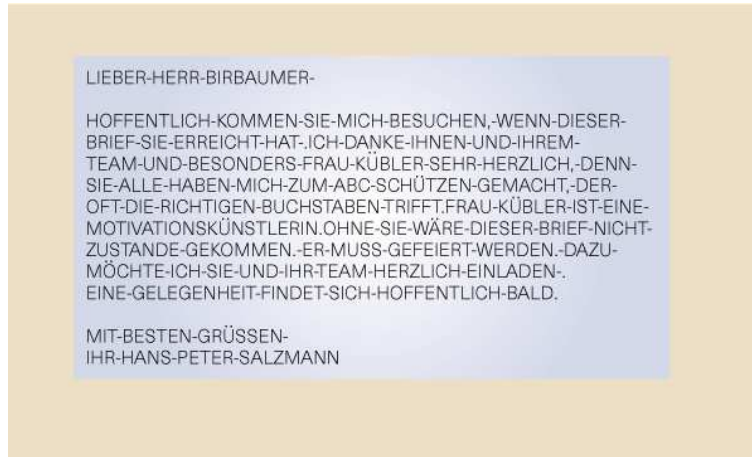


Figure 2.4: The first message from Subject A (extracted from [47]).

Both subjects were trained at a BCI system operating by means of the Slow Cortical Potentials (SCPs). After a number of different sessions both the subjects achieved such a high level of performance that they could easily use an electronic spelling device to write. Famous has remained the first full message of Subject A to professor Birbaumer reported in Fig.2.4 in which he warmly thanked the research team for the help they provided him.

Despite of the highly significant historical value of this step in the advancement of medicine, this kind of systems did not become a gold standard for the health-care of this severe impairments, anyway. This was mostly due to some consistent disadvantages affected such systems: actually, not much higher than the 2 words/min rate of the first Subject A's message has been reached yet; moreover, long training periods are still required to satisfactory using the P300 speller or other similar devices.

Since no further progresses were achieved, in the recent decades the focus of the BCI community moved from the alternative communication targeting complete paralysed people towards the motor rehabilitation of severe impaired patients suffered from stroke, spinal cord injury and tetraplegia [49] [50] [51].

The most common approach is to employ a robotic arm or a prosthesis controlled by the cerebral activity of the patients and recover his/her ability to grasp, reach and hold objects by means of such a technological help. Successful results in this field were recently achieved all over the world: firstly, Hochberg and collaborators at the Donoughe's Laboratory at Brown University, Providence, USA in 2012 made a tetraplegic woman to use a robotic arm to autonomously drink from a can placed over the table in front of her wheelchair [52]. Secondly, in 2013 Collinger and colleagues at the Schwartz's Lab in Pittsburgh, USA found high performance in the 3D movements of a robotic arm neurally controlled by a tetraplegic woman that had been operating the system for only two days [53].

Although these two results opened the frontiers of the rehabilitative medicine, a further step has not been accomplished yet: the passage from the invasive setup exploiting an ECoG (as in the case of Providence and Pittsburgh) to a totally non invasive platform based on EEG, MEG or other recording methods that collect data from the subject's scalp without any surgical intervention for electrodes implantation.

Therefore, there were implemented several other non invasive BCI applications that reached good performance, even if not as high as in the two cases presented before: works of Millan’s group at EPFL of Losanne, Switzerland [54], Pfurtscheller’s laboratory at the Technical University of Graz, Austria [55], and the laboratory of Birbaumer in Tubingen, Germany [56] represent the most famous and successful examples. They implemented telemonitoring and telepresence neurally-guided robots, BCIs for web browsing, P300 speller devices, virtual reality BCI controlled navigations environments and many others.

Although they all represent successful prototypes of feasible BCI systems, some weak points have already to be addressed: above all, it has to be observed that BCI is still mostly confined to the experimental laboratory, being the devices too expensive and the training not possible without the assistance of people with quite large expertise. Secondly, output commands are usually given on a discrete scale, even in a binary mode, while an ideal supportive tool should operate in a continuous way miming a more natural behaviour. Similarly, turning on and off the machine should always shifted from the caregiver control to the complete user responsibility, providing him/her the total independence they need in their life.

Besides that, the above mentioned groups are leaders in another field of research of BCI technology applied to rehabilitation: robotic-assisted motor recovery.

To this purpose, system to train grasping [57] and reaching [58] functions were realized and tested on different groups of patients. Several kinds of platforms have been already suggested for motor rehabilitation of the hand and the arm: FES-BCIs and BCI driven by the combination of EEG and EMG are two of the most common recently investigated systems [59].

## 2.2.2 Principles and Setups

Despite of the particular kind of recording method or final output, a BCI system always exploits two already introduced principles of neuroplasticity and operant-conditioning. This section will give a more extensive explanation of them and, in the second part, the typical BCI setup will be shown along with the description of several categories of BCIs.

**Basic Principles** The ability of the brain to adapt its functionalities to altered internal or external conditions was so far referred as brain plasticity or neuro-plasticity [4]. This is, for example, the main actor during the developmental period in which a baby begins to discover the world and his/her knowledge about it continuously changes. Newborns and young children have indeed to adapt themselves to life time by time, e.g. new environments, people’s reaction to their behaviours and so on. Neuroplasticity has, therefore, a major role in the learning process. Unfortunately, it has to be mentioned that this same powerful property of the brain can have some negative drawbacks: plasticity and adaptability can bring the brain to be over excited. This is the case, for example, of the focal dystonia of the hand in the so-called *writer’s* and *musician’s cramps* where a continuous repetition of the same gestures, postures or both, e.g. write or play, can lead to an abnormal overflow muscles activation [60]. This brings people who suffered from this kind of disease to the impairment of that gesture or posture. But, in the case of stroke recovery, neuroplasticity acts in its positive way and has to be strengthen: in fact, when a stroke event occurs, neurons in that area can’t work anymore and functions

like the motor and the cognitive ones become impaired. Nowadays it is well-known that immediately after the injury a spontaneous process of recovery begins and lasts for three months at least [18]. It allows brain to regain or to delegate compromised functions to other areas of the brain.

Neurophysiological researches on animal models of stroke have revealed indeed that, after a cerebral infarct, a change in the brain architecture takes place along with promising phenomena like neural sprouting, dendritic branching and synapto-genesis [14] [15] [16] [17] as already mentioned. It is also known from literature that motor training and physical exercises promote those kinds of neural changes: thus, recovery is suspected to be a complex combination between spontaneous and learning-dependent processes [61].

Therefore, generally rehabilitation programs include several activities such as occupational therapy, VR training and many others, besides the standard physical therapy, manipulations by clinicians and pharmacological treatments (see also 1.2 [2][18]). Particularly, when an individual suffers from a stroke he/she loses functions like grasping, reaching and holding. These basic abilities are products of a very ancient experience-training performed in the early stages of the youth, during an intense learning period. Then, the aim of a rehabilitation program is to induce patients to re-learn such functions without the usual neural resources exploited in the past of their life. Thus, two basic strategies can be employed to induce such a learning or re-learning mechanism: the *classical* and the *operant conditioning*.

On one hand classical conditioning [62] is a way to learn that occurs when a conditioned stimulus is paired with an unconditioned stimulus that causes an organism to exhibit an automatic unconditioned response to the unconditioned stimulus. After pairing is repeated the organism exhibits the unconditioned response as a reaction to the conditioned stimulus when presented alone. On the other hand, the operant-conditioning strategy requires the subject to perform an active behaviour following an external stimulus depending by that behaviour itself. Subsequently, he/she receives either a reward or a punishment for either a correct or a wrong response of the subject, respectively [63] [64] [7] [65]. Therefore, a loop is created and, repeating many times the same task, the subject should learn to correctly accomplish it in a more effective way and in a shorter time.

In this specific case, as reported in [49] and [67] and as it will be recalled in section 3.1, the operant learning strategy is employed in order to strictly and contingently relate the cerebral activity of the patient with his/her motor behaviour. Specifically, while he/she is performing a reaching movement, a feedback of his/her neural activity is provided and, if this agrees with the study hypothesis, he/she receives also a force feedback that helps him/her in completing the movement. Repeating this exercise several times, the learning process takes place.

In this way, the modification of the neural activity becomes an alternative tool for controlling the impaired reaching ability bypassing the damaged brain area.

**Typical Setup** Since its origin in the late 70s, BCI was defined and implemented as any other communication or control system with an input, signal processing and a translation algorithm that transforms the input in the output signals. Fig.2.5 extrapolated from [1] shows a schematic block diagram that illustrates how a typical BCI works.

Therefore a typical BCI platform is made by:

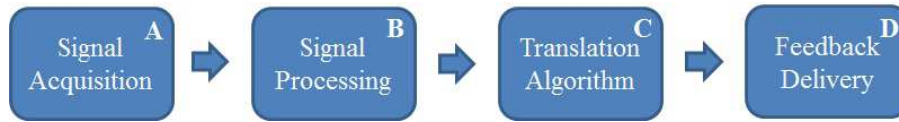


Figure 2.5: The typical BCI scheme.

- a signal acquisition unit;
- a signal processor;
- an output device.

In particular, electrophysiological signals of the subject performing the experiment are acquired, amplified and digitized in the first block.

Two main classes of BCI can be distinguished in dependence on the acquisition method and the kind of neurophysiological activity produced or modulated by the user: as already cited, they can be either *invasive* or *non-invasive*; moreover they can exploit *evoked* or *spontaneous* activity of the brain. In an invasive BCI signals are acquired inside brain either on the cerebral cortex by means of an ECoG or even deeper inside it among a neural population measuring the LFPs of a group of neurons or the firing rate of single neurons. Non invasive methods, instead, prevent the subject to undergo any surgical intervention of electrodes implantation like in the invasive case and gather, on the contrary, neurophysiological information from the scalp of the subject by means of either the EEG, the MEG, or by other methods like fMRI and Functional Near Infrared Spectroscopy (fNIRS) applied from outside the brain [68].

In case of EEG employment, different types of activity can be decoded and used to control the BCI system. Specifically, Evoked-Related Potentials (ERPs) consist in short waveforms (lasting less than 1 second) that appear after a cognitive stimulus to be recognized. This is the case of the so-called (and already mentioned) P300, a positive peak rising around 300 ms (see Fig.2.6) after such a stimulus (presented among many meaningless others)[46][69].

On the other side, spontaneous oscillations can be also detected and quantified (not only in EEG but also in MEG recordings) by the BCI system during their voluntary modulation operated by the subject. The most common rhythmical activity (see Fig.2.7) used in BCI are the SMR recorded from the sensorimotor areas [26] [11] [9] of brain where movement and somatosensory information are usually processed [44] [1] as explained in 1.1 and 2.1.

A similar phenomenon named as SCPs can be acquired from the fronto-central areas of the scalp and can be also modulated by a subject controlling the movement of a cursor on a screen. Different time-domain waveforms (see Fig.2.8) are associated with different cursor motion directions [1].

A further distinction can be made about the physiological information that is put in charge of the BCI control: there exists a *dependent* and an *independent* operation way. The clearest description of such two classes was provided by Wolpaw and collaborators in 2002 [1]: "A *dependent BCI* does not use the brain's normal output pathways to carry the message, but activity in these pathways is needed to generate the brain activity (e.g.

### P300 Evoked potential

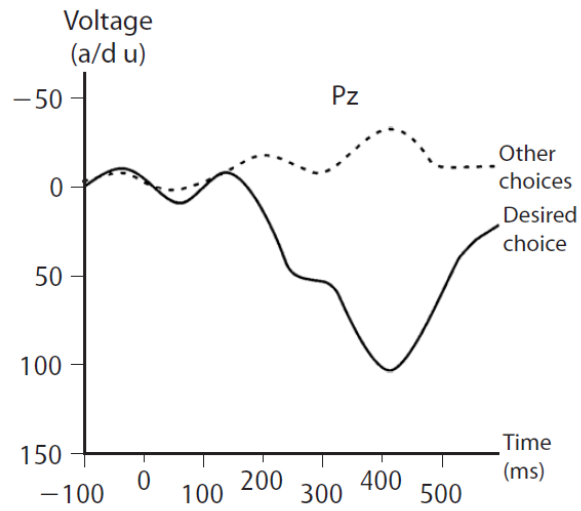


Figure 2.6: P300 Evoked Potential (extracted from [1]).

### Sensorimotor rhythms

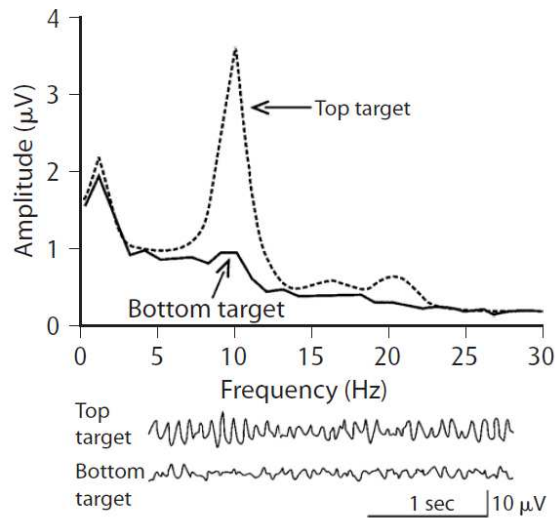


Figure 2.7: Sensorimotor Rhythms (extracted from [1]).

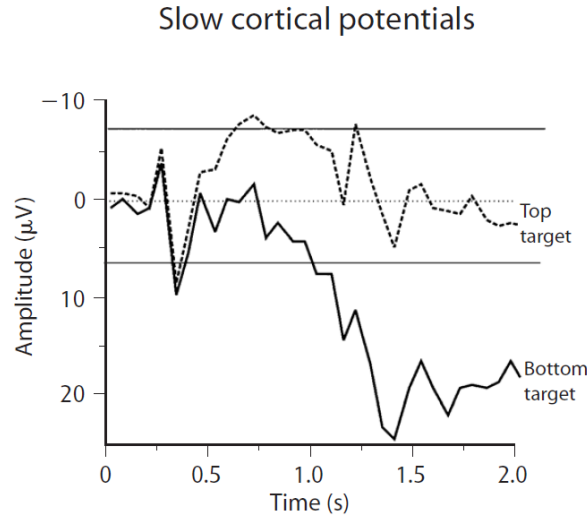


Figure 2.8: Slow Cortical Potential (extracted from [1]).

*EEG) that does carry it*"; while an *"independent BCI does not depend in any way on the brain's normal output pathways. [...] (It) provide(s) the brain with wholly new output pathways"*. As an example, in case the Visual Evoked Potentials (VEPs) are employed they are produced by a flashed letter on a matrix containing the whole alphabet, The generation of VEPs within the brain depends on the gaze direction and, consequently, on *"extra-ocular muscles and cranial nerves that activate them"*. This is the most common case of dependent BCI. On the contrary, when a P300 is elicited by the subject during (purely cognitive) identification of the meaningful stimulus among many others, the information about the supporting cognitive processes is carried only in the brain and does not depend on any other communication pathway. Therefore, such a BCI can be viewed as independent.

The second step of a typical BCI is the signal processing one. This could be subdivided into two further operations: (a) the feature extraction and (b) the translation phase.

Features extraction procedure includes spatial and temporal filtering, voltage amplitudes measurements, spectral analysis, single-neuron separation or a combination of some of them, and aims at identifying the encoded user's intentions or commands.

Afterwards a translation algorithm transforms the signal features (independent variables of the system) into proper device control commands (dependent variables).

It depends on both the output device and the specific application, and it could operate by means of either linear or non linear transformations.

Furthermore, the most important characteristic that has to be embedded at this step is *adaptability*. As far as BCI is a loop in which two agents, i.e. the subject's brain and the computer, have to continuously change their behaviour in dependence on each other, three levels of adaptability have to be implemented:

1. an initial adaptation of the computer to the neurophysiological characteristics (e.g. bandwidth of SMR, amplitude of P300, ...) of the new subject operating the system;

2. a periodical online adjustment that accounts for spontaneous short and long-term variations of cerebral activity due to environmental properties or subject's conditions (illness, awareness, drowsiness,...)
3. user's development of higher skills in controlling the BCI has to be recognized and encouraged to enhance efficiency of this new form of communication.

The third and last BCI step is the output device. In most cases this is represented by a computer screen showing a cursor moving towards a predefined target or a set of letters or icons to select. In the recent years prosthesis, orthosis, haptics and other robotic devices replaced or were added to the more commonly used screen to give the users a richer feedback of their performance or to provide them a useful artificial tool for accomplishing simple actions of their daily life.

# Chapter 3

## An Example of EEG based BCI Platform for Stroke Motor Recovery

This Chapter provides an example of EEG based BCI platform in the rehabilitation field and, at the same time, it represents the background that gave reason to this Ph.D. work. The detailed description of this particular system reported in this Chapter will clarify, indeed, the need of that specific and carefully designed signal processing that was the major topic of this work and that will be presented in Chapter 4 and discussed in Chapter 5. Specifically, the Chapter deals with the exposition of all the features characterizing the EEG based-BCI platform implemented at IRCCS San Camillo Hospital Foundation at Lido of Venice for the recovery of the reaching function of mildly impaired stroke patients hospitalized at the Institute. The Chapter will open with the description of the clinical case to treat and the neurophysiological assumptions of the experiment along with the thesis that was expected to be proved by the end of the study. Moreover, a protocol was established to state all the specifications of the experimental setup and course in order to scientifically prove the experimental thesis from the hypothesis. The hypothesis and the main goal of the study will then be reported, along with the measures and performance evaluations to assess the effectiveness of the system. Finally, the last section will highlight the principal strong points of the study as well as the improvements that were required in order to make the platform more effective for the patients. Those improvements, indeed or at least partially, were deeply investigated and implemented through the design of algorithms and Matlab routines and represent the core of the two following Chapters.

### 3.1 Study Protocol and Participants

**Experimental thesis** As previously mentioned in the introduction and in section 2.2, the contingency between a *correct* cerebral activity and a *good* motor output is of fundamental importance in the realization of an operant-conditioning scheme aiming at making stroke patients to relearn partially or totally lost motor functions.

The experimental thesis established, based on literature exposed in the previous Chapters, that a proprioceptive and contingent feedback controlled by the voluntary and continuous modulation of the injured area's SMR produced by the subject performing a reaching movement can properly act as the *reward* mentioned in section 2.2. After several repetitions of the exercise that reward would create the conditioned association of

the subject's expected cerebral activity, i.e. the contralateral SMR modifications, with the reaching movement, i.e. the motor output, preventing in such a way the subject's brain to arbitrary reallocate that motor function in another less effort-demanding but maybe also less useful area, thus promoting a more effective, faster and longer lasting recovery beneficial effects comparing with a spontaneous process of cerebral adaptation to the new injured condition. The experimental thesis was based also on the key and well-known hypothesis that every subject, even a stroke patient, is able - after proper training implementing an operant-learning strategy - to modulate their SMR.

However, to prove the experimental thesis proposed so far, a detailed and suitable protocol was designed and is going to be described in the following.

**Inclusion and exclusion criteria** It preliminarily required to include in the study only patients with some residual motor abilities, as far as the feedback acts as a helping reward to complete the reaching task, not to initiate it. Moreover, since a more severe impairment can be expected to come with a larger injured brain area, a mild impairment would assure the existence of some still healthy sensorimotor path that could be put in charge of the motor control of the limb during the course of the experiment. The only exclusion criterion required to discard from the study patients with cognitive deficits, because of the major need to be absolutely confident about the subjects' comprehension of the experimental task. Actually, the platform could be potentially used also by individuals affected by other cerebrovascular diseases with mild impairments in their upper limbs even though not originated from a stroke injury. Nevertheless, the choice to involve only stroke survivors in the study can be explained by the fact that in case of chronic condition after stroke, neuroplastic changes that can be largely exploited by any rehabilitation technique had been already worldwide observed.

The above mentioned strict inclusion criteria limited, as a consequence, the number of recruited subjects: indeed, usually more severe patients are admitted to San Camillo Hospital for a long period, while mild motor impaired ones are administered by some therapies for a shorter period or not even come to the Institute preferring to attend some physiotherapeutic sessions by their own in their home towns.

**Participants** Then, four only stroke patients were admitted to this BCI protocol till now and their description will be reported in the while. They all had been hospitalized at the IRCCS San Camillo at the moment of their participation into the study. This means that they were following a rehabilitation program - for the upper affected limbs, specifically - that included typical treatments like manipulations, physical and occupational therapies.

Fig.3.1 and Fig.3.2 report the characteristics of the four patients recruited in the period 2011-2013 at the Institute for the BCI protocol with their clinical evaluations at the admission time.

Clinical evaluations were performed by a physical therapist at the beginning of the treatment as well as at its end to assess any clinical improvement. A battery of six tests were administered to each patient to evaluate both the general and the more task-specific abilities of the patient in moving his/her upper limbs.

Therefore the Functional Independence Measure (FIM) (maximum score: 126), the Fugl-Meyer Assessment for the Upper Extremity (FMA-UE) (maximum score: 66), the

	Age	Gender	No.Ses.	Type	Damaged Arm
P1	26	F	all	all	right
P2	47	M	all	all	left
P3	58	M	all	all	right
P4	28	M	3	screening	left

Figure 3.1: Stroke subjects data.

	FIM	FMA-UE	BBT	RS	NHPT	MAS
P1	/	40/66	/	21/36	5p/50"	4
P2	126/126	66/66	41	36/36	19'94"	0
P3	126/126	64/66	40	36/36	20'21"	0
P4	126/126	66/66	/	36/36	16'	0

Figure 3.2: Clinical evaluations of the patients.

Modified Ashworth Scale (MAS) (best score: 0), the Nine Hole Peg Test (NHPT) (measured in seconds), the Box and Blocks Test (BBT) (measured in number of cubes/min) and the Reaching Score (RS) (maximum score: 36) were performed and provide the clinical assessment of their impairment.

In particular, patient n.1 (P1) was a 25-years old woman who suffered from an arteriovascular malformation (AVM) that caused her bleeding (that can be assimilated in this context to a hemorrhagic stroke) when she was 16. She underwent a surgical intervention, but six years later the edema in the peri-lesional area led her to a right-sided moderate hemiplegia. Admitted at San Camillo, she underwent a rehabilitative program that covered a wide range of treatments, from the more traditional (see section 1.2) to more innovative ones including the use of the VR, an haptic device for the hand motricity rehabilitation and the whole BCI-Phantom protocol.

Patient n.2 (P2) was a 47-years old man who was injured by a right-sided capsular ischemic stroke in 2009 when he was 44. Admitted at the S. Camillo Hospital in 2012; his rehabilitation period at the Institute consisted almost exclusively of this new BCI protocol that he completely performed. Besides that, he only underwent standard physical therapy. His mild upper limb disabilities do not prevent him from performing all daily life activities without any difficulty and, as a consequence, he achieved the maximum score at all the clinical assessments.

Patient n.3 (P3) was a 58-years old man who survived after a subcortical left-sided parietal ischemic stroke occurred in 2011 when he was 57. As in the case of P2 he was left with a mild motor impairment in his right-hand side. Such a disability did not limit him in accomplishing to his normal daily life. Moreover, as the previous patients he attended the whole BCI protocol along with other rehabilitative therapies during his hospitalization period.

Finally, patient n.4 (P4) was a 28-years old man suffered from a AVM similarly to P1. In 2009, when he was 24, a fronto-parietal bleeding in the right-hand side hemisphere caused him a mild left-sided hemiplegia that impedes him in controlling upper limb precise motor functions. P4, differently from the other patients, attended the only screening

phase: that singular session was scheduled with the solely purpose to gather new data to test the software advancements made in the previous months.

For the sake of completeness it can be said that all the patients signed an informed consent which established the experimental guidelines, goals, risks (no one, except for eventual uselessness) and expected benefits in accordance with the Declaration of Helsinki. Furthermore, the experimental protocol received approval by the Ethical Committee of the IRCCS before to be actually tested on any patient.

Furthermore, for a standard and complete analysis of results of P1 see [66], whereas for a preliminary explanation of the findings about P2 read [67].

As far as the experimental main variable was represented by the proprioceptive (force) feedback delivered by an haptic device, two experimental groups of patients are needed to verify the assumption of the study and to exclude that kinematic and functional improvements were simply due to the training effects caused by the repetitiveness of the task (as realized in [58]). Specifically, the first group - which includes P2 as the very first subject - experiences an helping robotic feedback while the second group - with P3 as first subject - receives a fake feedback, completely random, not related to the cerebral activity.

Patients recruitment is still currently in progress because a number of about twenty patients per group has to be reached in order to assess the statistically significance of the experimental thesis.

Coming back to the protocol description, patients were asked to performed a very standard task and to repeat it several times along a period of three weeks with each trial of reaching scheduled by a precise timing sequence. In the next paragraph the structure of a single trial and of the whole experiment course will be presented.

**Study design** Specifically, the required task was a standard 2D centre-out reaching one (as can be seen from Fig.3.3) performed with the patient sit on a comfortable armchair in front of a 1 meter-distant screen showing the interface of the experiment. One out of four targets at the four cardinal point locations was randomly presented on the screen with an inter-stimulus period of about 5 seconds.

Each reaching trial had, as mentioned before, a very detailed structure, as provided by Fig.3.4: it started with a 500 ms (*pre-trigger time*) blank screen following by the target appearance and a simultaneous cue sound. After a 1500 ms (*post-trigger time*) another sound was heard and the patient was allowed to move towards the target. Usually a reaction time of about 500 ms was recorded and a variable period of time between 400 and 800 ms had to be waited until the patient had completed the task (*movement period*). If he/she reached the target in the (500, 740) ms interval of time, the target *exploded* on the screen; otherwise, too slow movements led the target to be depicted of blue while too fast ones made the target become red. A *post-movement time* was necessary to return with the arm at the plane centre and with the cursor at the initial point on the screen. This completed the trial.

A series of 80 trials were repeated in each run (see Fig.3.5) with an equal occurrence of each target (20 per type). Moreover an initial rest period of 40 seconds was waited by the subject in a relaxed way.

On one-day test a session made by three runs was performed by the patient with the healthy arm and another with the damaged one.

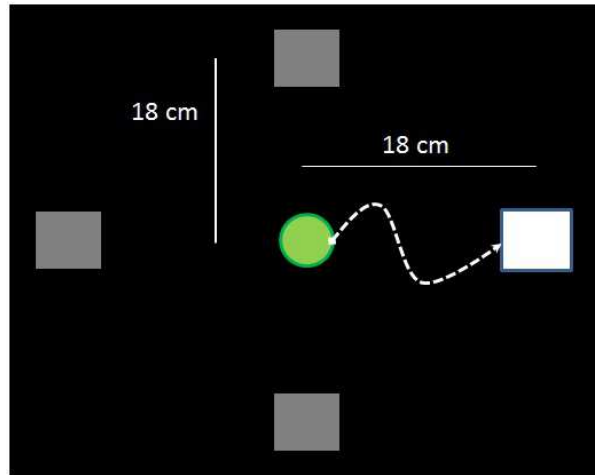


Figure 3.3: Standard 2D reaching task.

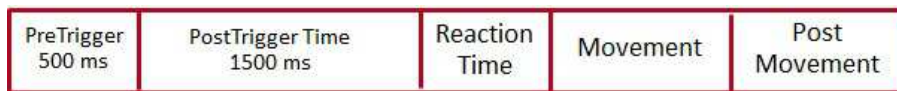


Figure 3.4: Single trial structure.

The overall study protocol is represented in Fig.3.6 and it was scheduled with a first screening session where the patient was evaluated by means of the afore presented standardized clinical scales and he/she performed a BCI session per arm without any help by the robot. At this stage a set of EEG features were chosen to be associated with the movement: a frequency band around 10 Hz and two electrodes were then selected for this purpose. Then, the patient underwent the actual BCI training with the force feedback related to the selected features given as an help to complete the reaching movement while he/she was learning to modulate the SMR of the cerebral area surrounding the damaged one. After such a two weeks training period, an end test session -identical to the screening one- was finally scheduled in order to obtain a final evaluation of the performance of the subject after the BCI treatment.

## 3.2 System Description

According to the general BCI scheme and as anticipated above, the experimental setup for this study was made of three main blocks: the acquisition unit, the signal processor and the feedback module. A further detailed representation is shown in Fig.3.7.

It has to be said that in this context the technical features of the specific BCI system operating at San Camillo Hospital are reported to allow any other research group to repeat the same identical experiment. Nevertheless, it has not to be excluded that an alternative system implementation based on literature and further experience can bring to similar results.

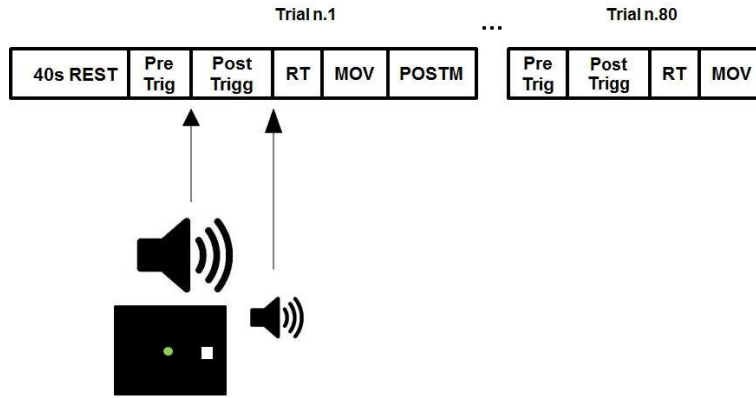


Figure 3.5: Single run structure.

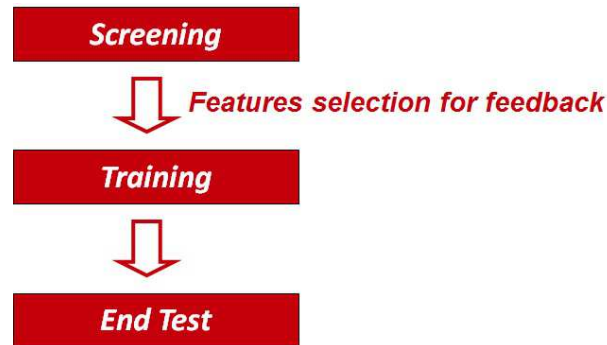


Figure 3.6: Different sessions of the experimental protocol.

1. *Acquisition unit.* The signal acquisition unit included an EEG cap provided with 29 recording Ag/AgCl electrodes in a modified 10-10 system arrangement and a 16 channels g.TEC amplifier g.USBamp version 3.09a[70].

Then the available EEG sensors were placed on the sensorimotor areas, e. g. primary motor cortex, primary somatosensory cortex and the associative somatosensory cortex: Fz, F3, F4, Fc5, Fc1, Fc6, C3, Cz, C4, Cp5, Cp1, Cp2, Cp6, P3 and P4 were selected (see Fig.3.8). Each of them was referred to the right ear lobe, whereas Poz channel (a site between P3 and P4) was chosen as ground. During the experiment, signals from the sixteen derivations were digitized by means of sixteen 24 bit Analog-to-Digital Converter (ADC)s at a sampling rate of 512 Hz. Then a Digital Signal Processor (DSP) applied a band pass filter between 0.1 and 60 Hz and a notch filter at 50 Hz to the data. Finally, the output amplified and digitized EEG signals are sent via USB connection to the processing unit.

2. *Signal processing module.* The platform adopted for the signal processing at this stage is BCI2000, a world widespread software implemented by Schalk and colleagues in 2004 [71].



Figure 3.7: Experimental setup.

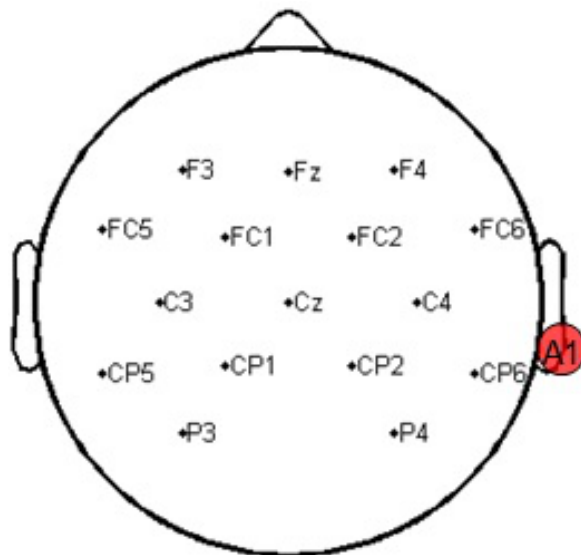


Figure 3.8: EEG Channels location.

Since the role of this module was to continuously quantify the MRD occurring during the movement, the spectral power decrease in the selected (11, 14) Hz band of the chosen two electrodes had to be computed in real-time. The latter was estimated by means of the Maximum Entropy Method (MEM) algorithm and a 500 ms sliding window that shifted by a 4 samples step along all the EEG trace. Then the results were linearly combined and the overall outcome was normalized on the spectral power of the baseline (initial rest).

This final quantity is called Neurofeedback (NFB) and can be viewed as a measure of the MRD phenomenon: the higher the NFB, the stronger the MRD and, thus, the stronger the assistive force feedback provided to the subject (during the training period). Actually, at each time sample, the target-directed force was delivered only if the correspondent NFB value exceeded a minimum threshold in order to ensure an effective MRD-BCI control. Otherwise no force assistance was given. Anyway, when feedback was present, its magnitude was computed through a linear positive coefficient applied to the thresholded NFB (Actually, relationship between NFB and the feedback force is *almost* linear because of some factors added to provide a smooth growth and decrease of the force, in order to avoid abrupt changes in the feedback that would be annoying and useless for the rehabilitation purposes).

Furthermore, the proportionality factor was conveniently chosen to guarantee a maximum force feedback of 6 N with the aim to avoid excessively large forces that could be misunderstood by the afferent nervous system of the participant making him/her uncertain if the robot was helping or obstructing him/her in the task accomplishment.

Finally, an UDP communication protocol allowed the signal processing unit to transmit the final modified NFB value to the feedback block.

3. *Feedback block.* At this stage such a modified NFB value - updated every 8 ms - was used to provide the contingent assisted target-directed force to the patient performing the task. This was accomplished through a robotic arm device called Phantom (PHANTOM, Premium 3.0/6 DOF Sensable Technologies)[72]. In the same time, the feedback block was continuously sending the task execution status to the previous unit thus enabling it to synchronize the EEG recordings with the experiment course. This scheme is strictly necessary to effectively control the BCI system and to correlate, in the following offline analysis, the neurophysiological data with the kinematic performance. Indeed, the Phantom device could record the end-effector real-time trajectory and instantaneous speed with a sampling rate of 100 Hz. Other kinematic parameters as trial duration, mean speed and displacement from an ideal straight path connecting the starting point and the target, were also computed and used offline as measures of motor performance. In particular, the displacement was calculated both as the maximum distance from the ideal trajectory (*orthogonal error*) and as the area between the straight and the actual walk (*area error*). The moment these kinematic data were collected during the experiment, they were analysed along with the EEG samples in order to assess the effectiveness of the BCI treatment.

Some of the parameters implemented in this system could be finally set after pre-

	Age	Gender	No.Ses.	Type
H1	31	M	3+12	Screening + Training
H2	34	M	9	Screening (only right arm)
H3	26	M	6	Screening

Figure 3.9: Healthy subject data.

liminary tests performed over few healthy subjects. For example, as mentioned in [49], initially the reaching path was set to 10 cm, a too low value that led participants not to completely develop the MRD within the limited time of the task accomplishment. In the following, the path was lengthen to 18 cm thus. Besides that, feedback force was delivered in an abrupt way, simply and roughly following the NFB (i.e. the MRD on the EEG) course. Subsequently, the Fitts' law[73] was employed to compute the most suitable time interval to include the reaction time, living all the rest of the movement time to the MRD actual development. For the sake of completeness, in the following Fig.3.9 reports a brief description of the healthy participants involved in the experiment.

As it can be noted, no one of the them performed the whole BCI protocol, but the only screening session along with some training runs for suitably setting up the force feedback. On the contrary, as stated above, the investigation about the improvement of the performance due to the proprioceptive feedback was not considered for the healthy subjects.

### 3.3 Performance Evaluation

Improvement due to BCI training were quantified by comparing clinical, kinematic and neurophysiological outcomes respectively provided by the clinical assessments administered to the patients by the physical therapists, by the tracking of the robotic arm movement through the Phantom device and by the EEG measurements and their offline analysis.

Usually, the treatment efficacy was evaluated at the end of the BCI training by comparing the aforementioned three classes of measurements obtained in the end-test session in regard to the initial screening session.

It has to be noted here that as far as only mild to moderate patients could be involved in the study and since the sensitivity of clinical scales is satisfactory only for severely impaired subjects or in case of large improvements, the difference of the tests scores did not significantly differ between the initial and the final phase of the study, at least for the last three subjects. They were, indeed, really mild impaired cases but P1 showed a visible improvement of the clinical scores because she presented a moderate dysfunction of the motor system (see [66]). For the remaining patients only kinematic and neurophysiological assessments gave significant findings about the effectiveness of the BCI system.

**Kinematic Measures** In addition to the clinical outcomes, from the movement kinematics recorded during all the sessions, both those with the haptic feedback and those without any robotic help, a series of measurements were gathered. The latter can be subdivided in three categories:

- The *general motor behaviour* category takes into account how many times the subject successfully completed the task all over the three runs of a session and, on the contrary, the number of too slow or too fast movements he/she produced.
- A second group of measures includes reaction time, duration and mean speed characteristics, giving an idea of the *rough arm control* during the task course.
- Features like orthogonal displacement, area error and speed peak can finally quantify improvements in the *finer control* and accuracy of the reaching movement, and provide a more robust indication of the quality of the patient's motion.

Statistical significance was generally tested through a Wilcoxon rank sum test except for the correct number of trials (as well as its percentage) and the number of the slow ones that were evaluated by a Kruskal-Wallis test.

**Neurophysiological Outcomes** Finally, EEG signals provided features that distinguish the different phases of a single trial: specifically, as mentioned above, the MRD of the SMR  $\mu$  and lower  $\beta$  was expected to occur - especially in the contralateral sensorimotor cortex - during the movement and even before it, during its preparation - in the post-trigger time - when the subject saw the target to reach but he/she was not allowed to move toward it, yet.

Desynchronization occurring in such a situation is a measure of the *reactivity* i.e. rapidity and entity of modification of the EEG sensorimotor rhythms in relation to altered conditions of stimulation: in this specific case, the more strongly rest period differs from an active period (planning or actual movement) - in terms of spectral power of the  $\mu$  and lower  $\beta$  bands - the higher the reactivity and the desynchronization. Neurophysiologically speaking, the larger that quantity, the stronger the expected (correct) cerebral pattern to associate to the movement in that scheme of operant-conditioning that underlyed the experiment.

The difference between the two conditions, i.e. rest and active period, is typically expressed through the so-called *Explained Variance* ( $R^2$ ). This is a well-known statistical measure that quantitatively describes how much the means of two distributions  $x_1$  and  $x_2$  differ from each other in relation to their variances. In this BCI application rest period distribution and movement one were compared to determine the strength of the MRD.

Mathematically  $R^2$  is computed as the ratio between the squared covariance of a single bivariate distribution constructed from the two sets of measures and the product of their variances.

Specifically, let  $x_i$  with  $i = 1, \dots, N$  the first random variable formed by the set of  $N_1$  samples of  $x_1$  and  $N_2$  samples of  $x_2$  with  $N_1 + N_2 = N$ , and  $y$  the second random variable with an equal number of samples  $N$  where:

$$y_i = 1, \quad \text{if } x_i \text{ is a sample of the first distribution } x_1$$

and

$$y_i = -1, \quad \text{if } x_i \text{ is a sample of the second distribution } x_2$$

with  $i = 1, \dots, N$ .

$R^2$  is then computed as in formula below:

$$R^2 = \frac{\text{cov}(x, y)}{\sigma_x^2 \sigma_y^2}$$

where, given  $m_x$  and  $m_y$  the averages of the two distribution  $x$  and  $y$ , their covariance is obtained by:

$$\text{cov}(x, y) = E[(x - m_x)(y - m_y)].$$

Operatively, as provided by the software BCI2000, the  $R^2$  value between two sets of samples, the first  $q$  made by  $N_1$  samples from a rest condition and the second  $r$  formed by  $N_2$  samples from an active period was obtained as in the following.

Let firstly define  $G$  as:

$$G = \frac{(\sum_{n=1}^{N_1} q(n) + \sum_{n=1}^{N_2} r(n))^2}{N_1 + N_2}$$

Then  $R^2$  results from formula below:

$$R^2 = \frac{\frac{(\sum_{n=1}^{N_1} q(n))^2}{N_1} + \frac{(\sum_{n=1}^{N_2} r(n))^2}{N_2} - G}{\sum_{n=1}^{N_1} |q(n)|^2 + \sum_{n=1}^{N_2} |r(n)|^2 - G}$$

Therefore  $R^2$  is in fact the most compact measure to express movement-related desynchronization of EEG rhythms. It can distinguish rest from motion probability distribution: the higher values of  $R^2$ , the larger the distance between the two conditions, the more considerable the MRD phenomenon.

### 3.4 Strong Points and Further Improvements

Previous sections provided a comprehensive and detailed overview of the BCI system for motor rehabilitation of the arm currently used at IRCCS San Camillo Hospital. Comparing this platform with literature and with other BCIs adopted in the rest of the world ([74] [75] [76] [77] [78] [79] [80] [57] [81] [82] [52] [83]) by other research groups with which there was information exchange, discussions, observations and listened oral presentations at conferences and meetings, several considerations could be pointed out.

In this section, then, the main strong points and advantages from this BCI application as well as some remarks for the general improvement of the system will be advanced. If on one hand, advantages are already available and adopted in the experiment, on the other hand some further advancements still have to be taken into account. Moreover, a partial improvement will be provided by the new algorithm proposed in next Chapter.

It has to be recalled here that this kind of BCI platform was designed to implement the operant-learning strategy as many other BCIs. This conditioning technique is considered one of the most powerful way to learn (or re-learn in the case of recovery from a stroke) because of the active involvement of the subject in the learning process. Furthermore, in

this specific application the operant-learning potentialities are exploited along with the neuroplasticity property of the brain that could create - especially during childhood and after a cerebrovascular disease like stroke - new neural connections and promote in such a way new information coding, i.e. (re-)learning.

The experimental hypothesis stating that it is possible and advantageous to use the area surrounding the lesioned one to regain - partially, at least - the motor control should provide the double benefit to recover from the impairment in a faster and more reliable manner since the neural area originally designated to motor functions is artificially made responsible for the same abilities again. On the contrary, in other rehabilitative approaches no attention is paid to the area that is artificially made in charge of the recovered functions through the treatment, even if it was not the responsible area for that before the injury.

Exploiting the natural functional areas [68] of the patient's brain, the recovery should be achieved in a shorter time and benefits of the rehabilitation should be longer lasting, persisting even further the hospitalization period.

Besides the previously highlighted advantages, one of the strongest points of this BCI application and the major feature of novelty is the use of a proprioceptive force feedback [84] [83] that is contingently modulated by the cerebral activity of the subject performing the reaching task and, more importantly, that is continuously provided to him/her helping them in completing the motion [58]. Indeed, the most BCI systems with haptics and robotic devices operating as outputs of the BCI loop usually implements a binary control that allows the patient to only perform very rough movements of reaching and grasping.

This system is one of the first attempts to make patients control their robotic arms in a continuous and, consequently, finer way. As mentioned in section 2.2, this goal had been already successfully reached by Hochberg and colleagues in 2012 [52] and by Collinger and his team in 2013 [53] using an ECoG that implies that the subject had to undergo a surgical intervention for electrodes implantation facing all the risks arising from a neural surgery and the infections problems rising from the implantation of non-physiological materials inside the brain. Therefore, another major point of the system is its complete non-invasiveness that could bring it to become - in the future - a common tool of the daily rehabilitative practise.

As well as strong good points, the platform requires the modification of some weak points of the protocol in order to ensure the rehabilitative benefits of this experiment. Some of them represents questionable choices in the paradigm design, others - the most - regard the EEG signals processing and its usage in transforming the cerebral activity into commands for the BCI output device.

First of all, continuously slight changes of the force feedback could lead patients to a confusing state in which system reaction is misunderstood or totally ignored. Different solutions were prospected: a fixed force at a preselected value or a force with a constant value equal to the modified version of NFB computed at the beginning of the movement, both delivered whenever the MRD is detected (before the actual motion).

As regard as the choice of the neurophysiological features for adapting the force feedback, they were usually selected in a semi-quantitative manner. Indeed, after the screening session, a grid plot sketching the  $R^2$  values at each frequency bin and each electrode (see Fig.3.10) was obtained. Following, the most significant three or four features (cor-

responding to the three or four maximum  $R^2$  values), i.e. each one represented by a combination of a frequency bin and an electrode, were selected for the feedback purpose.

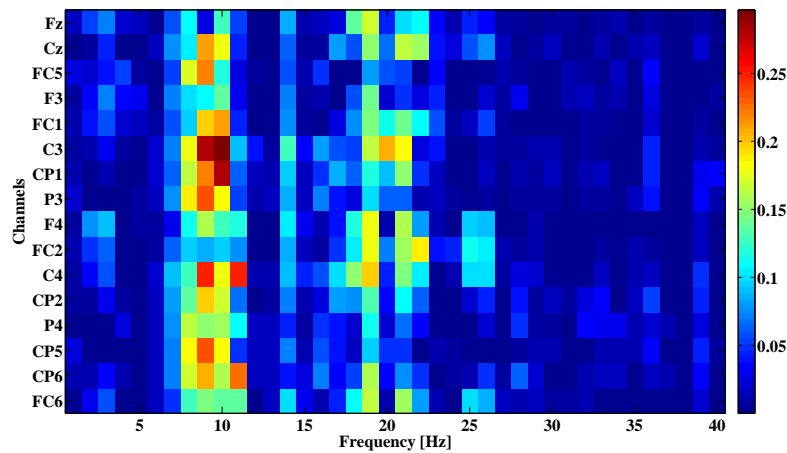
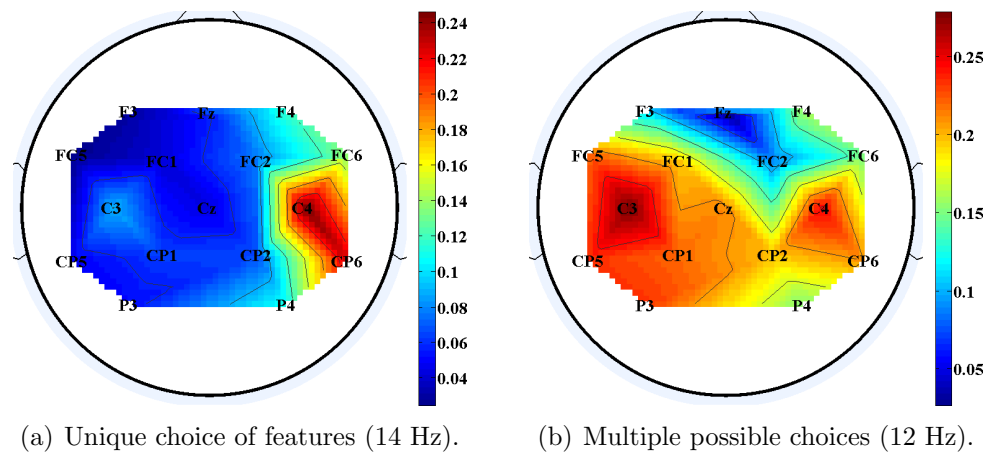


Figure 3.10:  $R^2$  grid plot from a screening session.

It has to be noted that while in some cases this choice was clearly unique like in Fig.3.11(a) such that the final decision could be automatically taken, sometimes multiple choices should be manually evaluated or discussed on the basis of other more complex neurophysiological considerations (as in Fig.3.11(b)).



(a) Unique choice of features (14 Hz).

(b) Multiple possible choices (12 Hz).

Figure 3.11: Features selection from the  $R^2$  values grid for specific frequencies within the SMR after a screening run performed with the left arm by a healthy participant.

Therefore, it has to be highlighted that such a semi-quantitative approach with the qualitative features selection is not repeatable and, thus, can not be perfectly replicated by another research group, wasting the possibility to establish a useful comparison. Nevertheless, this is a very common approach in the BCI community: the quantitative part allows to discard non-significant or non-physiologically meaning features, but the final

decision is usually qualitatively assumed in order to avoid abnormal behaviours or meaningless activity localizations.

EEG artefacts, for example, can occur and distort the task-related signals consequently causing the  $R^2$  to take unlikely values or distant electrodes to present a larger activity than the task-related channels (see Fig.3.12)

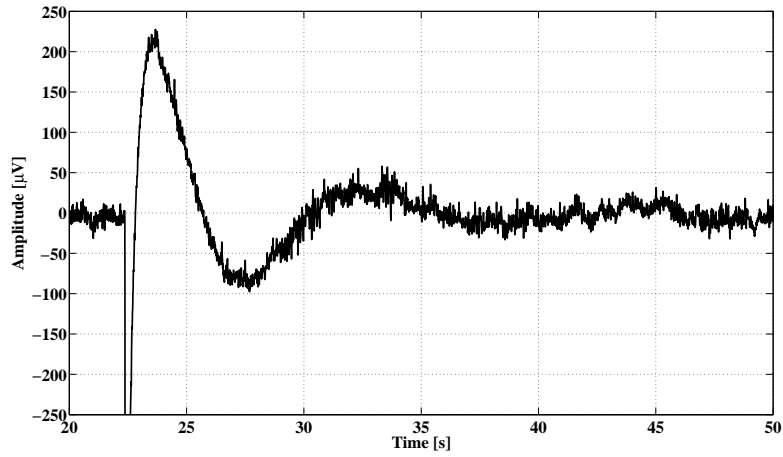
If, on one hand, during the offline analysis some results can be easily addressed to an artefactual origin (as in the case of the clearly artefactual  $R^2$  topography of Fig.3.12), on the other hand the online procedures require more carefulness. Actually, one of the most critical aspects of the current BCI platform is the lack of a robust and real-time operating algorithm to detect and suppress artefacts during the experimental runs.

Such artefacts, the electrode-pop ones for example, can indeed completely distort the EEG signal for a long period of time during which an unreliable force feedback will be provided with the consequent useless for the rehabilitation aim or, even worse, the complete misunderstanding by the subject.

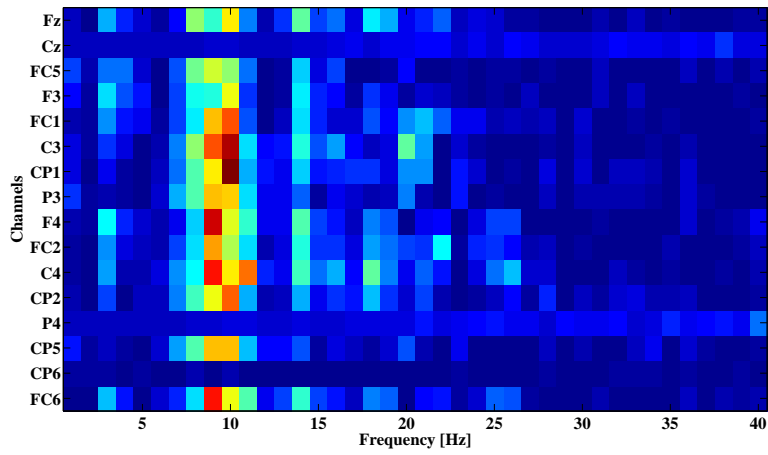
Besides that, the extreme inter-individuals and even intra-individual variability of the EEG signal led to an intrinsic difficulty into the artefact real-time detection along with the following identification of the task-related desynchronization of the SMR.

It has to be recalled that the most important aim of the BCI system is to release a real-time correct force feedback to the patient. In order to accomplish this purpose, a comprehensive and accurate offline analysis of the EEG signals was considered as mandatory to identify the characteristics of the artefacts and to properly design the real-time algorithms for cancelling them out. In the worst case in which no complete cancellation is possible, a significantly lowering action of their effects at the noise level has to be performed producing at most a few hundreds milliseconds of EEG signal *black out*. This would be an acceptable amount of time for missing the feedback, meaning that only one trial at most would be lost, while from the subsequent one the MRD value would be reliably computed and the correct feedback would be applied to the BCI system again.

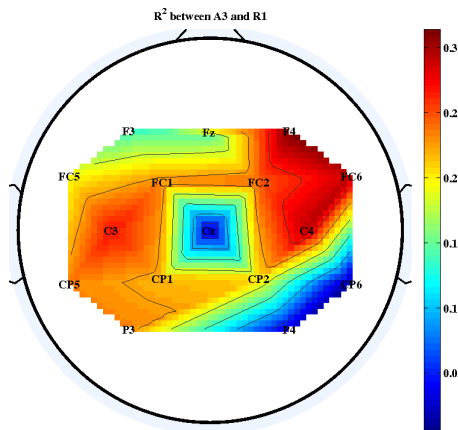
With this purpose, Chapters 4 and 5 will explain this analysis, a preliminary proposed artefacts solution and the final results of an alternative MRD identification with its advantages along with some residual weak points to address in the future.



(a)  $C_z$  channel with the electrode pop artefact.



(b) Distorted  $R^2$  values grid.



(c) Distorted  $R^2$  topography.

Figure 3.12: Electrode-pop artefact in the  $C_z$  channel affects the  $R^2$  computation (abnormally negative values in  $C_z$ ).



# Chapter 4

## EEG Signal Processing for BCI based Motor Rehabilitation

### 4.1 Electrode Pop Artefacts

This section deals with that specific kind of EEG artefact already mentioned in the previous Chapter that can arise from the displacement of an electrode during recordings, the so-called electrode-pop artefact. This event can cause the subject to fail in operating a BCI at least for a limited period of time - because of the artefactual analysis of the correspondent EEG signal is affected by the huge abnormal peak and by the large oscillations following the displacement and which can last for several seconds.

#### 4.1.1 Description

EEG recordings at the scalp of a subject are a combination of useful signal and disturbance [25] [26]. To be precise, the former is constituted by the neural response of the subject to an experimental task or, simply, it carries the information about the status of the individual. On the other hand all the other components of the EEG traces are labelled as disturbance. As mentioned before, there can be several causes of disturbance but, generally, they are classified as follows:

- *External interferences.* The main element of this set is the power line noise that usually corrupts the EEG recordings. For this reason, a notch filter around 50 Hz or 60 Hz is implemented to remove this considerable interference during EEG evaluations or experimental sessions.
- *Physiological interferences.* They can be further divided into two subclasses: muscular and neural noises. Eye-blinks, eye-gaze changes, chewing, gnashing, swallowing and head slight movements are muscles activations that can compromise the whole recordings. Skin sweat can be also a relevant phenomenon to cope with sometimes. Finally, distractions, habituation and other collateral cognitive phenomena can elicit neural populations of different cortical regions to spike and, at the scalp level, to show interfering waveforms. The latter are considered disturbance and are usually removed on the basis of their spatial and/or frequency occurrence.

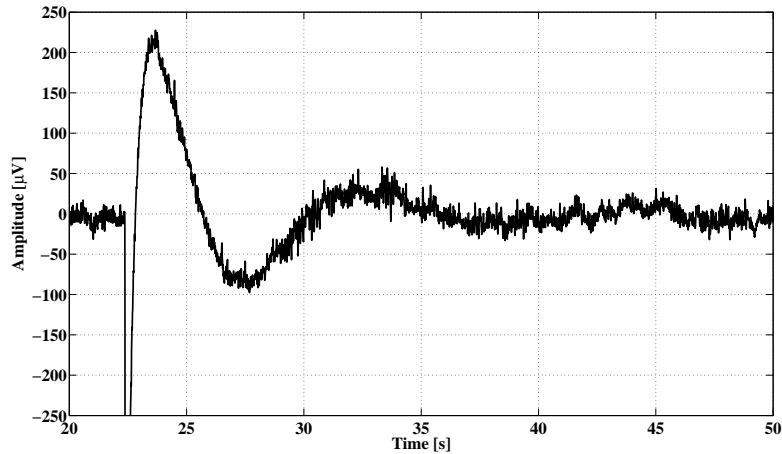


Figure 4.1: Signal with electrode pop artifact. A detail.

Then artefacts can occur either accidentally or along the whole recording. For instance, artefactual activity due to mains is usually present along the entire registration while muscular contraction is in the most cases a very short phenomenon that can seriously corrupt a relatively short-lasting recording segment.

One of the most impacting cause of artefact is the previously cited electrode-pop: although quite rare, this kind of noise can be completely superimposed over the low amplitude useful signal and make the identification procedure of the EEG characteristics almost impossible. A typical example of its shape is captured by Fig.4.1 where the usual abrupt negative fall, overshoot and slow-oscillating return to baseline values are clearly visible.

Fig.4.2 then shows an overview of the entire recording coming from the same EEG sensor.

It can be easily expected that such an artefactual activity compromises any kind of automatic features identification. Cautions in order to avoid this kind of artefacts can be taken during the recording preparation: clinical technicians are trained to pay attention on this type of occurrence.

In the following, after a brief excursus of the literature on this topic, a new real-time signal processing algorithm is presented with the aim to identify and remove this electrode-pop artefact before to estimate the EEG features required to assess the patient's status or to operate an EEG-based external device in a BCI scheme.

### 4.1.2 Literature Solutions

Pop artefacts have been treated in many different ways in the literature. Following, two main approaches both software and hardware are reported: the former was proposed by Durka and colleagues in the context of polysomnographic recordings [86] and it consists in the rough elimination of long EEG segments exceeding a fixed threshold during an offline analysis phase after recordings. The hardware solution proposed by Barlow [87], instead, required a circuit to cancel out the incoming pop artefact based on a previous

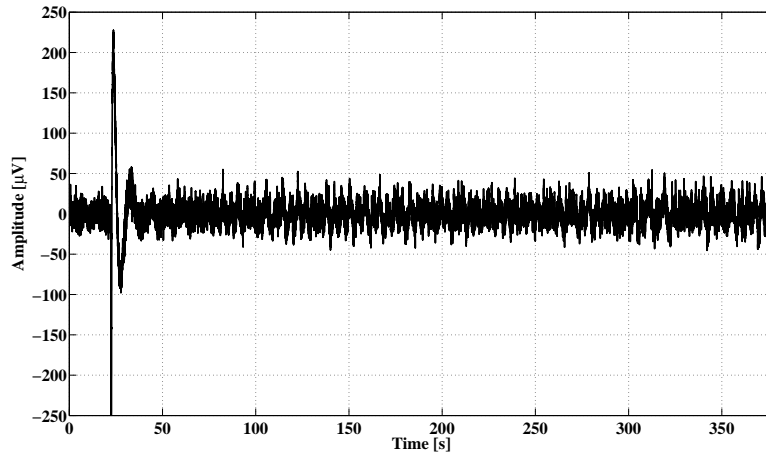


Figure 4.2: Signal with electrode-pop artifact. The whole recording.

simulation study of its typical waveform.

Nevertheless, both solutions were not suitable for the purposes of this study: indeed, on one hand the hardware solution was proposed without a rigorous quantification of performance and moreover data of the study under analysis had been already recorded, on the other hand discarding whole long segments of EEG traces like during polysomnographic experiment can not be the solution of a real-time system that has to continuously take decisions about the robotic feedback within a hundred of milliseconds at the latest.

Other studies ([88],[89],[90],[91],[92],[93]) proposed several Independent Component Analysis (ICA) based methods to remove artefactual components from EEG recordings. They also suggested a rejection algorithm based on higher order statistics of EEG to identify and exclude artefactual EEG components. In both cases, computation requires too much time to be performed in real-time as required in BCI applications: in fact, ICA has a  $O(NM^3)$  complexity defined by the ( $M$ ) sources decomposition of a set of EEG  $N$  time samples long signals. Methods based on higher order statistics need for, instead, a high number of clean EEG segments before to become reliable: this can be not the case of the BCI application studied in this Ph.D. work.

These kinds of algorithm can satisfactory be employed in the offline analysis of different applications or in experiments using Event-Related-Potentials (ERPs) where a large number of trials has to be collected before to take a decision about the output feedback. In that case an ICA-based or even a threshold-based method can effectively work.

In BCI systems like the one described in Chapter 3 real-time detection of electrode-pop artefacts is really crucial. Since no specific algorithms have been elected as the gold-standard for the real-time detection and rejection of this particular artefacts, a home-made solution was studied and implemented via software.

### 4.1.3 Proposal for a Rejection Algorithm

Therefore, the proposed solution is based on a non linear procedure and it could be accomplished in two different ways: either by estimating the main pulse and cancelling it

or by detecting the time instant when the main pulse starts and setting the signal to zero in that interval. The first solution would be more precise but it would require a bunch of computations and an accurate model of the artefact to estimate the main pulse with enough precision. On the contrary the new algorithm is based on the second instance and has two main steps: first of all, a single EEG trace is taken into account and its first derivative is computed as the simple difference between each sample and the previous one.

In order to properly identify the pop-up artefact some considerations resulted helpful. It has to be recalled that the EEG signals were preliminarily low-pass filtered before the amplification step with a filter bandwidth smaller than 100 Hz. Thus, an ideal unit step pulse given as an input to such a filter will show a rise time of several milliseconds. Moreover an additive delay is due to the signal passage through the input circuit of the amplifier leading to an output signal with a further longer rise time. From experimental observations it could be noted that a typical pop-up artefact had a rise time longer than 20 ms. Thus, aiming at identifying the actual pop-up artefact and avoiding false positive errors at the same time, a set of some consecutive derivative samples with significantly negative values (a suitable threshold had been previously selected) was subjected to the artefact detection analysis. Particularly, in the study, 8 was chosen as a suitable set width for this analysis. Then, the samples identified as artefactual were replaced by zero values and discarded from the feedback procedure that decides the entity of the BCI system reaction given to the subject performing the rehabilitative exercise.

During the interval of time where artefact is removed no feedback is intended to be provided to the subject but the system is thought to be waiting for new reliable values.

An example of application of this method is reported in Fig.4.3 where the sum of an original artefact-free signal (recorded from the FZ site on the scalp) and a synthetic electrode-pop is displayed as a black curve along with its first derivative (red curve) and the two time instants labelled as the edges of the artefactual period are highlighted with cyan dots. The limited interval in which the artefact occurred and was detected is shown in the figure for the convenient purpose of a better visualization.

**The Purpose** With regard to the BCI treatment for motor recovery of the upper limb in stroke survivors described in [67], the current signal processing unit running the world-spread software BCI2000 [71] does not care about the electrode-pop artefact. Unfortunately, some recorded sessions of the whole BCI treatment were affected by this electrode displacement. Therefore, the novel algorithm was designed and implemented to cope with this lack of artefact detection. The procedure was realized with the further goal to be performed in real-time during the BCI experiment. This means that it has to be as little time-consuming as possible to allow the BCI system to process the remaining on-line analysis and provide the robotic feedback to the subject performing the experiment before he/she starts to execute the movement task.

**Filtering** After these two first steps, the standard BCI2000 or another procedure involving a high-pass filtering above 1 Hz can run as usual. Here, for example, a band pass filtering in an extended (7,14) Hz  $\mu$  band is considered. The filtering operation leads to the cancellation of the large remaining slow oscillation following the huge negative abrupt fall just removed, bringing back the signal to fluctuate around reliable values

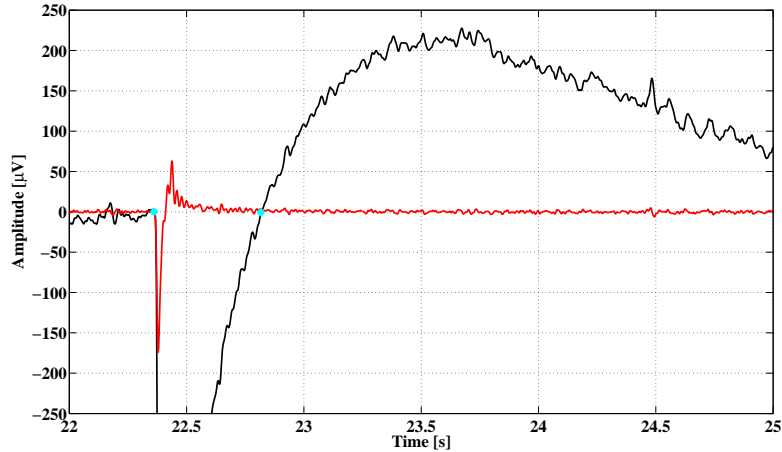


Figure 4.3: Artifact addicted EEG signal (black), its derivative (red) and the artefactual interval edges (cyan dots).

again. The zeros-fulfilled artifactual interval is filtered too and small oscillations arise at the filter output: however this does not represent an issue since this period of time is completely discarded from the following analysis. The difference between the (7,14) Hz band filter output with a previous step of artefact detection and removal and the same output without that preliminary operation is plotted in Fig.4.4 and Fig.4.5 (in more detail). The (7,14) Hz band filtered version of the original raw signal without the synthetic artefact is also reported in both figures as a comparison. Moreover, two magenta vertical lines define the artifactual interval that is discarded from the following analysis.

From Fig.4.4 and Fig.4.5 it can be noted that ideally-filtering a signal with an electrode-pop artefact causes an evident non-causal response that compromise the following analysis. Moreover, a real case filter would also introduce a significant delay that must be limited to make the BCI feedback effective. On the contrary, filtering the EEG signal with the artefact preliminarily removed do not cause any significant disturbance. The latter considerations are confirmed by the analysis of the performance presented later on.

**Performance Computation** In order to quantify the algorithm performance, the Signal-to-Noise Ratio (SNR) had to be computed. This would be possible only if a version of the same signal with and without the disturbance was available. To this purpose, a synthetic electrode-pop artefact was constructed and then added to a real EEG signal where no disturbance affected the trace. Then, the SNR could be easily computed. Different shapes of synthetic artefacts were evaluated and the most similar to the real one chosen for the following analysis. In particular, two different choices of artefacts are displayed in Fig.4.6 with a detail in Fig.4.7.

A trade-off between the similarity along the slope and that during the subsequent slow oscillation has to be defined.

Let the original EEG signal filtered in the (7,14) Hz band be denoted as  $x$  while the filter output without the algorithm application as  $y_1$  and the same quantity with the artefact previously detected and removed as  $y_2$ . Then  $e_1$  and  $e_2$  are defined as the

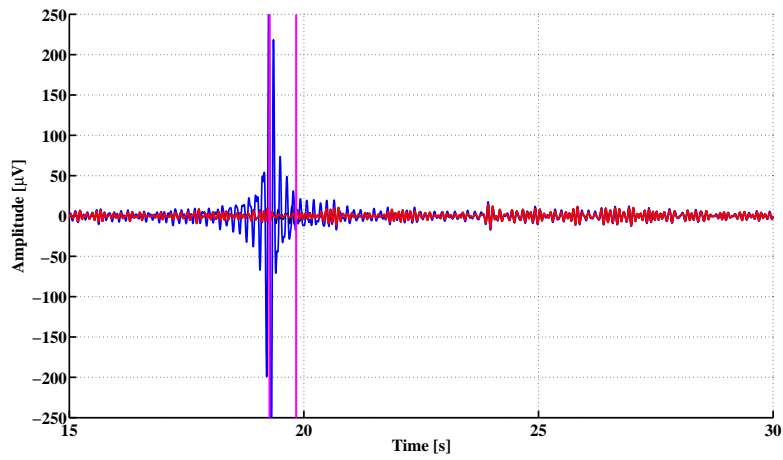


Figure 4.4: The original raw signal filtered in the (7,14) Hz band (black curve), the filter output after the application of the proposed algorithm (red curve), the filter output without any artifact detection algorithm (blue curve) and the artefactual interval (magenta vertical lines).

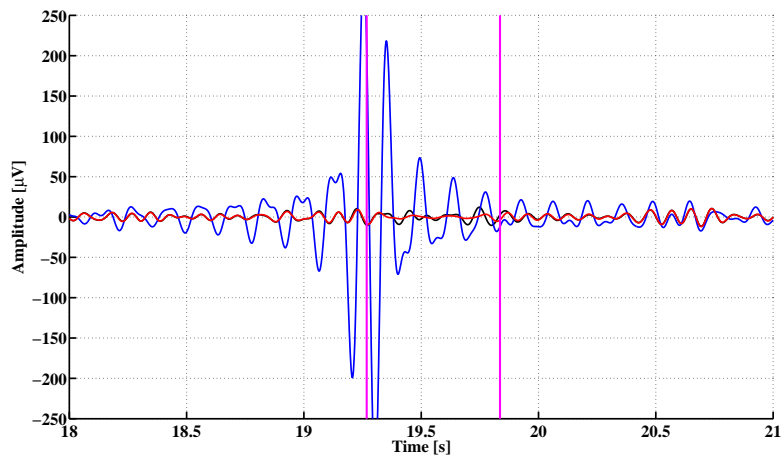


Figure 4.5: A detail of Fig.4.4.

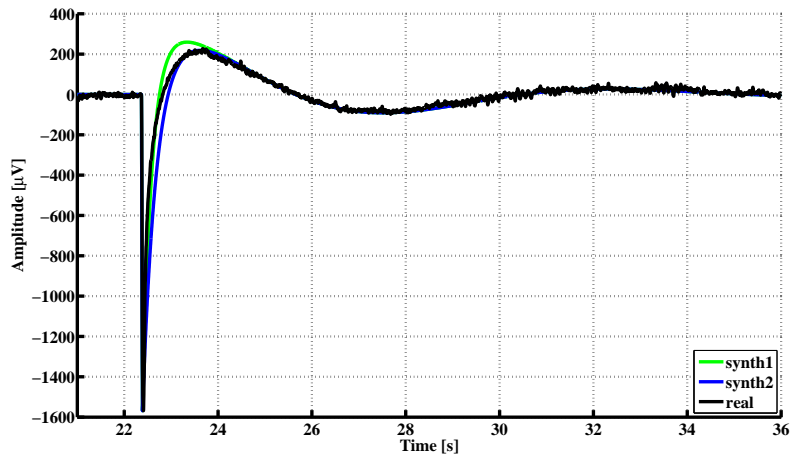


Figure 4.6: Raw signal (black) with two different shapes of synthetic artifacts.

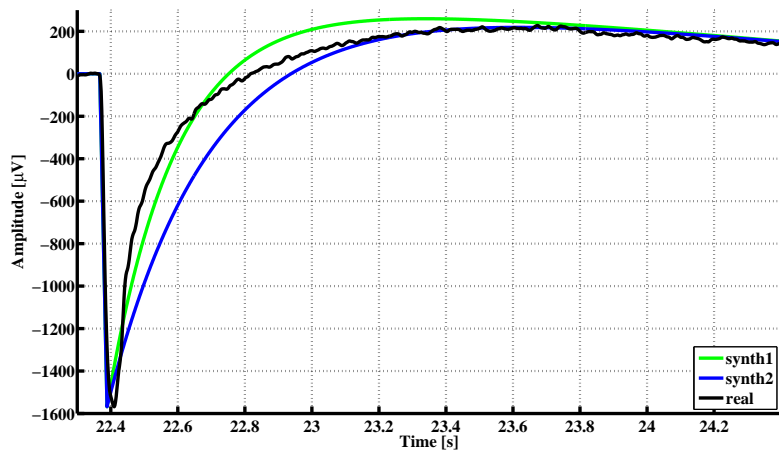


Figure 4.7: Raw signal (black) with two different shapes of synthetic artefacts. A detail.

	$A_1$ [ $\mu\text{V}$ ]	$A_2$ [ $\mu\text{V}$ ]	$\tau_1$ [s]	$\tau_2$ [s]	$f_0$ [Hz]	$\phi_0$ [rad]
<b>Blue artifact</b>	-1866	350	-0.3	-4	0.10352	0.55287
<b>Green artifact</b>	-1866	350	-0.2	-4	0.10352	0.55287

Figure 4.8: Table with the parameters values of the two synthetic electrode-pop artifacts.

following differences:

$$e1 = y1 - x \quad \text{and} \quad e2 = y2 - x$$

and represent the errors between the filter output and the original artefact-free signal. In order to quantify the algorithm performance, the error energy  $M_e$ , the signal energy  $M_x$  and the  $SNR$  (computed as the ratio between  $M_x$  and  $M_e$ ) at the filter output were computed over 256 samples-wide time windows. Such a window width was chosen to be the same as that used by the BCI2000 software currently operating in the online procedure during the BCI experiment. Then the new algorithm was employed in an offline analysis to assess its effectiveness in an MRD identification and localization procedure.

To reach this goal a preliminar description of a synthetic electrode-pop artefact is needed. Then, the  $SNR_s$  of an artefact corrupted EEG signal and an EEG signal with the artefact previously removed can be compared.

Let  $s$  be the original raw EEG signal and  $a$  the synthetic artefact. The latter was implemented as the formula below:

$$a(t) = A_1 \exp(-t/\tau_1) + A_2 \exp(-t/\tau_2) \cos(2\pi f_0 t + \phi_0)$$

where the constants  $A_1$ ,  $A_2$ ,  $\tau_1$ ,  $\tau_2$ ,  $f_0$  and  $\phi_0$  are reported in Fig.4.8 for the two synthetic artefacts shown in Fig.4.6 and Fig.4.7 as an example.

In both the cases the synthetic artefact shape is pretty close to that of the real one, but the blue artefact was selected to perform the following computations. Then the linearly combination of signal  $s$  with signal  $a$  ( $s + a$ ) drives the filter in the (7,14) Hz band. If the signal  $s + a$  has been previously processed by the algorithm for the electrode-pop artefact detection and removal, the filter output is  $y_2$ , otherwise  $y_1$  is obtained. The above mentioned signal  $x$  is the filter output when the raw signal  $s$  drives the filter. The energy of the two errors  $e_1$  and  $e_2$ , and the correspondent  $SNR_1$  and  $SNR_2$  were computed on the limited time intervals of 256 samples and compared to assess the advantage of the application of the new algorithm. Fig.4.9 shows indeed the energy of the two different errors computed within the above defined windows shifting by 8 samples at time.

The correspondent SNRs behaviours are displayed in Fig.10 where the ratio between the signal energy  $M_x$  and the error (either  $e_1$  or  $e_2$ ) energy  $M_e$  is computed over the same 256 samples time interval. Fluctuations of the SNRs curves are due to those of the original EEG signal. From Fig.4.9 and the next Fig.4.10 the advantage to apply the algorithm to remove the electrode-pop artefact becomes definitely clear.

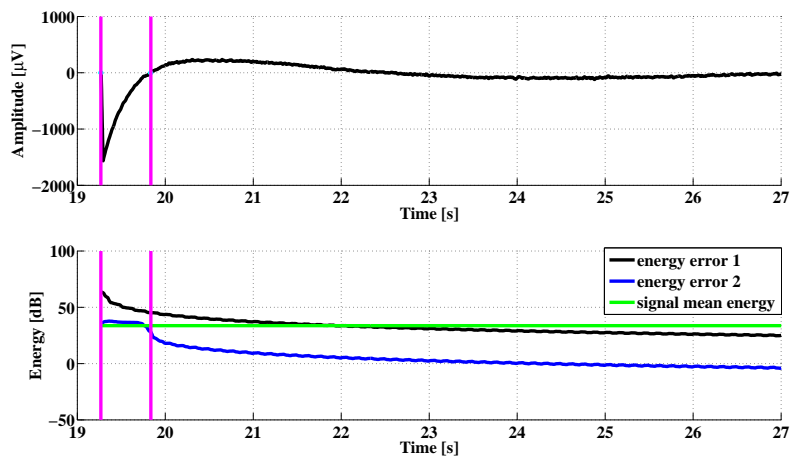


Figure 4.9: Energy of the errors at the filter output along with the mean energy level of the original artifact free signal  $x$  (green line) and the artefactual interval (magenta lines).

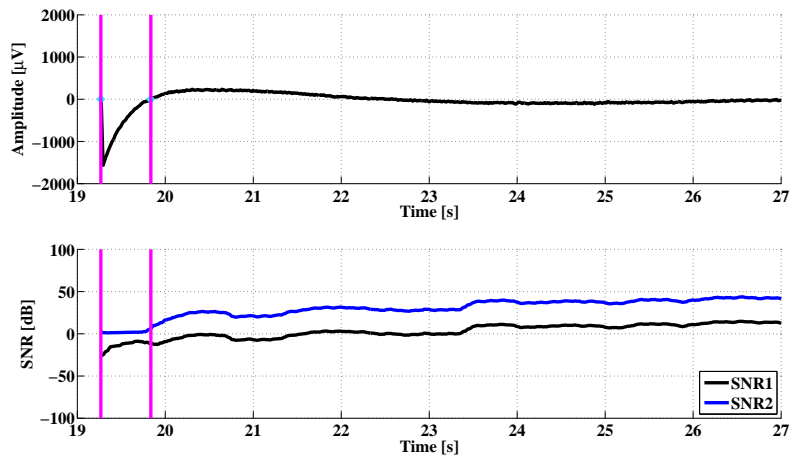


Figure 4.10: SNRs at the filter output with the artefactual interval (magenta vertical lines).

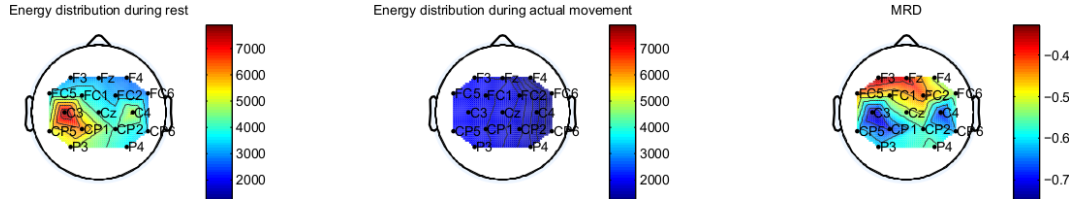


Figure 4.11: MRD topography of an artifact-free EEG recording.

In fact, from Fig.4.10 it can be noted that  $SNR_2$  evaluated after the artefact algorithm employment is constantly 30 dB larger than  $SNR_1$  obtained with the standard procedure and is suddenly higher than 0 dB after the artefactual interval where the signal were reset and its values discarded from the following MRD analysis. Indeed, it has to be incidentally mentioned again that the part of the EEG trace within the magenta edges is not taken into account for the following analysis of the MRD and, since the signal in the same interval was cancelled, the correspondent SNRs values are unreliable. After proving the quantitative advantage of the proposed procedure, the algorithm was tested in a real BCI application.

**Consequences on MRD identification** As explained in Chapter 3, the BCI platform taken into consideration aimed at improving the reaching movement accuracy in mild-impaired post-stroke chronic patients by means of a force contingent feedback that acted as a mirror of the cerebral activity related to that action. In particular, the MRD, as sign of that cerebral activity, was computed in real-time by the BCI2000 software as the normalization of the spectral power around 10 Hz estimated at the current time instant on mean and standard deviation of the analogous quantity gathered during the initial relaxation period. Moreover, these computations are performed on the basis of the recordings coming from specific locations, i.e. the sensorimotor cortex, on the subject's scalp. If an electrode-pop occurs, all these estimations become affected by abnormal values obtained by filtering the huge impulse present in the signal due to the temporary electrode displacement. Fig.4.11 to Fig.4.13 show the mean energy values obtained during the initial relaxation period, the movement and the correspondent MRD estimation. It has to be recalled from Chapter 3 that the larger the MRD, the stronger the robotic help and very likely the more efficient the BCI training.

Specifically, Fig.4.11 is plotted by analysing the artefact-free dataset where  $x$  represents the signal coming from the  $F_z$  location.

Then, Fig.4.12 shows the disastrous effect of an electrode-pop artefact occurred in the  $F_z$  sensor during the initial rest period. The MRD values of this artefactual signal were computed based on  $y_1$ .

As clearly visible from Fig.4.12, an artefactually huge energy value is focused at the  $F_z$  location in the scalp frontal area. While energy distribution during the movement periods of all the following trials is almost within the range of normality, it can be easily expected that the normalization process based on the rest period will lead to unreliable estimation of the patient's cerebral activity, i.e. the MRD values, with a consequent feedback production not related to the physiological activity of the subject and thus useless for him/her motor training. Finally, Fig.4.13 reports the analogous

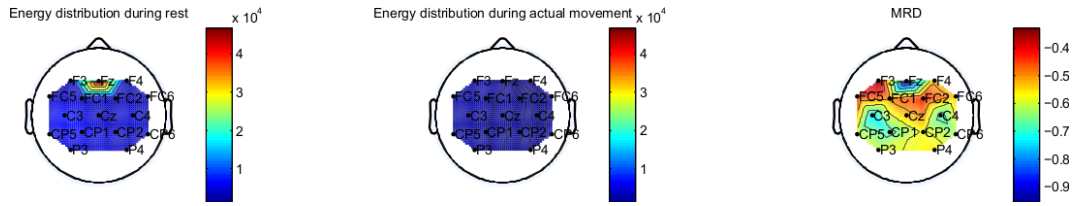


Figure 4.12: MRD topography of an artifact-addicted EEG dataset with a synthetic electrode-pop artifact on the FZ site.

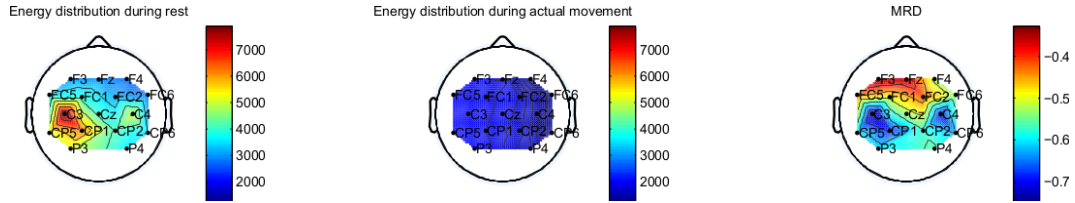


Figure 4.13: MRD topography after removing the synthetic electrode-pop artefact from the same EEG dataset of Fig.4.11.

energies distributions and MRD estimations gathered after the application of the proposed algorithm that removes the artefactual peak and correctly filters the remaining and large overshooting oscillation. Therefore the MRD value of the  $F_Z$  termination was computed based on  $y_2$ .

The figure assesses, then, the benefit of such preliminary procedure to remove this kind of artefacts. Indeed, a focus of the activity in  $C_3$ ,  $C_{P1}$  and  $C_4$  is a reasonable expectation since those sites are locations above the sensorimotor cortex. Moreover, energy values of the rest period are significantly lower than those of the previous case (Fig.4.12) when the electrode-pop artefact destroyed the EEG physiological waveforms.

**Discussion** The previous results have assessed the necessity and the effectiveness of the proposed algorithm to detect and remove the electrode-pop artefact in real-time. From the topographical distribution of the MRD values displayed in Fig.4.11, Fig.4.12 and Fig.4.13 it can be noted that a huge artefact like an electrode-pop occurred in one location of the scalp can compromise the MRD identification and, in particular, increase the number of false positive or false negative detections of this cerebral phenomenon: indeed, if such an artefact occurred during the rest period the MRD in that scalp location would be always identified since the energy of the artefactual EEG signal in that period would likely be much higher than that during the movement periods. If on one hand the artefact happens in a location outside the sensorimotor area, the unreliability of the results can be easily deduced as far as the MRD is expected to appear in the area representative of the sensory and motor cortex. If on the other hand, an electrode of the above cited part of the scalp pops up, a similar conclusion can be hardly taken. In that case a further investigation would be needed but, more importantly, the current online procedure would computes artefactual MRD values providing, as a consequence, an erroneous and useless feedback to the subject performing the exercise at the BCI platform. On the contrary,

in the case of electrode-pop during a movement period, the MRD would become not identifiable since the artefactually large values of the energy would be much higher than that of the initial rest period: thus, the MRD would mistakenly not be recognized.

Moreover, the effectiveness of the algorithm is also based on its real-time application: in fact, a simple difference operation between consequent amplitude samples (the first derivative step) and the check of its large decrease in few samples - less than 10, i.e. 20 milliseconds in this case - allow the detection of the artefact due to an electrode pop. Furthermore this online identification comes at a very good performance since, as shown in Fig.4.10, the  $SNR_2$  is constantly much better than the procedure that excludes this detection ( $SNR_1$  curve). As expected, a constant increase of the  $SNR$  can be observed as far as the impact of the artefact on the regular signal decreases as the recording goes on. A final consideration can be highlighted both from Fig.4.9 and Fig.4.10: the first part of the artefactual interval has to be excluded from the following analysis of the MRD because of the artefact abrupt negative slope. An additional interval of time where signal values have to be discarded can be roughly estimated in  $1/B$ , where  $B$  is the filter bandwidth ( $B = 7$  Hz in this particular case, then  $1/B = 150$  ms). In this prolonged period of time - lasting at most one second - the  $SNR_s$  values are unacceptable ( $SNR_1$ ) because of the artefact presence or unreliable ( $SNR_2$ ) because of the signal cancellation in that period.

But the most interesting note is that the proposed algorithm suddenly regains a good SNR into respect to the procedure without the artefact detection. As clearly visible from Fig.4.9, the error energy of the signal preprocessed with the electrode-pop algorithm becomes smaller than the mean energy of the signal immediately after the above defined interval, allowing a much early MRD identification.

Concluding, it has to be one more time remarked that the proposed procedure removes one only second of the signal content from the analysis which is a fairly trade-off to have an artefact-free signal, while the current procedure should discard much more time to wait for the  $SNR_1$  to overcome 20 dB (that is the minimum value to have the error energy less than 1% of the useful signal energy, a satisfactory threshold for the MRD evaluations). Finally, it can be observed that if an artefact occurs during the initial long rest period (40 seconds long), both the standard procedure and the new one can correctly estimate the MRD value from the artefact-free remaining part of the rest recording. On the contrary, if it happens during a movement trial (lasting at most one second) it disastrously impacts and the current procedure can not estimate the MRD along several trials, while the new algorithm allows this operation just one second later, that is losing at most one trial (where the BCI feedback is not provided and the  $SNR_2$  is not high enough).

## 4.2 Energy Analysis

### 4.2.1 Preliminary Steps

The algorithm to identify and remove pop-artefacts from the incoming signals was used in the offline analysis of the already existing data about the experiment and it specifically represented the first step of the energy analysis described in the following.

Particularly, each raw signal from the dataset of sixteen channels was scanned to find any pop artefacts and, if any, the correspondent samples were marked as artefactual.

	Fz	Cz	FC5	F3	FC1	C3	CP1	P3	F4	FC2	C4	CP2	P4	CP5	CP6	FC6
Fz	0	1	0	1	1	0	0	0	1	1	0	0	0	0	0	0
Cz	1	0	0	0	1	1	1	0	0	1	1	1	0	0	0	0
FC5	0	0	0	1	1	1	0	0	0	0	0	0	0	1	0	1
F3	1	0	1	0	1	1	0	1	1	0	0	0	0	0	0	0
FC1	1	1	1	1	0	1	1	0	0	1	0	0	0	0	0	0
C3	0	1	1	0	1	0	1	1	0	0	1	0	0	1	0	0
CP1	0	1	0	0	1	1	0	1	0	0	0	1	0	1	0	0
P3	0	0	0	1	0	1	1	0	0	0	0	0	1	1	0	0
F4	1	0	0	1	0	0	0	0	0	1	1	0	1	0	0	1
FC2	1	1	0	0	1	0	0	0	1	0	1	1	0	0	0	1
C4	0	1	0	0	0	1	0	0	1	1	0	1	1	0	1	1
CP2	0	1	0	0	0	0	1	0	0	1	1	0	1	0	1	0
P4	0	0	0	0	0	0	0	1	1	0	1	1	0	0	1	0
CP5	0	0	1	0	0	1	1	1	0	0	0	0	0	0	1	0
CP6	0	0	0	0	0	0	0	0	0	0	1	1	1	1	0	1
FC6	0	0	1	0	0	0	0	0	1	1	1	1	0	0	1	0

Figure 4.14: Adjacency matrix.

Then, as explained in more detail in the following, every interval of every signal which included some artefactual samples was discarded from the subsequent analysis.

After removing this kind of artefacts from the raw EEG signals, a Fast Fourier Transform (FFT)-based filtering [94] step was performed. Each signal was thus band-passed in the (4,40)Hz band where the edge frequencies were chosen to avoid other kinds of artefacts.

Indeed as previously described in section 4.1 blinks, current drifts, sweat over the scalp surface and other physiological as well as non physiological components occur in the low frequency spectrum and can distort the EEG signal. Similarly, muscular contractions can obscure the BCI-control signal in the spectrum mainly above 30 Hz.

Moreover, interference phenomena due to volume conduction during the propagation of the signal from the physiological sources inside the brain to the scalp surface are also present. Among other factors, a propagation loss can easily be accounted to model the signal power loss during that pathway: as a matter of fact, higher voltages are measured in the cortical areas nearer the source and, on the opposite, lower amplitude signals are acquired in farther sites. This kind of consideration leads to the further observation that two different EEG electrodes acquire two signals that have common components: their entity depends on the location of the two electrodes into respect of the original sources and the relative distance between the two sensors. Distance thus becomes a significant factor to quantify the interference level and to improve the Signal-to-Interference Ratio (SIR). Since the aim of the signal processing in this application (as in many others in the BCI and neuroscience community in general) is to detect signals as they are originated from the inherent sources, this kind of interference phenomena has to be reduced as much as possible.

A first step in order to reject common-mode components due to signal propagation between neighbouring channels was then to perform a differential operation among the raw signals, based on an adjacent matrix as reported in Fig.4.14

Therefore, sample-by-sample difference between every pair of signals corresponding to a 1-valued cell in the adjacent matrix was computed.

Consequently, a set of thirty-three signals was obtained and then sorted in such a way to have left-hemisphere regarding signals, right-hemisphere and inter-hemispheres ones respectively sequenced. Specifically, the final set of differential signals contained fifteen left-hemisphere signals, an equal number of right-hemisphere EEG traces and the last three signals related to connections between the two hemispheres. This facilitated the researchers during a preliminary visualization phase in which all signals were plotted together in order to provide a comprehensive view of the cerebral activity of the subject and a starting point for the discussion with the clinicians.

Afterwards, the elementary intervals for the following energy computation were identified: these were selected to fulfil the paradigm-stimuli occurrence provided by the trigger variables that came with the EEG data after each run of the experiment (they were defined in the protocol implementation phase). Specifically, five phases could be distinguished in every trial of the experiment, as recalled from 3:

- The *pre-trigger* interval which consists of 500 ms before the target appearance as already mentioned in section 3.1 about the system description.
- The *post-trigger* time lasting 1500 ms and aiming at making the subject planning the movement towards the visible target without actually moving.
- The *reaction time* which defines the temporal interval between the second cue sound that allowed the subject to move towards the target and the instant in which he/she actually started the movement. Therefore, this quantity includes the propagation time of the cue sound from the ears to the brain, its processing time in the brain and the transmission of the motor output from the brain to the arm's muscles. Typically this interval lasts about 400 ms.
- The *movement* period which consists of the time span for the actual 18 cm long path from the starting position to the target. It usually covers a period in the range (400,1000) ms. Nevertheless, the experimental task required the subject to perform the reaching movement within the limited (500, 740) ms time window. As previously mentioned in section 3.1, the movement speed corresponded to a visual feedback: particularly, faster movements (lasting less than 500 ms) made the target change color to red, while slower ones (lasting more than 740 ms) caused the target become blue.
- The *post-movement* phase covered the period of recovering from the hit target to the starting position.

Then, a 256 samples (corresponding to a 500 ms given a sample frequency of 512 Hz) interval was considered as the elementary period for the energy computation. This choice was supported by the literature about BCI where this period was selected to update the feedback provided to the subject performing the experiment.

Although EEG literature points out a time of two seconds for the analysis of reactivity of the EEG rhythms, in this context this quantity would be excessively large: two seconds would cover, indeed, different trial phases so that it would not be possible to distinguish any change among them.

<b>Pre Trigger</b>	<b>Post Trigger 1</b>	<b>Post Trigger 2</b>	<b>Post Trigger 3</b>	<b>Reaction Time</b>	<b>Movement 1</b>	<b>Movement 2</b>
------------------------	-------------------------------	-------------------------------	-------------------------------	--------------------------	-----------------------	-----------------------

Figure 4.15: The seven trial's phases.

A collection of seven 256 samples intervals were identified in each trial: pre-trigger represented the first one, post-trigger were subdivided into three 500 ms intervals, while during reaction time the first 256 samples were collected and during movement, finally, the first two were selected. Fig.4.15 shows the time course of the trial in terms of 256 samples intervals.

It has to be noted that in the reaction time and movement cases both the selected intervals could overlap the subsequent phases respectively. The latter introduces an error in the computed data that involves at most 20% of the total amount of samples of the current interval. However, due to the signal continuity and the further filtering operation explained in the next subsection involving filters bandwidths of 4 up to 6 Hz, the smoothing time is on the order of 100 ms, which is roughly the duration of the overlapping data. Based on this consideration the energy values computed during the reaction times and movement periods are ensured to be valid for the feedback purposes.

Nobody knows yet the perfect time-line of the physiological reaction to such a stimuli-rich paradigm: therefore, it has to be always kept in mind that a certain physiological delay could occur during the experiment coming from distractions or different reaction speeds among people. With the 256 samples intervals structure of Fig.4.15 the energy analysis could be performed.

## 4.2.2 Energy Computation

Energy was indeed computed in every elementary interval of each trial, each differential signal and different frequency bands only excluding artefactually-labelled intervals.

Specifically, energy was computed by means of the classical formula of energy for digital signals reported here for the sake of completeness:

$$E(p, t, s, f) = \sum_{n=1}^{256} |x_{p,t,s,f}(n + n_0 - 1)|^2$$

where  $p$  states for phase,  $t$  for trial,  $s$  for differential signal,  $f$  for frequency band and  $n_0$  for the initial time sample of the (p,t) segment. Each quadruplet  $(p, t, s, f)$  will be named as *condition* in the following. It has to be observed that computing the energy is equivalent to the power computation of the specified interval in this case, as far as the time interval is the same for each computation. Only a  $\frac{1}{256}T_s$  factor, with  $T_s$  being the sampling period, would make the difference between the two possible evaluations: however, this does not influence the comparative analysis among different conditions.

As the frequency bands regards, the most common choice is to select the standard bands used in the clinical practise for the EEG evaluation operated by clinicians. Then, recalling section 2.1, the  $\mu$  band (8,12) Hz and the lower  $\beta$  band (12,18) Hz were analysed.

However, since a comprehensive overview of the signals originated while the subject was performing the experiment was required, some other frequency bands were analysed to live the researchers free to be agnostic and to be always critical towards standards de-facto and generally accepted *magic numbers*. Therefore, the standard  $\theta$  band (4,8) Hz along with some other frequency bands defined in a logarithmic-like logic were considered: (10,14) Hz, (16,24) Hz, (20,28) Hz, (24,36) Hz and (28,40) Hz were added to the previous frequency analysis.

A final (10,20) Hz band was considered in order to assess the performance of the algorithm in this larger band and, possibly (if similar performance was found) use it in place of other smaller standard ones. This could provide notable advantages in terms of real-time computation: a larger frequency band would require a filter with a shorter delayed output signal. In fact, it can be observed that since the filter's impulse response transient could be assumed (roughly speaking) to equal the inverse of the filter's frequency bandwidth (at 3 dB), a 4 Hz bandwidth like in the case of the standard  $\mu$  band (8,12) Hz will produce a 250 ms delay in the output signal, while a 10 Hz bandwidth as in the last suggested frequency band case will introduce 100 ms delay only, that could eventually affect the only initial part of an analysis interval.

After these considerations multiple components of delay can be distinguished: specifically, the delay due to the filtering operations described above adds to those mentioned in section 4.1.

## 4.3 Movement Related Desynchronization (MRD) Quantification

### 4.3.1 MRD Definition

In section 1.1 few notions about the neurophysiology and the neuroanatomy of motor functions were described. In this section the EEG correlates of the sensorimotor circuit, as already briefly introduced in section 2.1, will be highlighted and deeply analysed.

Since the 30s of last century neurophysiological studies developed by Berger, Gastaut, Jasper, Penfield, Magnus and many others reported observations about the recurrent behaviour of the *arcade wave* or *wicket rhythm* or even *en arceau*, i.e.  $\mu$  rhythms, during movement of patients: indeed, this EEG component was noted to *disappear* during motor activities.

Afterwards, several studies assessed those observations in a number - actually the most - of patients, but only since the 70s the development of a quantitative method to measure this phenomenon [95] [96] [97] [98] allowed to extend the results of the previous studies to the whole population. Since that moment,  $\mu$  disappearance was indeed verified in all the subjects. Pfurtscheller, the father of the quantification algorithm aforementioned, called *desynchronization* this behaviour. As previously cited in section 2.1, desynchronization of  $\mu$  rhythms was then observed not only as a consequence of a movement, but even when a subject only imagines to accomplish it, plans an action or watches somebody else performing it. Moreover it could be observed also after sensory events like burn's of hand or arm, vibration perception and so on.

That led Pfurtscheller to complete the denomination as Event-Related Desynchroniza-

tion (ERD). For the purpose of this thesis work, however, where only desynchronization related to a *movement* is taken into account, the original ERD name was substituted with the previously used MRD name.

From the neurophysiological point of view, desynchronization could be roughly explained as the change in the neuronal behaviour from a *synchronized* condition where the most neural populations (at least locally) are working in the same frequency band to a *desynchronized* one where different functions have to be accomplished at a time so that some neural populations need to modify their working frequency causing the *laser-effect* due to a number of neurons contingently firing to vanish.

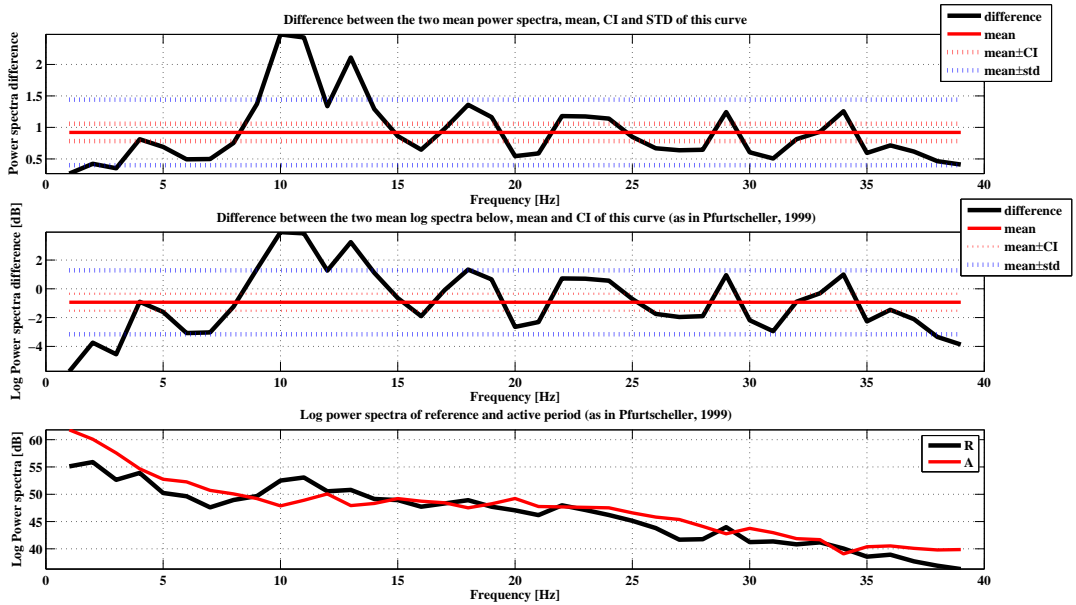
Actually, as pointed out above, the desynchronization term can not be used without its opposite, the synchronization status leading to the definition of the Event-Related Synchronization (ERS) and the Movement-Related Synchronization (MRS), respectively [99] [100]. Particularly, in the case of motor activities the desynchronization of  $\mu$  rhythms can be observed along with the synchronization of  $\beta$  rhythms. This can be explained, as already indicated before, as the requirement of some neural districts to change their working frequency (around 10 Hz) towards higher frequency ranges (around 20 Hz).

Pfurtscheller in many papers written with collaborators ([101], [102], [103], [104]) stated a quantitative method to measure the desynchronization as well as the synchronization of EEG rhythms.

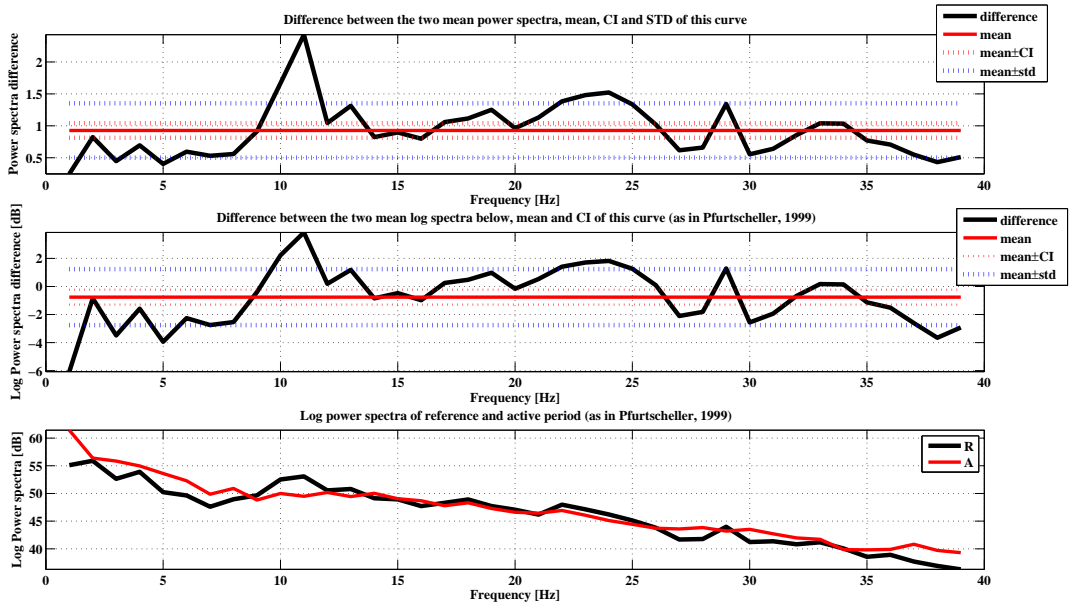
Before to actually compute those quantities, the individual frequency bands where to look for the ERD and the ERS respectively have to be preliminarily defined for each subject: such bands should be chosen as the most reactive bands of frequencies showing a modulation correlated with the movement. Usually, the individual desynchronization band lays around 10 Hz (a slightly modified  $\mu$  band) while the synchronization band around 20 Hz (in the  $\beta$  rhythms range), but widths and band centres have to be evaluated person-by-person because of the large variability that competes to these cerebral features.

One more time, Pfurtscheller and collaborators developed an algorithm to evaluate these quantities. Specifically it requires the following steps:

1. A 1 second interval in a reference, e.g. rest, period ( $R$ ) is selected and its power spectrum is estimated. Usually this period is chosen few seconds (three or four) before the movement onset.
2. Similarly, a 1 second of activity ( $A_1$ ) is identified as the most desynchronized period and its power spectrum is evaluated.
3. In the recovery phase after the task accomplishment, 1 second of the trial ( $A_2$ ) is taken into account, as well, to verify the  $\beta$  synchronized condition. As in 1 and 2 the power spectrum of this trial token is computed.
4. Average within each set of a different condition ( $R, A_1, A_2$ ) is then operated over the all available trials.
5. Averaged power spectra of the reference period and an active one are compared and their difference is computed along with the 95% confidence intervals as showed in Fig.4.16(a) and (b).



(a) Active period chosen before the movement.



(b) Active period chosen from the onset of the movement.

Figure 4.16: Individual frequency band identification method by Pfurtscheller in case of a healthy subject.

Specifically, Fig.4.16(a) illustrates the output of the individual frequency band computation algorithm in the case in which the active period is chosen before the movement onset, during the planning phase of post-trigger time. On the other hand, for Fig.4.16(b) an active 1 s period starts from the actual movement onset time. ERD band is defined as the interval of most significant power decrease (around 10 Hz, usually), while ERS as that with a power increase (in the  $\beta$  band).

Once the individual ERD and ERS frequency bands are found, desynchronization and post-movement synchronization can be estimated. To this purpose the method suggested by Pfurtscheller and colleagues accounts the following steps:

1. Raw signals recorded with a hardware implemented band pass filter between 0.5 and 50 Hz are divided into trials lasting some seconds (about eight) and centred on the movement on-set;
2. Raw trials are further band passed in the individual ERD/ERS bands respectively;
3. The power traces are obtained from each of the raw trials squaring sample-by-sample;
4. A number of squared trials is averaged;
5. A time compression is operated averaging over some consecutive power samples. As previously mentioned, a power decrease means a desynchronized status while, on the contrary, a power increase corresponds to ERS.
6. Eventually, the relative percentage power is computed as the ratio between the ERD and the ERS quantities sample-by-sample from the averaged ERD and ERS curves.

As regard as the ERD and ERS localization, literature showed that, for hand or arm movement [24][103][44] a general lower  $\alpha$  (6,10) Hz band is obtained after almost any kind of task, whereas an upper  $\alpha/\mu$  and lower  $\beta$  desynchronization is specifically localized over the sensorimotor areas. To further particularize those observations, desynchronization was found to start contralaterally - over the hemisphere on the opposite side to the moving limb tract - and become bilaterally symmetrical with execution of movement [104].

Then, it has to be mentioned that  $\mu$  rhythms were observed to generate mainly in the somatosensory area while  $\beta$  rhythms in a little more frontal region, over the motor areas. Therefore, computing  $\mu$  ERD and  $\beta$  ERS means to select also the proper locations to find the electrophysiological correlate of the sensorimotor cortical activity supporting the movement. Usually, when motor execution or motor imagery tasks are required to the subject under test,  $C_3$  is monitored for right-side limb movements,  $C_4$  for left-side, both  $C_3$  and  $C_4$  for simultaneous movement of right and left arms or hands and, finally,  $C_z$  is the standard location to observe feet motor control.

From the neurophysiological viewpoint, in an arm reaching task following a proprioceptive feedback (like a force stimulus, as in the current experiment described in section 3.2) two phases of cortical information processing could be expected:

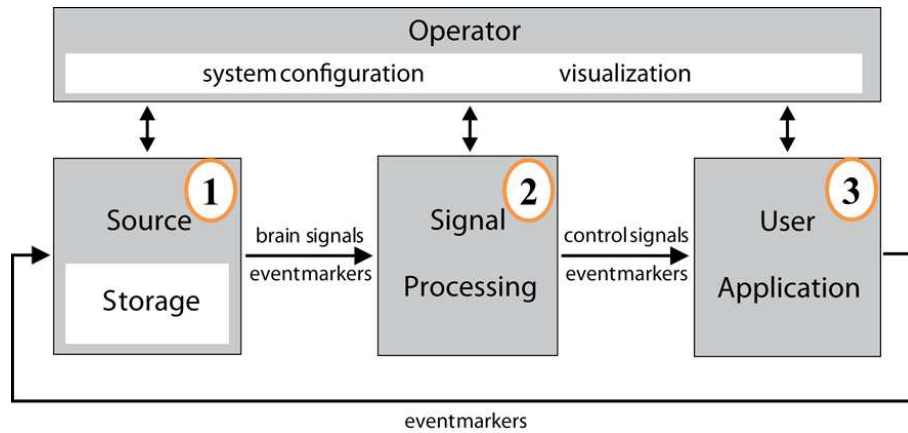


Figure 4.17: BCI2000 modules (modified from [71]).

- proprioceptive *afferent vias* transport the external stimulus information from the *receptors*, i.e. the muscles and nerves located in the distal district of the hand, to the contralateral somato-sensory areas of the brain located in the parietal lobe;
- with the proprioceptive information, a motor output is processed (even through the pons and the other hemisphere) and transmitted by means of the motor areas in the frontal lobe of the brain down to the final actuators of the movement, i.e. the muscles, by using the *efferent vias*.

However such a time line has not been proved yet, but only the bilateralization phenomenon in the whole sensorimotor areas as mentioned above.

### 4.3.2 BCI2000 Software

Operatively speaking, as already said in Chapter 3, the experiment was implemented by means of the world-wide spread (in the BCI community) software BCI2000 designed by Schalk and colleagues in 2004 [71].

Implementing the standard BCI structure formed by the four blocks already presented in section 2.2 (see Fig.2.5), Schalk and collaborators defined a similar software architecture, as shown in Fig.4.17.

While blocks 1 and 3 of Fig.2.5 perfectly match the analogous blocks *A* and *D* of Fig.4.17 representing the signal acquisition and digitalization steps and the device control operated by the features obtained as outputs of the signal processing block, respectively, block 2 is made by two further subroutines labelled in Fig.2.5 as *B* and *C*.

Signal processing indeed consists of the feature extraction module and the translation algorithm. In particular, raw signals from the source module become inputs of the signal processing block where a *spatial filter*, a *temporal filter*, a *linear classifier* and a *normalizer* could be applied to the raw traces.

Each of them can be defined by a block scheme as in Fig.4.18, where  $s_{in}$  is the signal input of any of the four filters and  $s_{out}$  its output that, in turn, will then become input for the next filter.

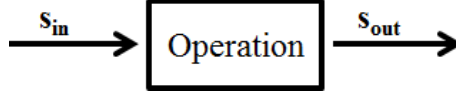


Figure 4.18: Single operation in the signal processing module of BCI2000.

Despite the particular choice of filter, to obtain the signal output each operation block performs a product between matrices as the following formula states:

$$S_{CHxN}^{OUT} = C_{CHxCH} S_{CHxN}^{IN}$$

where  $S^{OUT}$  is the  $CHxN$  matrix of the  $CH$  output signals with  $N$  samples,  $S^{IN}$  is the same quantity at the input and  $C$  is the matrix of weights.

This leads to the linear equation below:

$$s_{out}(i, n) = \sum_{j=1}^{CH} s_{in}(j, n) c(i, j)$$

where  $s_{out}(i, n)$  is the output sample  $n$  of the  $i$ -th output signal, while  $s_{in}(i, n)$  is the analogous measure at input and  $c(i, j)$  is the weight of the  $j$ -th channel in the computation of the  $i$ -th output.

Specifically:

- spatial filtering can operate a Laplacian derivation, a Common Average Reference (CAR) analysis or even a Common Spatial Pattern (CSP) identification;
- temporal filtering could implement a slow wave filter, an autoregressive spectral estimation, a Finite Impulse Response (FIR) filter, a peak detection or the average of single evoked responses;
- classifier computes each output as the linear combination of the input as given from a classification matrix;
- normalizer acts on the classifier's output in order to provide a zero mean signal at its output and a specific value range or a pre-selected standard deviation.

It has to be mentioned that coefficients for the classifier and, even more importantly, for the normalizer are defined either by the experience of the experimenters about the specific participant or by the statistics tool embedded in the BCI2000 software that can provide adaptation of the output features to the spontaneous changes of the cerebral activity thanks to a previous statistical analysis conducted over the signals.

BCI2000 is thus a very flexible and scalable tool for a variety of BCI applications and, moreover, it is constantly updated by the whole BCI community.

A further consideration concerns about the real-time constraint: as highlighted several times in the previous Chapters, BCI experiments require the system to perform all the acquisition, processing and output actuation within few tens of milliseconds range of time. This is ensured by BCI2000 software whose performance in some of the possible pc-amplifier configurations was reported in [71]. In fact, a maximum delay at the output level of 15 ms was found with minimal variations (i.e. latency jitter < 0.75 ms).

In the current experiment's settings as detailed described in 3.2 the combination of a CAR spatial filter, a Butterworth band pass filter in the individual  $\mu$  band (identified after the screening session) and a notch filter was chosen to process raw input signals. Then, a linear classifier computed the sum of the spectral power estimated in the (two or three) most significantly task-related channels and in the individual frequency band. Classifier's output was finally adapted to spontaneous cerebral activity changes thanks to the normalizer step which imposed a zero mean and unit variance to its output.

Although BCI2000 is that powerful and comprehensive software, the current implementation (see 3.2) for the EEG signals processing worked quite well but not in a complete satisfactory way. Some remarks especially remained for what the possible presence of large artefacts and the semi-automated features selection concerned. This was the reason that gave rise to the development of the algorithm for electrode-pop up artefacts detection and suppression presented in section 4.1 and to the subsequent detailed energy analysis performed in section 4.2. Those preliminary steps led to a slightly modified definition of MRD that allowed an earlier identification of the intention to move, that is the scope of the signal processing module in compliance with the operant-conditioning strategy to restore motor functions.

Next section will then explain the last step of the overall new algorithm for the MRD identification. It was thought to cope with the remarks expressed so far, but it could be generally exploited in every similar BCI application for motor recovery.

### 4.3.3 Proposal for an MRD Quantification Algorithm

As mentioned before, in this section the final MRD computation in a real-time design will be illustrated. This step is accomplished thanks to the previous energy analysis of section 4.2. After such a comprehensive statistical analysis, four definitions of MRD, slightly different from the original Pfurtscheller's one are suggested and, in next Chapter, they will be proved to be beneficial for an earlier identification and quantification of the phenomenon. Indeed, the four definitions were expressed as the following ratios  $r_i, i = 1, \dots, 4$ :

1. The ratio between the first 500 ms of post-trigger time and the pre-trigger one;
2. The ratio between the second 500 ms of post-trigger time and the first 500 ms of post-trigger;
3. The ratio between the third 500 ms of post-trigger time and the second 500 ms of post-trigger;
4. The ratio between the reaction time and the third 500 ms of post-trigger time;

Then, in order to identify an actual MRD, the following rule was adopted:

if  $r_i < THRESHOLD$ , then MRD is detected.

where *THRESHOLD* was initially set to 1 and then lower to 0.8 and even 0.6, meaning that an MRD event could be identified only if a more significant power decrease (of the

20% or 40%, respectively) were measured. Furthermore, the condition in the expression above had to be verified for half the number of channels, i.e.  $\frac{CH}{2}$  to actually decode an MRD.

As it will be discussed in the following and last chapter, this definition - based on the computation of the ratio between spectral powers in subsequent intervals - increased the performance of the MRD offline identification and allowed also to distinguish between healthy control participants and stroke survivors.

Its feasible implementation in the real-time operations will result more clearly from the quantitative findings shown in the next chapter where the early MRD identification will be highlighted in the most cases, both for healthy and stroke subjects.

A final mention has to be pointed out about the threshold choice. Initially it was set to 1, i.e. the minimum value for each ratio to ensure an energy decrease (that is the desynchronization); then it was lower down leading to the idea that a trade-off has to be matched: tighter than 1 limit for the threshold was selected to test the entity of the desynchronization amount, but no more than 50% energy decrease was found to have significant performance in any case. Further notions about the neurophysiological processes occurring during the trials could probably give reason of that qualitative considerations. Finally, a systematic optimization procedure has been already planned to find the optimal threshold value for obtaining more precise and customized results on the MRD identification performance.

This section concludes the exposition of the new proposed algorithm for the MRD identification during movement trials in a BCI experiment. Its fundamental steps are represented by the specific procedure for the electrode-pop artefacts detection and suppression described in section 4.1, the energy comprehensive statistical analysis performed in section 4.2 and the so far presented quantification method for MRD identification.

In the next Chapter, the results of the application of such an algorithm to the already recorded EEG data will be reported and a discussion section will provide comments about its performance, strong points and further possible improvements.



# Chapter 5

## Results and Discussion

As previously mentioned this Chapter deals with the presentation of the results from the energy analysis described in section 4.2 and the following MRD identification performance obtained by the application of the algorithm of section 4.3.

### 5.1 Results from the Signal Processing

As extensively explained in section 4.2, a complete energy analysis was performed on all the available differential signals, frequency bands, trials and phases with the aim to describe the energy behaviour during such kind of reaching task. A large amount of data was there collected and a statistical analysis could be performed.

In the following, Fig.5.1 provide a compact representation of those values both for the case of a healthy subject (Fig.5.1(a)) and of a stroke patient (Fig.5.1(b)).

Each boxplot represents the energy statistics measured during trials of the screening session in the correspondent phase (rest, pre-trigger, and so on) displayed below, in the standard  $\mu$  band (8,12) Hz in the  $C_4 - C_z$  differential signal ( $C_4$  would be the usual channel to find the MRD for a left-sided movement).

As it can be noted from Fig.5.1 a large variability was found both for the healthy and the stroke patient cases. This could be explained by the overlapping physiological and non-physiological components arising during such tasks and recorded at the scalp level.

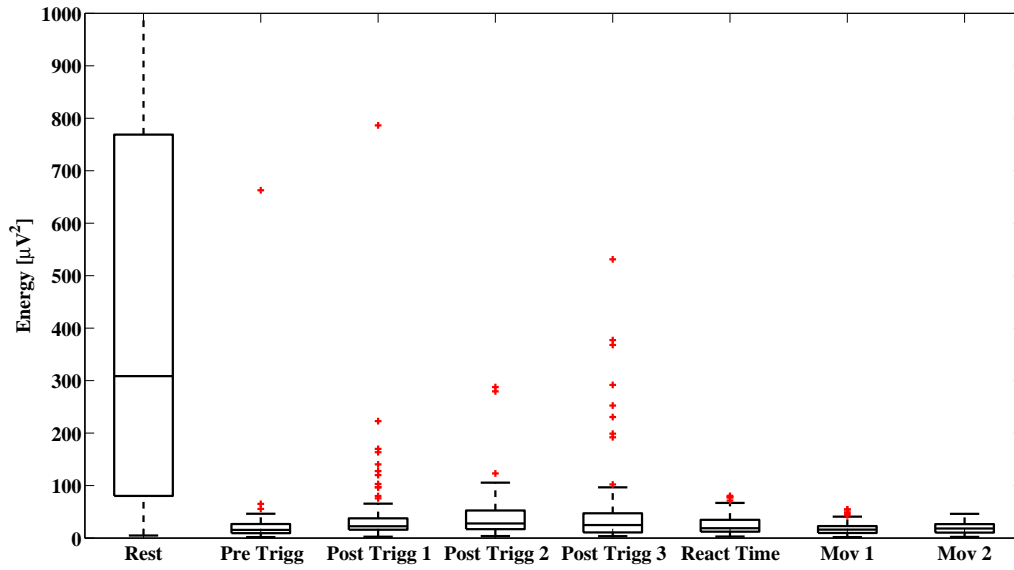
Moreover, a considerable amount of variability could be addressed to the inter-sessions variations that a subject produces when performing the experiment in different times.

Therefore, in Fig.5.2 the analogous boxplots for the energy statistics are displayed in the case of three single runs of the screening session for a healthy subject.

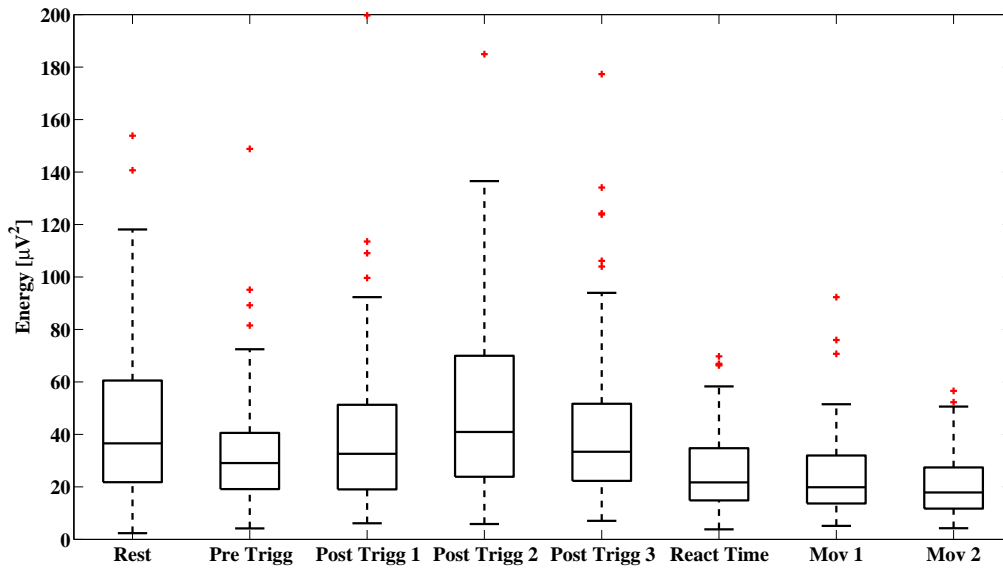
One more time, a large quantity of variability still clearly remains. This is due to the inter-trials and the intra-subject variations that occur even during different trials of the same daily session as a consequence of the physiologically changes continuously happening in a multi-tasking operating brain.

To this purpose a bunch of single trials energy profiles are reported in Fig.5.3.

From those profiles the cerebral activity variations can be clearly appreciated. But, more importantly, the different timing of the energy decrease (i.e. the MRD beginning) phenomenon strongly results. This means that, no matter the trigger events would state, the cerebral activity does not strictly follow their *rules*. It is only partially conditioned by cue sounds or target appearance, but it reacts with very different patterns to very



(a) Healthy case.



(b) Stroke case.

Figure 5.1: Statistical analysis of energy for all the phases in the (8,12)Hz band during screening with left arm for signal  $C_4 - C_z$  for a healthy subject.

similar tasks. Practically speaking, the energy decrease due to the movement processing can arise in a large time window: sometimes it starts just after the target appearance, some others it comes later till almost the end of the post-trigger interval or even at the reaction time period.

Nevertheless, with a robust identification technique the energy decrease related to the movement is detectable and quantifiable. Therefore, an algorithm that can reliably recognize the different situations (adaptability of the algorithm) and provide the correspondent robotic feedback at the most suitable moment was needed. This was indeed the main issue the new proposed algorithm aimed to give answer.

It has to be highlighted that two main factors can also influence the MRD identification: the localization of the phenomenon and the baseline level selection.

As the localization as regard, no clear situation could be described: indeed, a general energy decrease all over the sites (of differential signals) was found. Topographical maps of Fig.5.4 report one case (Fig.5.4(a)) that matches with the neurophysiological expectation of a contralateral activation (i.e. energy decrement) of the sensorimotor cortex, along with one (Fig.5.4(b)) of the most common case found during the energy analysis where a diffuse or a bilateral activation is present.

If the baseline selection is taken into account, a double choice can be made: in fact, either the inter-trials, i.e. pre-trigger time, period could be evaluated as the reference energy for the remaining trial phases or the initial 40 seconds rest could be used at the same scope. Both the solutions present their advantages as well as their drawbacks, so that a trade-off has to be accepted. Indeed, as found in a comparative analysis of performance (not reported here for compactness purposes), the MRD identification based on the second choice usually leads to higher detection performance, since the baseline energy is evaluated from a longer period of registration before the experiment beginning in which the relaxation (and the consequent  $\mu$  enhancement) of the subject is thus ensured.

However, sometimes the subject conditions at the current trial are so different from those at the beginning that a nearer (in time) reference would be a better choice, in order to avoid many false positive errors. In these cases, the inter-trials period of EEG signals, that is the pre-trigger time, should be used. This is the choice underlying the remaining results presented in this section. The same option would result beneficial in case of large and long-lasting artefacts corrupting the rest, as for example the electrode pop ones. By its side, pre-trigger lasts only 500 ms then it could be subjected to the drawback to make the patient not able to completely relax, leading to a number of false negative errors in the identification process.

In this final part, results and comments from the MRD computation explained in section 4.3 will be reported. In particular, as it can be reminded from that section, MRD was defined as the ratio between the energies of one phase and a baseline period (i.e. its preceding phase, in particular). The ratios between consecutive periods of time were evaluated with the aim to detect the instant in which the energy maximally decreased.

All the results will be presented in form of tables with a number of rows equal to the number of ratios and a number of columns equal to the number of frequency bands considered in the analysis. Rows can be viewed, thus, as kind of time axis in which the first row represents the MRD identification at about 2 s before the actual movement, the second one the MRD detection 1.5 s about before the motion and so on.

As the frequency bands as concern, the all standard and the logarithmically-logic

selected ones were included in the analysis and reported here. Moreover the larger (10,20) Hz band will be also taken into account with the purpose already mentioned in section 4.2 to be evaluated as possible alternative to smaller frequency bands introducing higher delays in the filter implementation phase.

Finally, each element of a table represents the percentage of detections of the MRD within one run (that is made by 80 trials or less if artefacts were present). It is worth to be reminded that an MRD identification occurs when the most channels presented a ratio correspondent to the current row at the frequency band related to the current column lower than a prefixed threshold. As mentioned before, that threshold was initially set to 1 and then it was lower to 0.8 and even 0.6, in order to make more strict the MRD identification requiring in this way an energy decrease of 20% or 40% into respect of the reference period.

A first example of such tables is provided in Fig.5.5. They sum up results from the MRD identification of a single run within the screening sessions performed by H3 and P2 in the three upper and three lower panels, respectively.

Moreover, the changes in the performance in correspondence with different values of the threshold in the MRD identification are also displayed, as reported by the captions of the figures.

Going further deep into the analysis of the pathological case, given a threshold value of 0.8, Fig.5.6 shows findings from each single run of the screening session for both the impaired and the healthy arms of P2.

As a comparison, the performance during the correspondent three runs of the end test session is given in Fig.5.7.

As already said in the previous sections, performance of this BCI system were usually evaluated by means of three different kinds of measures: clinical scales scores, kinematic outcomes and neurophysiological results.

As far as the latter have been just completely investigated in this section and the clinical scores reported in Fig.3.2 of section 3.1 are not significantly sensitive for such mildly impaired stroke patients, a brief presentation of some kinematic findings is due in the final part of this section to complete the overview about patient's improvements after this BCI experiment. Reference to these results will be mentioned in the discussion section as a proof of the reliability of the neurophysiological data of the patients correspondent with some kinematic variables improvement.

Therefore, kinematic outcomes of patient P2, P3 and P4 are reported in Fig.5.8, Fig.5.9 and Fig.5.10, while for a detailed analysis of results about P1 please refer to [66].

It is convenient here to recall that the statistical significance at the 95% level of confidence of the improvement achieved at the end test session in comparison with the screening one, as already pointed out, was assessed by means of the Wilcoxon rank test sum for all the kinematic measures apart for the number of correctly scored trials evaluated by the Kruskal-Wallis test.

## 5.2 Discussion

This section deals with the discussion of the MRD identification performance presented in section 5.1 of the algorithm proposed in section 4.3 and its correlation with the kinematic

findings reported at the end of section 5.1 for two patients.

Generally speaking, the most important observation that can be highlighted from all the tables presented so far is that the new algorithm can detect the MRD phenomenon in an earlier way, during either the first possible interval in the healthy case or, however, about 1 s before movement in the patient case.

Specifically, looking at Fig.5.5, a 90% identification percentage is already reached in the first interval in the case of the healthy subject H3 even if the threshold was lower to 60% and a more strict definition of MRD was imposed (although a slight performance decrease has to be accounted). For what the frequency distribution of the MRD concerns, from those tables it is clear that MRD mostly occurs - as expected - in the  $\mu$  and lower  $\beta$  bands, the bands below 8 Hz and above 25 Hz showing definitely lower identification rates. The (10,20) Hz band showed performance comparable to the more common bands of analysis: this could lead to the choice of this frequencies interval with the consequent computational advantages already mentioned in section 4.2.

On the other side, the patients showed - as in the expectations - lower performance than the healthy case, as it can be infer from Fig.5.5. Given a threshold equal to 0.8, for example, the third time interval (i.e. ratio) has to be waited to achieve a 90% detection level. However, this means that 1 s would be already available for further signal processing operations so that the algorithm was found to be reliable and useful also in the pathological cases.

As in the results of the healthy subject, the most significant frequency bands are located in the lower part of the available spectrum ((4,40) Hz is broadest spectrum at the output of the preprocessing step). This is, one more time, in line with literature on the topic. Moreover, the (10,20) Hz band still shows top performance, similarly to other more standard bands.

If looking at Fig.5.6 and Fig.5.7, the improvements due to training are relevant both in the healthy and the impaired arm of the patients, especially for subject P2. Moreover, as expected, a higher identification percentage was achieved with the healthy limb than the affected one. Both the last two observations are, moreover, confirmed by the contextual kinematic improvements reported in Fig.5.8, 5.9 and 5.10.

After the BCI training (with an actual force feedback as in the P2 case), performance are lower than the final run of the screening session but higher than the very beginning of the protocol showing a further visible increment within the end-test session.

Herein, further considerations about the actual efficacy of the particular proprioceptive and contingent feedback have to be frozen and postponed to the end of the experiment still in evaluation with the recruitment of more subjects.

Indeed, no significant changes in the behaviour of the phenomenon arose at the end of the experiment as what frequency distribution or time course matters.

A final important note is worth: the proposed algorithm can distinguish between the control and the pathological conditions. This is not a common feature for an algorithm that aims in detecting the MRD and moreover this observation could lead to consider the proposed algorithm as a diagnostic tool instead of a simple single step in the overall BCI system. However, in order to prove the significant diagnostic value of the procedure, a rigorous correlation analysis between the MRD performance, the clinical scores and the kinematic measures would be also needed.

This could be considered one of the points that have to be addressed by the future

analysis. Accordingly, this consideration leads to the conclusive section of this chapter: section 5.3 will illustrate indeed some perspectives along with open issues that still have to be addressed in order to ameliorate the system and make this specific BCI application actually effective for the rehabilitation purposes that guided its original implementation.

### 5.3 Future Perspectives

In order to generate such advancements in this BCI platform, further work on the signal processing part would be necessary. Besides the hints for improvement already suggested at the end of section 4.3 about an optimization procedure to set a suitable threshold for the MRD identification and a rigorous correlation analysis between the MRD performance and the kinematic outcomes, other actions should be taken into consideration and have to be deeper discussed with the aim to optimize the current protocol and to make it available for the largest pathological population that could benefit of it.

The first (and already under work) improvement to realize is to increase the EEG electrodes grid density so that it would be possible to better differentiate between the various regions and to be allowed to use signal processing techniques like CSP, CAR or other spatial filters that require a higher number of channels to be efficient.

With this modification, a more focused spatial distribution of the MRD phenomenon could be hopefully found in order to better evaluate the spatial neural re-organization of cerebral functions related to movement occurring during the BCI training.

Afterwards, the real implementation of the solution proposed along chapter 4 has to be realized and test on the real platform. To this purpose, a temporal filter should be selected to limit the bandwidth of the signal to the individual frequency band previously computed (during a preliminary session). A simulation study has been already performed in [105] where the FIR filter of order 50 was found to represent the optimal choice for this kind of protocol. As part of a future work, the application of this study to the actual EEG data has to be carried on.

Another important aspect of this model of experimental paradigm is the analysis of the correlation between the frontal and the parietal cortex as main actors in the sensorimotor control: correlations in the time domain or coherence in the frequency one of specific frequency bands and between the somatosensory and the primary motor cortex have to be investigated as carriers of the external somatosensory stimuli and the subsequent (delayed) motor output, respectively. The time-line of these activations and a valid support in this kind of analysis could be represented by the EMG recordings. This device could indeed be added to the current system to monitor the muscles activation onset and their reaction time.

Finally, as already mentioned before, this BCI application could be suitable for other kinds of patients rather than only stroke survivors. Indeed, the only exclusion criterion is that patient should mildly suffered from a motor impairment due to a cortical or sub-cortical focused injure like stroke. But, other phenotypically similar pathologies (such as focal dystonia) could eventually be treated with the same rehabilitative method.

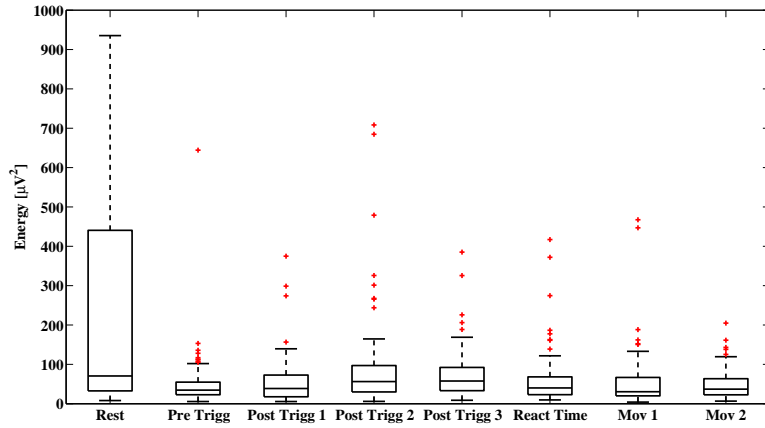
The protocol is actually being continued at San Camillo with the patient recruitment, although with some difficulties about the inclusion criterion that excludes more severe patients: actually, as previously mentioned, the most stroke survivors remains with really

severe impairments at the upper limbs, especially at the hands level. In many cases patients are completely blocked and they are not able to perform any movement; in many others they are defined as flaccid and can not sustain any movement with their affected upper limb.

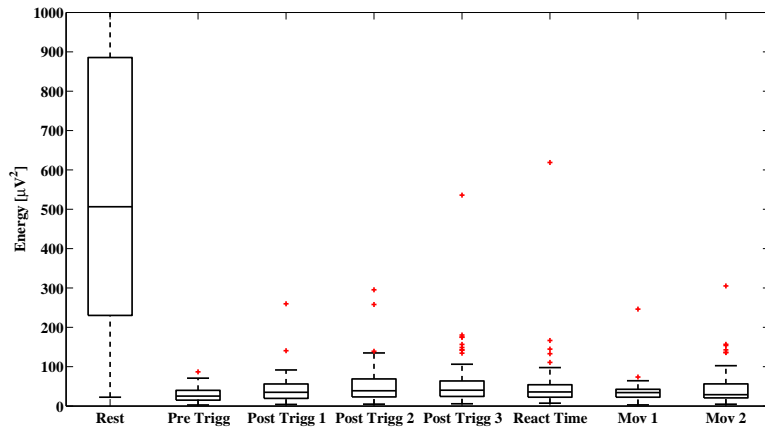
However, this BCI application aims, in a near future, at including these more severe patients in the rehabilitative program also. At the moment this is technically impossible but realistic solutions have been already suggested: for example, completely rigid patients can undergo a preliminary phase during which a physiotherapist would manipulate their arm making them to recover a minimal motricity to perform - partially, at least - the BCI reaching trials.

If this option was realized, the BCI-Phantom application could be completely tested and its efficacy would be proved in a shorter-term. Moreover, if the latter was verified to produce rehabilitative benefits (as already demonstrated in similar studies as [84] and [58]) the system could be suggested to enter the daily clinical rehabilitative practise of the Institute.

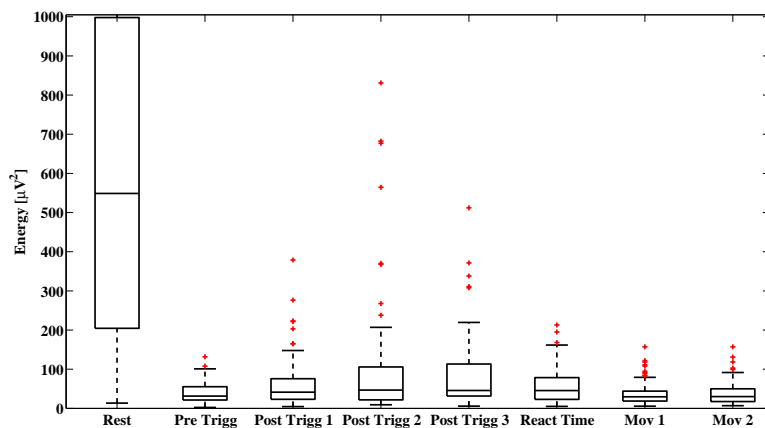
Furthermore, the project to make this system portable has been already advanced and many other portable BCI solutions are already available on the market nowadays. A portable and cheap EEG-based BCI solution for motor recovery of arms would allow patients to continue at home the treatment attended during the limited period of the hospitalization with a consequent benefit in terms of long-lasting and more effective recovery.



(a) Run no.1



(b) Run no.2.



(c) Run no.3.

Figure 5.2: Statistical analysis of energy for all the phases in the (8,12) Hz band of the signal  $C_3 - C_z$  during the screening session performed by the healthy subject H2 with the right arm.

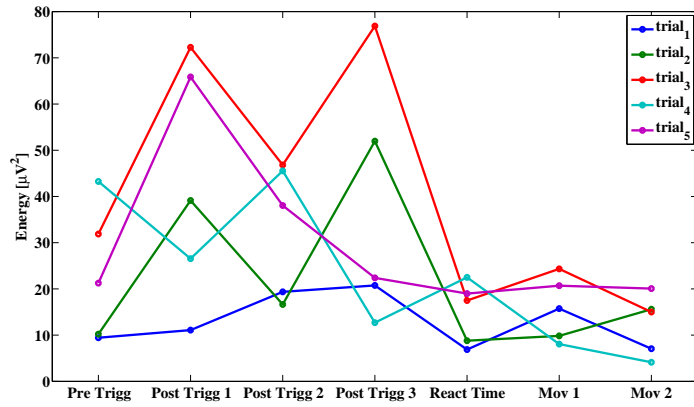
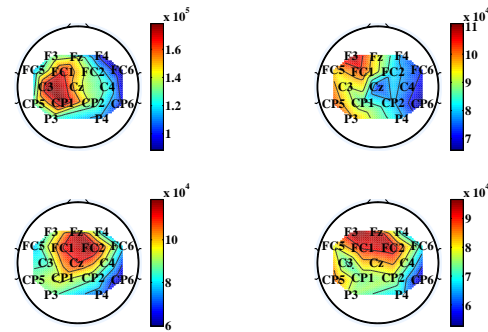
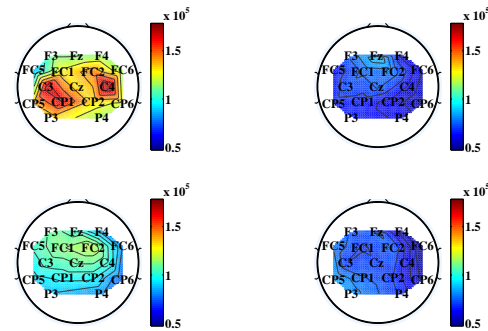


Figure 5.3: Example of single trials energies.



(a) Lateralized distribution (left hand movement) particularly visible in the right upward map.



(b) Diffuse distribution (right hand movement).

Figure 5.4: MRD localization in a healthy case. The topographical maps represent the distribution of the energy values in the reference interval during the initial rest (left up corner), in a first active period during the post-trigger time (right up), in a second active period from the onset of the movement (left down corner) and a final active period during the recovery phase (right down).

	(4,8)	(8,12)	(10,14)	(12,18)	(10,20)	(16,24)	(20,28)	(24,36)	(28,40)
Def 1	55	94	96	93	94	83	83	74	68
Def 2	67	97	98	98	98	92	97	96	87
Def 3	98	98	100	100	100	98	100	100	96
Def 4	100	98	100	100	100	100	100	100	100

(a) Healthy subject with threshold equal to 1.

	(4,8)	(8,12)	(10,14)	(12,18)	(10,20)	(16,24)	(20,28)	(24,36)	(28,40)
Def 1	39	91	93	89	93	77	72	48	43
Def 2	48	96	96	96	96	86	89	64	51
Def 3	92	98	98	98	98	94	92	74	56
Def 4	98	98	98	98	98	100	98	86	69

(b) Healthy subject with threshold equal to 0.8.

	(4,8)	(8,12)	(10,14)	(12,18)	(10,20)	(16,24)	(20,28)	(24,36)	(28,40)
Def 1	20	87	92	75	88	59	49	11	12
Def 2	21	89	96	78	89	69	60	13	12
Def 3	70	93	98	82	91	75	65	18	15
Def 4	81	94	98	86	91	81	72	22	18

(c) Healthy subject with threshold equal to 0.6.

	(4,8)	(8,12)	(10,14)	(12,18)	(10,20)	(16,24)	(20,28)	(24,36)	(28,40)
	61	55	60	42	51	47	38	25	25
Def 1	78	76	77	60	70	75	75	60	63
Def 2	98	97	97	96	98	100	91	90	91
Def 3	100	100	98	100	100	100	97	98	96

(d) Stroke subject with threshold equal to 1.

	(4,8)	(8,12)	(10,14)	(12,18)	(10,20)	(16,24)	(20,28)	(24,36)	(28,40)
Def 1	51	45	47	22	33	30	26	15	17
Def 2	66	66	57	32	48	48	38	25	30
Def 3	90	90	81	71	82	81	63	42	48
Def 4	100	95	88	83	88	90	80	52	62

(e) Stroke subject with threshold equal to 0.8.

	(4,8)	(8,12)	(10,14)	(12,18)	(10,20)	(16,24)	(20,28)	(24,36)	(28,40)
Def 1	36	38	32	8	15	13	15	10	6
Def 2	43	50	36	10	18	22	15	11	7
Def 3	78	72	52	37	42	46	23	12	12
Def 4	93	75	55	47	48	52	28	15	13

(f) Stroke subject with threshold equal to 0.6.

Figure 5.5: MRD identification performance with different thresholds for subjects H3 and P2.

	(4,8)	(8,12)	(10,14)	(12,18)	(10,20)	(16,24)	(20,28)	(24,36)	(28,40)
Def 1	21	27	46	53	52	55	68	76	68
Def 2	42	45	57	70	63	63	77	82	78
Def 3	92	76	80	85	86	85	86	85	78
Def 4	100	81	90	91	91	92	92	88	86

(a) Screening run no.1 with left affected arm.

	(4,8)	(8,12)	(10,14)	(12,18)	(10,20)	(16,24)	(20,28)	(24,36)	(28,40)
Def 1	18	33	45	34	28	22	28	29	20
Def 2	54	57	68	46	49	42	54	38	34
Def 3	85	77	81	70	70	69	76	52	49
Def 4	97	94	90	81	84	85	85	65	60

(b) Screening run no.1 with right healthy arm.

	(4,8)	(8,12)	(10,14)	(12,18)	(10,20)	(16,24)	(20,28)	(24,36)	(28,40)
Def 1	39	91	93	89	93	77	72	46	43
Def 2	48	96	96	96	96	86	89	64	51
Def 3	92	98	98	98	98	94	92	74	56
Def 4	98	98	98	98	98	100	98	86	69

(c) Screening run no.2 with left affected arm.

	(4,8)	(8,12)	(10,14)	(12,18)	(10,20)	(16,24)	(20,28)	(24,36)	(28,40)
Def 1	17	33	32	29	26	28	24	12	21
Def 2	44	57	47	47	37	46	37	33	29
Def 3	84	84	79	82	67	67	53	52	42
Def 4	100	96	83	94	85	91	71	56	48

(d) Screening run no.2 with right healthy arm.

	(4,8)	(8,12)	(10,14)	(12,18)	(10,20)	(16,24)	(20,28)	(24,36)	(28,40)
Def 1	51	45	47	22	33	30	26	15	17
Def 2	66	66	57	32	48	48	38	25	30
Def 3	90	90	81	71	82	81	63	42	48
Def 4	100	95	88	83	88	90	80	52	62

(e) Screening run no.3 with left affected arm.

	(4,8)	(8,12)	(10,14)	(12,18)	(10,20)	(16,24)	(20,28)	(24,36)	(28,40)
Def 1	47	40	37	40	36	41	31	28	35
Def 2	70	60	56	51	48	55	43	43	50
Def 3	91	92	72	70	70	71	57	56	68
Def 4	98	96	81	86	83	87	72	65	77

(f) Screening run no.3 with right healthy arm.

Figure 5.6: MRD identification performance for P2 (left affected arm) along the screening sessions.

	(4,8)	(8,12)	(10,14)	(12,18)	(10,20)	(16,24)	(20,28)	(24,36)	(28,40)
Def 1	51	42	36	35	37	27	21	5	2
Def 2	66	52	52	41	45	37	33	25	22
Def 3	95	81	73	67	62	61	58	42	35
Def 4	100	91	83	82	76	85	75	60	52

(a) End test run no.1 with left affected arm.

	(4,8)	(8,12)	(10,14)	(12,18)	(10,20)	(16,24)	(20,28)	(24,36)	(28,40)
Def 1	6	33	43	35	35	37	33	36	35
Def 2	18	57	60	45	45	50	52	43	47
Def 3	81	87	75	72	67	65	65	52	58
Def 4	97	95	81	88	86	85	86	62	61

(b) End test run no.1 with right healthy arm.

	(4,8)	(8,12)	(10,14)	(12,18)	(10,20)	(16,24)	(20,28)	(24,36)	(28,40)
Def 1	26	16	27	17	17	10	16	1	0
Def 2	33	38	50	26	26	22	27	25	30
Def 3	87	72	73	62	62	55	47	37	45
Def 4	98	81	83	78	75	82	67	53	62

(c) End test run no.2 with left affected arm.

	(4,8)	(8,12)	(10,14)	(12,18)	(10,20)	(16,24)	(20,28)	(24,36)	(28,40)
Def 1	31	33	31	16	18	8	12	7	15
Def 2	38	53	50	35	51	50	28	18	30
Def 3	90	81	66	58	60	50	45	36	47
Def 4	100	86	81	87	87	86	78	48	57

(d) End test run no.2 with right healthy arm.

	(4,8)	(8,12)	(10,14)	(12,18)	(10,20)	(16,24)	(20,28)	(24,36)	(28,40)
Def 1	41	35	32	28	27	26	33	26	17
Def 2	50	50	55	37	36	33	47	42	41
Def 3	95	82	75	63	62	58	61	55	55
Def 4	98	90	82	83	73	78	75	63	61

(e) End test run no.3 with left affected arm.

	(4,8)	(8,12)	(10,14)	(12,18)	(10,20)	(16,24)	(20,28)	(24,36)	(28,40)
Def 1	32	40	51	30	35	30	43	36	32
Def 2	45	52	71	51	53	53	65	55	48
Def 3	85	82	80	73	70	75	73	66	58
Def 4	96	87	88	93	83	96	87	76	70

(f) End test run no.3 with right healthy arm.

Figure 5.7: MRD identification performance for P2 (left affected arm) along the end test sessions.

	% Correct Trials	Duration [ms]	Area Error [mm <sup>2</sup> ]	Reaction Time [ms]
Screening	15 ± 5	902 ± 244	35 ± 3	422 ± 10
End-test	28 ± 5*	811 ± 27**	33 ± 7	449 ± 23*

(a) Left affected arm.

	% correct trials	Duration [ms]	Area Error [mm <sup>2</sup> ]	Reaction Time [ms]
Screening	31 ± 3	808 ± 313	23 ± 6	515 ± 207
End-test	39 ± 1*	729 ± 136*	22 ± 1	367 ± 9

(b) Right healthy arm.

Figure 5.8: Kinematic performance of P2.

	% Correct Trials	Duration [ms]	Area Error [mm <sup>2</sup> ]	Reaction Time [ms]
Screening	31 ± 7	757 ± 37	50 ± 17	350 ± 66
End-test	50 ± 8	741 ± 50	34 ± 11	284 ± 34

(a) Right affected arm.

	% correct trials	Duration [ms]	Area Error [mm <sup>2</sup> ]	Reaction Time [ms]
Screening	29 ± 6	783 ± 53	59 ± 23	343 ± 16
End-test	40 ± 2*	682 ± 3*	28 ± 3*	289 ± 19*

(b) Left healthy arm.

Figure 5.9: Kinematic performance of P3.

	% Correct Trials	Duration [ms]	Area Error [mm <sup>2</sup> ]	Reaction Time [ms]
Screening	59.2	0.646 ± 0.259	16.62 ± 48.2	372 ± 56
End-test	/	/	/	/

(a) Left affected arm.

	% Correct Trials	Duration [ms]	Area Error [mm <sup>2</sup> ]	Reaction Time [ms]
Screening	72	0.598 ± 0.131	13.25 ± 60.94	441 ± 126
End-test	/	/	/	/

(b) Right healthy arm.

Figure 5.10: Kinematic performance of P4.



# Conclusion

In the context of EEG-based BCI for motor rehabilitation for stroke survivors, the specific signal processing for providing a reliable and in real-time feedback was presented and discussed.

A particular BCI application aided by an haptic device that could release a force that helped the patient in completing the reaching task required in the experiment was considered.

The initial protocol and setup of the application were described in detail along with the strong and weak points arose during the operations. Then, the motivation for proposing new solutions especially in the signal processing module of the platform resulted clear: identification and correction of large artefacts due to electrode pop was addressed by means of a non linear algorithm that can run in real-time preventing from wasting large amount of data as in the initial setup of the experiment.

Afterwards, a comprehensive analysis of the energy distribution in the time, frequency and space domain was performed and reported for all the phases of a single trial of reaching movement and along the whole experimental session.

Since the purpose of this work was to detect in a precise and real-time way the cerebral pattern related to the movement (the MRD) during the experimental course and to quantify it in order to produce a consequent force feedback associated to that, new definitions of the MRD were proposed and evaluated.

In particular, early detection of the MRD was obtained in the expected frequency bands  $\mu$  - (8,12) Hz - and lower  $\beta$  - (12,18) Hz - with identification performance higher than 90% both for the healthy subjects and the stroke patients. Once implemented, this new solution would then allow to save time during a trial of movement before the actual accomplishment of the reaching task to operate further processing on the EEG signals, to combined in a more suitable way the extracted relevant features that should describe the condition of the subject, or to compute a more effective feedback from the point of view of the operant-learning strategy for recovering the arm functionalities.

Open questions still remain to be discussed and addressed, as mentioned in the final Chapter of this work but, nevertheless, promising perspectives arose from this study however: now, they need to be implemented to confirm the high performance shown in the offline analysis mentioned so far.

If such improvements in the signal processing steps of the platform will be verified during the online operations also, new frontiers of application could be opened from the extension of the same BCI platform: indeed, with a suitable adaptation of the haptic feedback and the integration of an EMG system the attempt to move by even more severely impaired patients could be detected, supported and promoted. Moreover, this system could be transformed into a substitutive tool for performing movement by reusing

the same EEG signal processing methods and applying an actual robotic arm in place of the current haptic feedback. Many other advancements could be prospected with some of them already planned, but a robust and reliable signal processing unit has to be previously implemented to suitably and optimally match the requirement of the system as well as of the task , adapting at the same time to the specific subject's characteristics and needs.

This Ph.D. thesis work represents in fact a step towards the realization of such a reliable system for the rehabilitative purposes, an adaptive tool for every kind of subject and, more importantly, a potentially portable, non invasive and relatively cheap platform for continuing the reaching training at patient's home after the hospitalization period, with the consequent much larger benefit from the rehabilitation underwent in the clinics.

# Bibliography

- [1] Wolpaw J.R., Birbaumer N., McFarland D.J., Pfurtscheller G. and Vaughan T.M., *Brain-Computer interfaces for communication and control*, Clin. Neurophysiol., 113, 767-791, 2002.
- [2] Langhorne P., Coupar F. and Pollock A., *Motor recovery after stroke: a systematic review*, Lancet Neurol., 8, 741-754, 2009.
- [3] Riemann B.L. and Scott M.L., *The sensorimotor system, Part I: the physiologic basis of functional joint stability*, J. Athl. Train., 37(1), 71-79, 2002.
- [4] Dimyan, M.A. and Cohen L.G., *Neuroplasticity in the context of motor rehabilitation after stroke*, Nat. Rev. Neurol., 7, 76-85, 2011.
- [5] Krakauer J.W., *Motor learning: its relevance to stroke recovery and neurorehabilitation*, Curr. Opin. Neurol. 19, 84-90, 2006.
- [6] Piron L., Turolla A., Agostini M., Zucconi C.S., Ventura L., Tonin P. and Dam M., *Motor learning principles for rehabilitation: a pilot randomized controlled study in post stroke patients*, Neurorehab. Neural Re., 24, 501-508, 2010.
- [7] Fetz E.E., *Operant Conditioning of Cortical Unit Activity*, Science, 163, 955-958, 1969.
- [8] Guyton A.C., *Neuroscienze : basi di neuroanatomia e neurofisiologia*, trad. it. Pietro D’Arcangelo, ed. Piccin, Padova, 1996 (orig. ed. W.B.Saunders, Philadelphia, 1995).
- [9] Brodmann K., *Vergleichende Lokalisationslehre der Grosshirnrinde in ihren Prinzipien dargestellt auf Grund des Zellenbaues*, Johann Ambrosius Barth Verlag, Leipzig, 1909.
- [10] Garey L.J., *Broadmann’s Localization in the Cerebral Cortex*, Springer, New York, 2006.
- [11] Jasper H. and Penfield W. L., *Epilepsy and the Functional Anatomy of the Human Brain*, 2nd ed., Brown and Co., 1954.
- [12] Scott S.H. and Norman K.E., *Computational approaches to motor control and their potential role for interpreting motor dysfunction*, Curr. Opin. Neurol., 16, 693-698, 2003.
- [13] World Health Organization (WHO) Statistics Annual Report, 2013 [http://www.who.int/gho/publications/world\\_health\\_statistics/2013/en/](http://www.who.int/gho/publications/world_health_statistics/2013/en/)

- [14] Carmichael S.T., *Cellular and molecular mechanisms of neural repair after stroke: making waves*, *Annals of Neurology*, 59 (5), 735-742, 2006.
- [15] Biernaskie J. and Corbett D., *Enriched rehabilitative training improved forelimb motor function and enhanced dendritic growth after focal ischemic injury*, *J. Neurosci.*, 21 (14), 5272-5280, 2001.
- [16] Adkins, D.L., Boychuk, J., Remple, M.S. and Kleim, J.A., *Motor training induces experience-specific patterns of plasticity across motor cortex and spinal cord*, *J. Appl. Physiol.*, 101 (6), 1776-1782, 2006.
- [17] Stroemer, R.P., Kent, T.A. and Hulsbosch, C.E., *Neocortical neural sprouting, synaptogenesis, and behavioral recovery after neocortical infarction in rats*, *Stroke*, 26(11), 2135-2144, 1995.
- [18] Langhorne P., Bernhardt J. and Kwakkel G., *Stroke rehabilitation*, *Lancet*, 377, 1693-1702, 2011.
- [19] Quinn T.J., Paolucci S., Sunnerhagen K.S., Sivenius J., Walker M.F., Toni D., Lees K.R., European Stroke Organisation (ESO) Executive Committee, ESO Writing Committee. *Evidence-based stroke rehabilitation: an expanded guidance document from the european stroke organisation (ESO) guidelines for management of ischemic stroke and transient ischemic attack 2008*, *J. Rehabil. Med.*, 41, 99-111, 2009.
- [20] Pfurtscheller G. and Neuper C., *Motor Imagery and Direct Brain-Computer Communication*, *Proc. IEEE*, 89(7), 1123-1134, 2001.
- [21] Broetz D., Braun C., Weber C., Soekadar S.R., Caria A. and Birbaumer N., *Combination of brain-computer interface training and goal-directed physical therapy in chronic state: A case report*, *Neurorehabil. Neural Re.*, 24(7), 674-679, 2010.
- [22] Birbaumer N. and Cohen L.G., *Brain-computer interface: communication and restoration of movement paralysis*, *J. Physiol.*, 579(Pt 3), 621-636, 2007.
- [23] Piovesan D., Morasso P., Giannoni P. and Casadio M., *Arm stiffness during assisted movement after stroke: the influence of visual feedback and training*, *IEEE Trans. Neural Sys. Rehab. Eng.*, 21, 454-465, 2013.
- [24] Klimesch W., *EEG alpha and theta oscillations reflect cognitive and memory performance: A review and analysis*, *Brain Res. Rev.*, 29, 169-195, 1999.
- [25] Nunez P.L. and Srinivasan R., *Electric Field of the Brain*, Oxford University Press, New York, 2006.
- [26] Niedermeyer E. and Lopes Da Silva F.H., *Electroencephalography: basic principles, clinical applications and related fields*, Lippincott Williams and Wilkins, Philadelphia, PA, 1999.
- [27] Miniussi C. and Ruzzoli M., *Transcranial stimulation and cognition*, *Handb. Clin. Neurol.*, 116, 739-750, 2013.

- [28] Pellicciari M.C., Brignani D. and Miniussi C., *Excitability modulation of the motor system induced by transcranial direct current stimulation: a multimodal approach*, Neuroimage, 83, 569-580, 2013.
- [29] Miniussi C. Cappa S.F., Cohen L.G., Floel A., Fregni F., Nitsche M.A., Oliveri M., Pascual-Leone A., Paulus W, Priori A. and Walsh V., *Efficacy of repetitive transcranial magnetic stimulation/transcranial direct current stimulation in cognitive neurorehabilitation*, Brain Stimul., 1(4), 326-36, 2008.
- [30] Dimyan M.A. and Cohen, L.G., *Contribution of transcranial magnetic stimulation to the understanding of functional recovery mechanisms after stroke*, Neurorehabil. Neural Re., 24, 125-135, 2010.
- [31] Berger H., *Über das electrenkephalogramm des menchen*, Archiv für Psychiatrie Nervenkrankheiten, 87, 527-570, 1929.
- [32] Nuwer M.R., Comi C., Emerson R., Fuglsang-Frederiksen A., Guafarit J.M., Hinrichs H., Ikeda A., Luccas F.J.C. and Rappelsburger P., *IFCN standards for digital recording of clinical EEG*, EEG Clin. Neurophysiol., 106, 259-261, 1998.
- [33] Jasper H.H., *The ten-twenty electrode system of the International Federation*, EEG Clin. Neurophysiol., 10, 371-375, 1958.
- [34] Oostenveld R. and Praamstra P., *The five percent electrode system for high-resolution EEG and ERP measurements*, Clin. Neurophysiol., 112(4), 713-719, 2001.
- [35] Pasqual-Marqui R.D., Michel C.M. and Lehmann D., *Low resolution electromagnetic tomography: a new method for localizing electrical activity in the brain*, Int. J. Psychophysiol., 18, 49-65, 1994.
- [36] Blinowska K.J. and Kaminski M., *Functional brain networks: random, "small world" or deterministic?*, PLoS One, 8 (10), 2013.
- [37] Vergallo P. and Lay-Ekuakille A., *Brain source localization: a new method based on Multiple Signal Classification algorithm and spatial sparsity of the field signal for electroencephalogram measurements*, Rev. Sci. Instrum., 84(8), 2013.
- [38] Puuronen J. and Hyvarinen A., *A Bayesian inverse solution using independent component analysis*, Neural Netw., 50, 47-59, 2014.
- [39] Liao K., Zhu M. and Ding L., *A new wavelet transform to sparsely represent cortical current densities for EEG/MEG inverse problems*, Comput. Meth. Prog. Bio., 111(2), 376-388, 2013.
- [40] Nievergelt Y., *Wavelets Made Easy*, Springer, New York, 2013.
- [41] International Federation of Societies for EEG and Clinical Neurophysiology, *A glossary of terms commonly used by clinical electroencephalographers*, EEG Clin. Neurophysiol., 37, 534-548, 1974.

- [42] Pineda J.A., *The functional significance of mu rhythms: Translating "seeing" and "hearing" into "doing"*, Brain Res. Rev., 50(1), 57-68, 2005.
- [43] Di Pellegrino G., Fadiga L., Fogassi L., Gallese F. and Rizzolatti G., *Understanding motor events: A neurophysiological study*, Exp. Brain Res., 91(1), 176-180, 1992.
- [44] McFarland D.J., Miner L.A., Vaughan T.M. and Wolpaw J.R., *Mu and beta rhythm topographies during motor imagery and actual movements*, Brain Topogr., 12, 177-186, 2000.
- [45] Vidal J.J., *Toward Direct Brain-Computer Communications*, Annu. Rev. Biophys. Bioeng., 2, 157-180, 1973.
- [46] Farwell L.A. and Donchin E., *Talking off the top of your head: toward a mental prosthesis utilizing event-related brain potentials*, EEG Clin. Neurophysiol., 70(6), 510-523, 1988.
- [47] Birbaumer N., Ghanayim N., Hinterberger T., Iversen I., Kotchoubey B., Kubler A., Perelmouter J., Taub E. and Flor H., *A spelling device for the paralysed*, Nature, 1999.
- [48] Kubler A., Kotchoubey B., Hinterberger T., Ghanayim N., Perelmouter J., Schauer M., Fritsch C., Taub E., Birbaumer N., *The thought translation device: a neurophysiological approach to communication in total motor paralysis*, Exp. Brain Res., 124(2), 223-32, 1999.
- [49] Silvoni S., Ramos-Murguialday A., Cavinato M., Volpato C., Cisotto G., Turolla A., Piccione F. and Birbaumer N., *Brain-Computer interface in stroke: A review of progress*, Clin. EEG Neurosci., 42, 4, 245-252, 2011.
- [50] Ang K.K. and Guan C., *Brain-Computer Interface in Stroke Rehabilitation*, J. Comp. Sci. Eng., 7, 139-146, 2013.
- [51] Curran E.A. and Stokes M.J., *Learning to control brain activity: a review of the production and control of EEG components for driving brain-computer interface (BCI) systems*, Brain Cogn., 51(3), 326-36, 2003.
- [52] Hochberg L.R., Bacher D., Jarosiewicz B., Masse N.Y., Simeral J.D., Vogel J., Haddadin S., Liu J., Cash S.S., Van Der Smagt P. and Donoghue J.P., *Reach and grasp by people with tetraplegia using a neurally controlled robotic arm*, Nature, 485(7398), 372-5, 2012.
- [53] Collinger J.L., Foldes S., Bruns T.M., Wodlinger B., Gaunt R. and Weber D.J., *Neuroprosthetic technology for individuals with spinal cord injury*, J. Spinal Cord. Med., 36(4), 258-272, 2013.
- [54] Leeb R., Perdakis S., Tonin L., Biasiucci A., Tavella M., Creatura M., Molina A., Al-Khodairy A., Carlson T. and Millan J.D., *Transferring brain-computer interfaces beyond the laboratory: successful application control for motor-disabled users*, Artif. Intell. Med., 59(2), 121-132, 2013.

- [55] Pfurtscheller G., Allison B.Z., Brunner C., Bauernfeind G., Solis-Escalante T., Scherer R., Zander T.O., Mueller-Putz G., Neuper C. and Birbaumer N., *The hybrid BCI*, Front. Neurosci. 21, 4-30, 2010.
- [56] Birbaumer N., Gallegos-Ayala G., Wildgruber M., Silvoni S. and Soekadar S.R., *Direct brain control and communication in paralysis*, Brain Topogr, 27(1), 4-11, 2014.
- [57] Pfurtscheller G., Muller G.R., Pfurtscheller J., Gerner H.J. and Rupp R., *"Thought"-control of functional electrical stimulation to restore hand grasp in a patient with tetraplegia*, Neurosci. Lett., 351(1), 33-36, 2003.
- [58] Ramos-Murguialday A., Broetz D., Rea M., Laer L., Yilmaz O., Brasil F.L., Liberati G., Curado M.R., Garcia-Cossio E., Vyziotis A., Cho W., Agostini M., Soares E., Soekadar S., Caria A., Cohen L.G. and Birbaumer N., *Brain-machine interface in chronic stroke rehabilitation: a controlled study*, Ann. Neurol., 74(1), 100-108, 2013.
- [59] Leeb R., Sagha H., Chavarriaga R. and Millan J.R., *A hybrid brain-computer interface based on the fusion of electroencephalographic and electromyographic activities*, J. Neural Eng., 8(2), 2011.
- [60] Albanese A., Bhatia K., Bressman S.B., DeLong M.R., Fahn S., Fung V.S., Mallett M., Jankovic J., Jinnah H.A., Klein C., Lain A.E., Mink J.W. and Teller, J.K., *Phenomenology and classification of dystonia: A consensus update*, Mov. Disord., 28(7), 863-873, 2013.
- [61] Buch E.R., Shanechi A.M., Fourkask A.D., Weber C., Birbaumer N. and Cohen L.G., *Parietofrontal integrity determines neural modulation associated with grasping imagery after stroke*, Brain, 135(Pt 2), 596-614, 2012.
- [62] Pavlov I.P., *Conditioned Reflexes: An Investigation of the Physiological Activity of the Cerebral Cortex*, Oxford University Press, London, 1849-1936, 1927 (translated and edited by G.V. Anrep, Dover 2003).
- [63] Konorski J., *Conditioned reflexes and neuron organization*, Cambridge University Press, page 89, 1948 (Tr. from the Polish ms. under the author's supervision).
- [64] Skinner B.F., *The behavior of organisms: an experimental analysis*, Oxford, England, Appleton-Century, 457, 1938.
- [65] Fetz E.E., *Volitional control of neural activity: implications for brain-computer interfaces*, J. Physiol., 579(Pt 3), 571-579, 2007.
- [66] Silvoni S., Cavinato M., Volpato C., Cisotto G., Genna C., Agostini M., Turolla A., Ramos-Murguialday A. and Piccione F., *Kinematic and neurophysiological consequences of an assisted-force-feedback brain-machine interface training: a case study*, Front. Neurol., 4 (173), 2013.
- [67] Cisotto G., Silvoni S., Cavinato M., Piccione F. and Pupolin S., *Brain computer interface in chronic stroke: an application of sensorimotor closed-loop and contingent force feedback*, Proc. of the IEEE ICC'13, 2972-2976, 2013.

- [68] Weiskopf N., Mathiak K., Bock S.W., Scharnowski F., Veit R., Grodd W., Goebel R. and Birbaumer N., *Principles of a brain-computer interface (BCI) based on real-time functional magnetic resonance imaging (fMRI)*, IEEE Trans. Biomed. Eng., 51(6), 966-970, 2004.
- [69] Donchin E., Spencer K.M. and Wijesinghe R., *The mental prosthesis: assessing the speed of a P300-based brain-computer interface*, IEEE Trans. Rehabil. Eng., 8(2), 174-179, 2000.
- [70] Guger Technology g.USBamp. Product details, from <http://www.gtec.at/Products/Hardware-and-Accessories/g.USBamp-Specs-Features>.
- [71] Schalk G., McFarland D.J., Hinterberger T., Birbaumer N. and Wolpaw J.R., *BCI2000: A general-purpose brain-computer interface (BCI) system*, IEEE Trans. Biomed. Eng., 51(6), 1034-1043, 2004.
- [72] PHANTOM, Premium 3.0/6 DOF Sensable Technologies. Product details, from <http://www.sensable.com/haptic-phantom-premium-6dof.html>
- [73] Fitts P.M., *The information capacity of the human motor system in controlling the amplitude of movement*, J. Exp. Psychol., 47, 381-391, 1954.
- [74] Carlson T., Tonin L., Perdakis S., Leeb R. and Millan J. R., *A hybrid BCI for enhanced control of a telepresence robot*, Proc. IEEE EMBS, 2013, 3097-3100, 2013.
- [75] Kapeller C., Hintermuller C., Abu-Alqumsan M., Pruckl R., Peer A. and Guger C., *A BCI using VEP for continuous control of a mobile robot*, Proc. IEEE EMBS, 2013, 5254-5257, 2013.
- [76] Lugo Z.R., Rodriguez J., Lechner A., Ortner R., Gantner I.S., Laureys S., Noirhomme Q. and Guger C., *A Vibrotactile P300-Based Brain-Computer Interface for Consciousness Detection and Communication*, Clin. EEG Neurosci., 2014.
- [77] Ortner R., Irimia D.C., Scharinger J. and Guger C., *A motor imagery based brain-computer interface for stroke rehabilitation*, Stud. Health Technol. Inform., 181, 319-323, 2012.
- [78] Yilmaz O., Cho W., Braun C., Birbaumer N. and Ramos-Murguialday A., *Movement related cortical potentials in severe chronic stroke*, Proc. IEEE EMBS, 2013, 2216-2219, 2013.
- [79] De Massari D., Ruf C.A., Furdea A., Matuz T., Van Der Heiden L., Halder S., Silvoni S. and Birbaumer N., *Brain communication in the locked-in state*, Brain, 136(Pt 6), 1989-2000, 2013.
- [80] Scherer R. and Pfurtscheller G., *Thought-based interaction with the physical world*, Trends. Cogn. Sci. 17(10), 490-492, 2013.

- [81] Daly J.J., Cheng R., Rogers J., Litinas K., Hrovat K. and Dohring M., *Feasibility of a new application of noninvasive Brain Computer Interface (BCI): a case study of training for recovery of volitional motor control after stroke*, J. Neurol. Phys. Ther., 33(4), 203-211, 2009.
- [82] Caria A., Weber C., Broetz D., Ramos-Murguialday A., Ticini L.F., Gharabaghi A., Braun C. and Birbaumer N., *Chronic stroke recovery after combined BCI training and physiotherapy: a case report*, Psychophysiology, 48(4), 578-582, 2011.
- [83] Grosse-Wentrup M., Mattia D. and Oweiss K., *Using brain-computer interfaces to induce neural plasticity and restore function*, J. Neural Eng., 8(2), 025004, 2011.
- [84] Ramos-Murguialday A., Halder S. and Birbaumer N., *Proprioceptive feedback in BCI*, Proc. IEEE NER, 279-282, 2009.
- [85] Gomez-Rodriguez M., Peters J., Hill J., Scholkopf B., Gharabaghi A. and Grosse-Wentrup M., *Closing the sensorimotor loop: Haptic feedback facilitates decoding of motor imagery*, J. Neural. Eng., 8(3), 2011.
- [86] Durka P.J., Klekowicz H., Blinowska K.J., Szelenberger W. and Niemcewicz S.Z., *A simple system for detection of EEG artifacts in polysomnographic recordings*, IEEE Trans. Biomed. Eng., 50, 526-528, 2003.
- [87] Barlow S., *Automatic elimination of electrode-pop artifacts in EEG's*, IEEE Trans. Biomed. Eng., 33, 517-521, 1986.
- [88] Jung T.P., Makeig S., Humphries C., Lee T.W., McKeown M.J., Iragui V. and Sejnowski T.J., *Removing electroencephalographic artifacts by blind source separation*, Psychophysiol., 37(2), 163-178, 2000.
- [89] Santillan-Guzman A., Heute U., Stephani U. and Galka A., *Muscle artifact suppression using independent-component analysis and state-space modeling*, Proc. IEEE EMBS, 6500-3, 2012.
- [90] Zeng H., Song A., Yan R. and Qin H., *EOG artifact correction from EEG recording using stationary subspace analysis and empirical mode decomposition*, Sensors (Basel), 13(11), 14839-59, 2013.
- [91] Sweeney KT, McLoone SF, Ward TE. *The use of ensemble empirical mode decomposition with canonical correlation analysis as a novel artifact removal technique*, IEEE Trans. Biomed. Eng., 60(1), 97-105, 2013.
- [92] Asaduzzaman K., Reaz M.B., Mohd-Yasin F., Sim K.S. and Hussain M.S., *A study on discrete wavelet-based noise removal from EEG signals*, Adv. Exp. Med. Biol., 680, 593-599, 2010.
- [93] Gao J., Yang Y., Sun J. and Yu G., *Automatic removal of various artifacts from EEG signals using combined methods*, J. Clin. Neurophysiol., 27(5), 312-320, 2010.
- [94] Cooley J.W. and Tukey J.W., *An algorithm for the machine calculation of complex Fourier series*, Math. Comput., 19(90), 297-301, 1965.

- [95] Pfurtscheller G. and Aranibar A., *Event-related cortical desynchronization detected by power measurements of scalp EEG*, EEG Clin. Neurophysiol., 42(6), 817-826, 1977.
- [96] Pfurtscheller G, and Aranibar A., *Evaluation of event-related desynchronization (ERD) preceding and following voluntary self-paced movement*, EEG Clin. Neurophysiol., 46(2), 138-146, 1979.
- [97] Pfurtscheller G, and Aranibar A., *Changes in central EEG activity in relation to voluntary movement. I. Normal subjects*, Prog. Brain Res., 54, 225-231, 1980.
- [98] Pfurtscheller G., Aranibar A. and Wege W., *Changes in central EEG activity in relation to voluntary movement. II. Hemiplegic patients*, Prog. Brain Res., 54, 491-495, 1980.
- [99] Pfurtscheller G., *Event-related synchronization (ERS): an electrophysiological correlate of cortical areas at rest*, EEG Clin. Neurophysiol., 83(1), 62-69, 1992.
- [100] Pfurtscheller G. and Neuper C., *Event-related synchronization of mu rhythm in the EEG over the cortical hand area in man*, Neurosci. Lett., 174(1), 93-96, 1994.
- [101] Neuper C., Wortz M. and Pfurtscheller G., *ERD/ERS patterns reflecting sensorimotor activation and deactivation*, Prog. Brain Res., 159, 211-222, 2006.
- [102] Graimann B. and Pfurtscheller G., *Quantification and visualization of event-related changes in oscillatory brain activity in the time-frequency domain*, Prog. Brain Res., 159, 79-97, 2006.
- [103] Pfurtscheller G. and Lopes Da Silva F.H., *Event-related EEG/MEG synchronization and desynchronization: basic principles*, Clin. Neurophysiol., 110(11), 1842-1857, 1999.
- [104] Pfurtscheller G., *EEG event-related desynchronization (ERD) and event-related synchronization (ERS)*, In: [26], 53, 958-967, 1999.
- [105] Sturaro S., *Design of a digital FIR filter with minimum delay for BCI applications*(Bachelor Thesis), Padova, 2013.

# List of Figures

1.1	The nervous system. . . . .	10
1.2	Brain hemispheres and lobes. . . . .	11
1.3	The Brodmann areas. . . . .	11
1.4	The main functional areas. . . . .	12
1.5	The sensorimotor system. . . . .	13
1.6	The neuron. . . . .	14
1.7	Pathway from the CNS to the muscles. . . . .	15
2.1	The 10-20 international EEG system. . . . .	20
2.2	The 5-10 extended international EEG system. . . . .	21
2.3	An example of cerebral rhythms. . . . .	24
2.4	The first message from Subject A (extracted from [47]). . . . .	26
2.5	The typical BCI scheme. . . . .	29
2.6	P300 Evoked Potential (extracted from [1]). . . . .	30
2.7	Sensorimotor Rhythms (extracted from [1]). . . . .	30
2.8	Slow Cortical Potential (extracted from [1]). . . . .	31
3.1	Stroke subjects data. . . . .	35
3.2	Clinical evaluations of the patients. . . . .	35
3.3	Standard 2D reaching task. . . . .	37
3.4	Single trial structure. . . . .	37
3.5	Single run structure. . . . .	38
3.6	Different sessions of the experimental protocol. . . . .	38
3.7	Experimental setup. . . . .	39
3.8	EEG Channels location. . . . .	39
3.9	Healthy subject data. . . . .	41
3.10	$R^2$ grid plot from a screening session. . . . .	45
3.11	Features selection from the $R^2$ values grid for specific frequencies within the SMR after a screening run performed with the left arm by a healthy participant. . . . .	45
3.12	Electrode-pop artefact in the $C_z$ channel affects the $R^2$ computation (abnormally negative values in $C_z$ ). . . . .	47
4.1	Signal with electrode pop artifact. A detail. . . . .	50
4.2	Signal with electrode-pop artifact. The whole recording. . . . .	51
4.3	Artifact addicted EEG signal (black), its derivative (red) and the artefactual interval edges (cyan dots). . . . .	53

4.4	The original raw signal filtered in the (7,14) Hz band (black curve), the filter output after the application of the proposed algorithm (red curve), the filter output without any artifact detection algorithm (blue curve) and the artefactual interval (magenta vertical lines). . . . .	54
4.5	A detail of Fig.4.4. . . . .	54
4.6	Raw signal (black) with two different shapes of synthetic artifacts. . . . .	55
4.7	Raw signal (black) with two different shapes of synthetic artefacts. A detail. . . . .	55
4.8	Table with the parameters values of the two synthetic electrode-pop artifacts. . . . .	56
4.9	Energy of the errors at the filter output along with the mean energy level of the original artifact free signal $x$ (green line) and the artefactual interval (magenta lines). . . . .	57
4.10	SNRs at the filter output with the artefactual interval (magenta vertical lines). . . . .	57
4.11	MRD topography of an artifact-free EEG recording. . . . .	58
4.12	MRD topography of an artifact-addicted EEG dataset with a synthetic electrode-pop artifact on the FZ site. . . . .	59
4.13	MRD topography after removing the synthetic electrode-pop artefact from the same EEG dataset of Fig.4.11. . . . .	59
4.14	Adjacence matrix. . . . .	61
4.15	The seven trial's phases. . . . .	63
4.16	Individual frequency band identification method by Pfurtscheller in case of a healthy subject. . . . .	66
4.17	BCI2000 modules (modified from [71]). . . . .	68
4.18	Single operation in the signal processing module of BCI2000. . . . .	69
5.1	Statistical analysis of energy for all the phases in the (8,12)Hz band during screening with left arm for signal $C_4 - C_z$ for a healthy subject. . . . .	74
5.2	Statistical analysis of energy for all the phases in the (8,12) Hz band of the signal $C_3 - C_z$ during the screening session performed by the healthy subject H2 with the right arm. . . . .	80
5.3	Example of single trials energies. . . . .	81
5.4	MRD localization in a healthy case. The topographical maps represent the distribution of the energy values in the reference interval during the initial rest (left up corner), in a first active period during the post-trigger time (right up), in a second active period from the onset of the movement (left down corner) and a final active period during the recovery phase (right down). . . . .	81
5.5	MRD identification performance with different thresholds for subjects H3 and P2. . . . .	82
5.6	MRD identification performance for P2 (left affected arm) along the screening sessions. . . . .	83
5.7	MRD identification performance for P2 (left affected arm) along the end test sessions. . . . .	84
5.8	Kinematic performance of P2. . . . .	85
5.9	Kinematic performance of P3. . . . .	85
5.10	Kinematic performance of P4. . . . .	85